Motion-based Thermal Sensing for Health Care Monitoring Systems (HMS) and Healthcare Applications

BY

OUDAY HANOSH
BSc, University of Baghdad, 1997
M.S., University of Baghdad, 2001

THESIS

Submitted as partial fulfillment of the requirements
for the degree of Doctor of Philosophy in Electrical and Computer Engineering
in the Graduate College of the
University of Illinois at Chicago, 2021

Chicago, Illinois

Defense Committee:

Rashid Ansari, Chair and Advisor
A. Enis Cetin, Co-advisor
Mojtaba Soltanalian
Pai-Yen Chen
Yusuf Ozturk, ECE dept., San Diego State University

To see a world in grain of sand

And a heaven in a wild flower,

Hold infinity in the palm of your hand

And eternity in an hour.

- William Blake

To my dad, mom, Nadeen, Louy, Firas, and Daniel for all the love, help, and support to fulfill my dream

To all family and friends for their unconditional love

ACKNOWLEDGMENTS

I would like to express my sincere gratitude and appreciation to everyone who played a role in my PhD journey and helped to make this dream achievable.

First, I would like to sincerely thank my PhD advisor, Dr. Rashid Ansari and my PhD co-advisor, Dr. A. Enis Cetin.

Dr. Rashid Ansari, Your scholarly guidance was indispensable. Thank you for the encouragement, trust, and support, especially when the path grew dark. I will always appreciate the opportunities and new research challenges you helped me to discover. You are the type of mentor that I will strive to be in the future.

Dr. A. Enis Cetin. From the first day that you joined our department, I was impressed with your enthusiasm and work ethic, and I did my best to follow your example. Thank you so much for introducing me to IR sensors and their use in medical applications. Your expertise and support were invaluable, and helped me to keep pushing.

I would like to express my sincere gratitude to my beloved Mom and Dad, who have sacrificed so much so that I can achieve my dreams. I am so proud to be your son and I will always do my best to honor you. Thank you for believing in me. You are the best role models imaginable. I would like to thank my brother Louy, my sister Nadeen, my brother-in-law Firas, and my nephew Daniel. Your love and support have given me so much strength.

ACKNOWLEDGMENTS (Continued)

I would like to dedicate my PhD to my family members here in the States. To my beloved Uncle Salah and Aunt Frances Khayyat, I will never forget your endless love, kindness, and warm hospitality. Aunt Frances, you were an angel on this earth and no words can express how much I miss you.

I would also like to dedicate this PhD to my best friend, Beshar, for all of his help and support, especially during the times that I felt so overwhelmed. Thank you for everything.

Finally, I would like to take this moment to thank my beloved brother, Adnan, and his family, for being there with me through the good and bad times. There are no words that can express my gratitude. This PhD is as much yours as it is mine!

OH

CONTRIBUTION OF AUTHORS

Chapter 1 shows the introduction of this thesis and the summery of all the research contributions.

Chapter 2 provides an introduction to passive sensors and reviews past work on detecting convulsive seizures during sleep. It also reviews recent research on estimating the pulse rate and respiratory rate.

Chapter 3 presents the work of the published manuscript (Hanosh et al., 2019 [1]), for which I was the main contributor and first author. Prof. Rashid Ansari and Prof. A. Enis Cetin were co-investigators.

Chapter 4 presents the work of the published conference paper Hanosh et al., 2019 [2]), for which I was the main contributor and first author. Prof. Rashid Ansari and Prof. A. Enis Cetin were co-investigators.

Chapter 5 shows the approach method that submitted to IEEE Journal, for which I was the main contributor and first author. Prof. Rashid Ansari and Prof. A. Enis Cetin were co-investigators.

Chapter 6 presents the method that submitted to IEEE Journal, for which I was the main contributor and first author. Prof. Rashid Ansari and Prof. A. Enis Cetin were co-investigators.

Chapter 7 provides the conclusion of this thesis and discusses the possible approaches for the future work.

TABLE OF CONTENTS

TABLE OF CONTENTS (Continued)

CHAPTER **PAGE**

LIST OF TABLES

LIST OF TABLES (Continued)

LIST OF FIGURES

LIST OF FIGURES (Continued)

FIGURE **PAGE**

LIST OF FIGURES (Continued)

FIGURE **PAGE**

LIST OF FIGURES (Continued)

LIST OF ABBREVIATIONS

HMSs	Health Monitoring Systems
WHO	World Health Organization
SUPED	Sudden Unexpected Death in Epilepsy
EEG	Electroencephalogram
ECG	Electrocardiography
MEMS	Micro Electro-Mechanical Systems
NREP	Non-Rapid EYE Movement
REM	Rapid EYE Movement
AASM	American Academy of Sleep Medicine
SWS	Slow-Wave Sleep
SU	Sensing Unit
IR	InfraRed
HMM	Hidden Markov Model
RELU	Rectified Linear Unit
NN	Neural Network
TP	True Positive
TN	True Negative

LIST OF ABBREVIATIONS (Continued)

FP	False Positive
FN	False Negative
HR	Heart Rate
RR	Respiratory Rate
AoD	Area of Detection
CDC	Centers of Disease Control and Prevention
CVDs	Cardiovascular Diseases
FORP	Fiber Optic Respiratory Plethysmograph
RF	Radio Frequency
CWT	Continuous Wavelet Transform
SPO2	Blood Oxygen Saturation
FG	Fiber Grating
RVSM	Radar Vital Signs Monitoring
CCD	Charged Coupled Device
SUDEP	Sudden Unexpected Death in Epilepsy

List of Algorithms

SUMMARY

Recent rapid advances in sensor technology and Internet of Things (IoT) have led to remarkable progress in medical applications and public healthcare. Consequently, there is a huge momentum to develop Health Monitoring Systems (HMSs) that can improve patient care and safety, the accuracy of the information, and the real-time assessment of the human health condition.

Sensors play a crucial role in healthcare technology and HMSs, with the aim of improving the quality of human life. The sensors can capture vital signs and other patient information and convert them into electrical signals that can be analyzed for follow-up action by caregivers as appropriate. A key challenge in HMSs is to find low-cost and accurate sensors that can be fitted on to non-intrusive, affordable, reliable, small, lightweight, and easy-to-use devices. The objective of these devices is to help achieve an accurate diagnosis, and to monitor patients not only in clinical settings but also in home environments.

In this dissertation we investigated the use of low-cost, non-contact pyroelectric and thermopile passive infrared sensors for motion detection in health monitoring applications. The research focus is on exploring the use of these sensors for the tasks of

i. convulsive body motion detection targeted at monitoring patients with epilepsy during sleep, seeking to prevent sudden unexpected death in epilepsy (SUDEP), and

ii. subtle body motion detection aimed at estimating two vital signs: heart rate and respiratory rate.

We also investigate the design of efficient and low-cost algorithms and their practical implementation to perform the tasks and validate the methods experimentally. For the task of detecting convulsive

motion aimed at epileptic seizure monitoring during sleep, we propose a novel approach that uses low-cost, non-intrusive, contact-free pyroelectric infrared sensors to sense convulsive body motion and distinguish it from other body motions. The method is tested on the signals captured from healthy subjects, recruited after getting IRB approval. We investigate the use of different machine learning algorithms and attain a maximum accuracy of 98.98% for our data. We also examine the use of a low-cost, low-power, and low-resolution (8×8) thermopile sensor array implemented with a Convolutional Neural Network (CNN). We demonstrate that a 99.2% accuracy is achieved in classifying convulsive movements and non-convulsive body motion. For task of measuring subtle body motion aimed at estimating one of the vital signs, the human respiratory rate, we again investigate the use of the thermopile infrared sensor array and the pyroelectric infrared sensor. We propose and experimentally validate a novel method that human respiration rate may be reliably estimated from respiration-induced body movements. We devised computationally efficient algorithms to analyze the data collected from human subjects with IRB approval. We demonstrate that a 97.7% correlation between the actual respiratory rate and the estimated rate in our dataset is attained. We also propose a novel approach to estimate the human respiratory rate and heart rate by investigating the use of a low-cost, contact-free, and non-invasive pyroelectric infrared sensor. The respiratory rate and the heart rate are inferred from the time-varying sensor signal due to the subtle movements of the head caused by the flow of air from the lungs and blood from the heart to the head via the carotid artery, respectively. The PIR sensor is placed behind the human head without direct contact with the body. Experimental results show a 96.4% correlation between our heart rate estimates and the pulse oximeter measurements is achieved in our dataset. Also, 95.37% correlation is achieved between the respiratory rate estimates and the chest movements monitoring as a ground truth.

CHAPTER 1

INTRODUCTION

1.1 Introduction

Recent developments in microelectronics and sensor technology have led to design and implementation of light weight, small size, and affordable sensor devices that play a fundamental role in transforming how healthcare service is provided [3]. Traditional healthcare systems are designed, implemented, and optimized to react to the treatments of the diagnosed illness rather than focusing on prevention. On the other hand, contemporary HMSs are implemented to react to prevention of illness with early detection of the disease [4]. Most of HMSs usually rely on using a combination of sensors, a microcontroller, and a workstation for data processing and decision making. Sensors are the kernel of the HMSs. They can monitor and measure the main physiological parameters of the patient that can assess his/her health condition status. Based on whether contact with a human body is made, sensors can be classified into contact-based sensors or contact-free sensors [5], [6].

Recently, there is an increased interest in the use of contact-free sensors in HMSs to measure the vital signs and early detection of some of the chronic diseases [7]. Such sensors include Infrared IR sensors, vibration and acoustic sensors, and different type of cameras [7], [8], [9], [10].

Several factors influenced the trend towards the increased used of contact-free sensors in HMSs. One factor is the low cost of such sensors that makes them affordable for use by many people, including the low-income segment of population. The small size and light weight of these sensors make them easy to

use in different setups, not only in hospitals or clinics but also in home environments for Assistive Living (AL) [11], [12], [13]. Another factor is the high accuracy and tolerable rate of errors in applications that can improve the quality of life of people. Finally some of the contact-free sensors such as an IR sensors and low-resolution thermal cameras are non-intrusive in the sense that they preserve the privacy of the patients [14].

1.2 Motivation

More than 65 million people world-wide, with 3.4 million in the United States, suffer from epilepsy [15]. Unfortunately, they carry a higher risk for death than the general population. Every year 1 out of 1000 people with epilepsy dies from sudden unexpected death in epilepsy (SUDEP) [16], [17]. SUDEP is a fatal threat to patients who suffer from convulsive seizures. The causes of the SUDEP are still not well-understood, and patients who suffer from epileptic seizures may face death during sleep, likely after an unwitnessed convulsive seizure. An important step towards SUDEP prevention is reliable seizure detection during sleep that is inexpensive and unobtrusive. This motivated our search for affordable, low-power, contact-free solutions to this problem. This led us to the investigation of two different type of passive sensors, the Pyroelectric Infrared sensor and the low -resolution thermopile sensor array for convulsive seizure detection based on our prior knowledge of the effectiveness of passive sensors in motion detection applications. Detection of an epileptic seizure during sleep may be used to issue alerts to caregivers to provide timely help to the patients. The contact-free nature of the passive sensors and their ability to detect seizures even in the dark make them attractive for patient use. We note that while a sleep stage can trigger the epilepsy, which is noticeable in some epilepsy syndrome cases like Rolandic seizures, epilepsy may in turn disorganize and confuse sleep during epileptic seizures [18].

Another key challenge in healthcare is the incidence of Cardiovascular diseases (CVDs), which is one of the leading causes death among both males and females in United States. According to the Centers for Disease Control and Prevention (CDC), about 6.5 million people in the United States suffer a heart failure every year, and a heart failure was a contributing factor in one in 8 deaths in 2017 [19]. Moreover, 30% of deaths around the world are due to CVDs [20]. Vital signs are critical in monitoring patients with CVDs. The Heart Rate (HR), Respiratory Rate (RR), blood pressure and body temperature are four vital signs which are indicators of the human body's most basic functions. Continuous monitoring of the HR and RR and accurate measurement of the HR and RR are important for monitoring the health status of patients with CVDs. This motivated us and led us to examine the use of PIR sensor and the thermopile sensor array as a low-cost, privacy-preserving and contact-free sensors to measure the HR and RR. We used the pyroelectric IR sensor to detect the HR and RR from the subtle head movement of the stationary subjects while the thermopile sensor array is used to measure the RR during sleep.

1.3 Research Contributions

The main contributions of this thesis are summarized as follows:

1. We propose a novel approach and implement and algorithm to detect convulsive body movements motivated by epileptic seizure detection using PIR sensors. (Hanosh et al., [1]).
2. We propose and demonstrate a new method of detecting convulsive movements during sleep using an (8×8) low-resolution thermopile sensor array. (Hanosh et al., [2]).
3. We propose a novel approach and carryout the implementation of an algorithm to measure the HR and RR from the subtle head movement using PIR sensor.

4. We devise and demonstrate the effectiveness of new method to detect the RR during sleep using an (8×8) thermopile sensor array.

The results were demonstrated using data collected from human subjects with IRB approval.

1.4 Thesis Outline

The rest of this dissertation is organized as follows. In Chapter 2, we provide an introduction to passive sensors and describe related work for detecting convulsive seizures. We also present the related work to estimate the heart rate and respiratory rate. In Chapter 3, we describe our novel approach to detect convulsive seizures using pyroelectric IR sensor. Chapter4 demonstrates our novel method for detecting convulsive movements using a low-resolution 8×8 thermopile sensor array. Chapter 5 describes our approach to estimating the respiratory rate using a thermopile sensor array. Chapter 6 presents our unique method to estimate the pulse rate and respiratory rate from a single signal that captures the subtle head movements using a contact-free pyroelectric IR sensor. The conclusion and possible future work are presented in chapter 7.

CHAPTER 2

PASSIVE SENSORS AND RELATED WORK

Recent developments in the design, technology, and manufacturing of sensors with a decrease in their size, power consumption and cost has led to expanding the role of the sensors in the healthcare application and assistive living [21]. To monitor patients with a variety of diseases, different types of contact-based sensors, contact-free sensor, passive and/or active sensors are incorporated in the HMSs to detect the early symptoms and initiate an alarm to the caregivers to help their patients. The need of non-invasive devices for continuous health monitoring and the need of early detection of many diseases motivate us to investigate two types of low-cost, contact-free and passive sensors, the pyroelectric Infrared PIR sensor and the thermopile sensor array, in selected healthcare applications. We investigate the use of these sensors to detect the convulsive seizures during sleep and to measure two vital signs,the Respiratory rate (RR) and the Heart Rate (HR), that play an important role in assessing patient's health. In this chapter we present an overview of the pyroelectric IR sensor and an (8×8) thermopile IR sensor array. A background of the sensors that are used to detect convulsive movements and the sensors that are used to measure the RR and HR, is provided.

2.1 Sensors classification

Sensors are entities that can capture physical input from the environments, and generate an electrical or optical output. The sensed physical input from the environment may be thermal energy , light intensity, temperature, humidity and other input. Each type of sensor has its own internal condition-

ing unit to generate the electrical output corresponding to the variation of the captured input [22]. The sensors can be classified in many different types. Based on whether contact is made with a subject's body, they are classified as contact-based sensors and contact-free sensors. Sensors also are classified based on the energy radiation into passive and active sensors, active sensors illuminate a scene with their own radiated energy. Passive sensors on the other hand, do not radiate energy. They are not equipped with transmitters to radiate any type of energy. Furthermore, the sensors can also be classified based on whether their output is digital or analog (see Figure 1) [23].

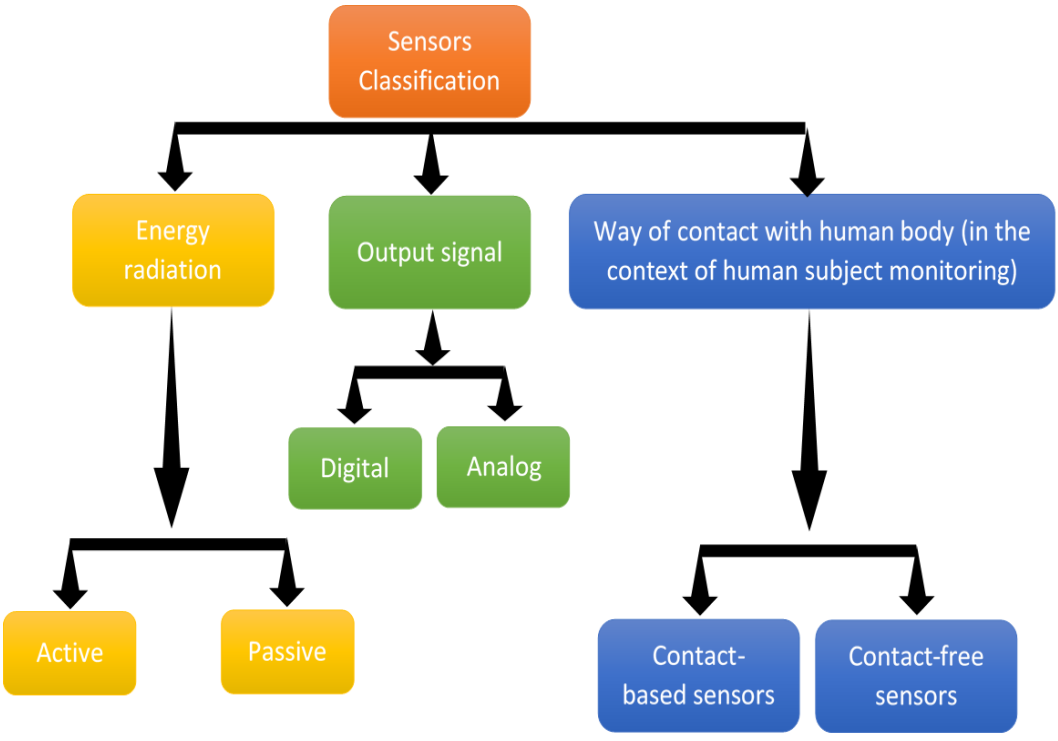

Figure 1: A block diagram of sensor classification based on the type of the output, the way of connection, and the energy radiation.

2.2 Thermopile and Pyroelectric passive sensors

Nowadays pyro-electric IR sensor and thermopile IR sensor are widely used in our daily life [24–28]. The thermopile and pyroelectric sensors are provide two ways of detecting infrared radiation emitted by humans in motion. They detect IR light with a wavelength between 8 and 13μm, which is not in the visible range of the human eyes. Both sensors can perform non-intrusive and contact-free detection, and are passive because they do not emit any radiation. In our work we used these sensors in two different systems to detect convulsive movements and, measure two vital signs: the heart rate and respiratory rate, which are important to assess the health condition of a human.

2.2.1 Thermopile sensor array

A thermopile sensor array is a set of thermocouples made of two dissimilar materials to detect the IR radiation from a moving subject. It works based on the Seeback effect phenomena [29]. Since an individual thermocouple generates a low output, several thermocouples are connected in series to boost the output level. Each thermocouple is made of two junctions: hot junction and cold junction [29]. The hot junction detects the IR radiation, while the cold junction is isolated from the IR radiation (see Figure 2). When the IR radiation is incident on the hot junction of the thermocouple (points A, B and C in Figure 2), a temperature difference between the hot junction and cold junction (point D, and E in Figure 2) is created, and an electrical output proportional to the intensity of radiation is produced (see equation 1).

$$V_{out} = N_{Thc} S_B \left(T_H - T_C\right) \tag{2.1}$$

where N_{Thc} is the number of thermocouples, S_B is the Seeback coefficient, T_H is the hot junction temperature, and T_C is the cold junction temperature. In our work we used a low-resolution Panasonic Grid-EYE 8×8 thermopile sensor array, consisting of 64 pixels, and a frame rate of 10 frames per second, with a low power consumption of approximately $15mW$.

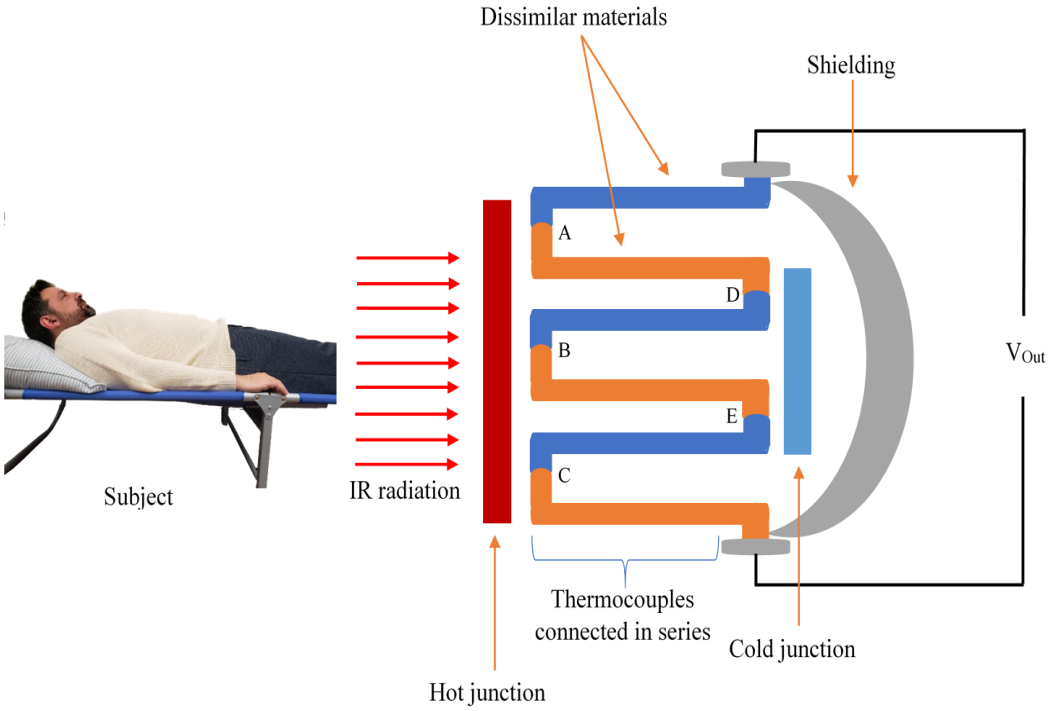

Figure 2: Internal structure of the thermopile sensor array made of a number of thermocouples connected in series.

2.2.2 Pyroelectric sensor

A pyroelectric sensor is used to measure IR radiation emitted from a moving object within its Area of Detection (AoD). It has two slots made of the same materials that are sensitive to the IR radiation. When there is no motion, the differential IR level between the two slots is equal to zero, because both slots have the same amount of charge, corresponding to the ambient light. If the IR radiation is intercepted in one of the slots due to motion, then PIR slot *a* (see Figure 3) has more IR level change than slot *b*, generating a positive differential charge. On the other hand, when the moving object exits the AoD of the PIR sensor, the level of IR radiation of the second slot *b* will be higher than that of slot *a*, generating a negative differential charge.

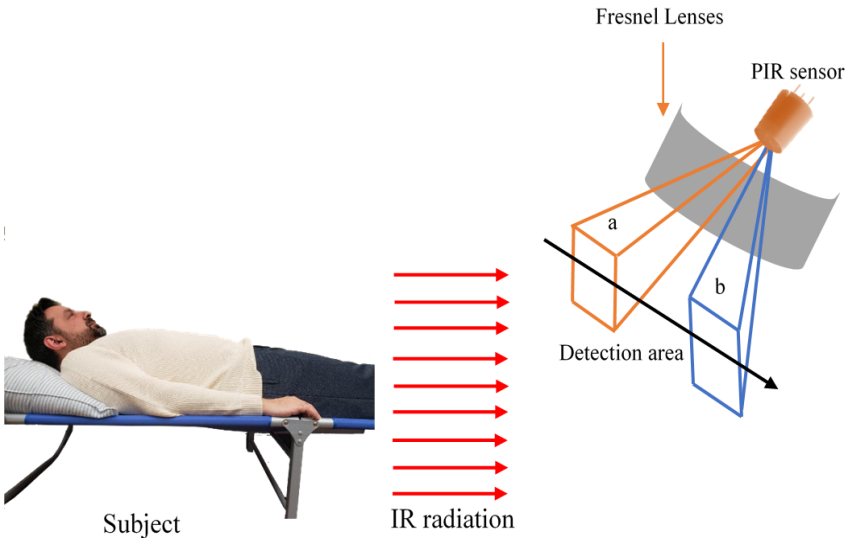

Figure 3: Internal structure of the Pyroelectric Infrared PIR sensor that has two slots made from the same material.

2.3 Review on epileptic seizure detection

More than 65 million people world-wide, with 3.4 million in the United States, suffer from epilepsy [30]. Unfortunately, they carry a higher risk for death than the general population. Every year 1 out of 1000 people with epilepsy dies from Sudden Unexpected Death in Epilepsy (SUDEP) [31], [32]. The cause of SUDEP is still unknown, but in most cases, death occurs in sleep and victims are found face down in bed [33]. Early detection of seizures and simple interventions could reduce the risk of SUDEP [33]. We seek to design a low-cost, contact-free, and privacy-preserving system to detect epileptic seizures during sleep.

Many methods are used to detect seizures [34–50], but most are not well-suited for in-home seizure monitoring that would be required for SUDEP prevention. The electroencephalogram (EEG) is the gold-standard method for seizure detection and measures the electrical activity of the brain. However, EEG electrodes are not suitable for routine home use since they are uncomfortable, and it is potentially harmful to have them attached to the scalp for a long period of time. Another approach is to indirectly detect seizures by monitoring a subject's heart rate with electrocardiography (ECG) [35]. Because the heart rate usually increases during an epileptic seizure, ECG is used as indicator of seizures in newborns and with implanted devices like the vagal nerve stimulator [35]. As with the EEG though, it is very difficult for a patient to wear the ECG electrodes for a long period of time.

Recently, non-electrode based wearable devices have been introduced to detect convulsive seizures. Most of the technologies rely on sensors attached to the body to detect body movements and/or heartbeat, such as micro-electromechanical sensors or pulse oximeters [34]. These sensors are typically coupled to a wireless communication channel to transmit the signal for processing. Although such wearable

sensor devices are small, the body contact needed for these devices may bother a patient during sleep or patients may not remember to wear the devices.

2.4 Type of Epileptic seizures

Epileptic seizures can be classified based on the area of the brain that involved in such a seizure into partial seizures and generalized seizures. In the partial seizures, the activity can occur in a certain area of one side of the brain, then it may transfer to another area or it could stay in the same area. Two main types of partial seizures can be observed: simple partial seizures, and complex partial seizures (see Figure 4). For the people who have a simple partial seizure, although they can be awake during the seizures, they are unable to move or speak. Complex partial seizures can affect a greater area of the brain compared with simple partial seizures, and they effect the consciousness. The other type of the epileptic seizures is the generalized seizures which involve both sides of the brain. It can be classified into absence; atonic; tonic clonic; and myoclonic. In this research study we detect convulsive movements similar to generalized tonic clonic or the compulsive seizures during sleep. This type of seizures can cause injures or even unexpected sudden death [51].

2.5 The Relation Between Epileptic Seizure And Sleep Stages

According to many studies, the relationship between sleep and epilepsy has been known since the ancient Greek times [52], [53], [54]. This relationship is based on two major factors: the epilepsy syndrome and the stage of sleep. Sleep is broadly divided into three stages - wake, Non-Rapid Eye Movement (NREM) stage, and Rapid Eye Movement (REM) stage. NREM sleep has been linked to strengthening of the connection between brain cells while the REM stage has been linked to dreams. According to the American Academy of Sleep Medicine (AASM), the NREM stage may be divided into

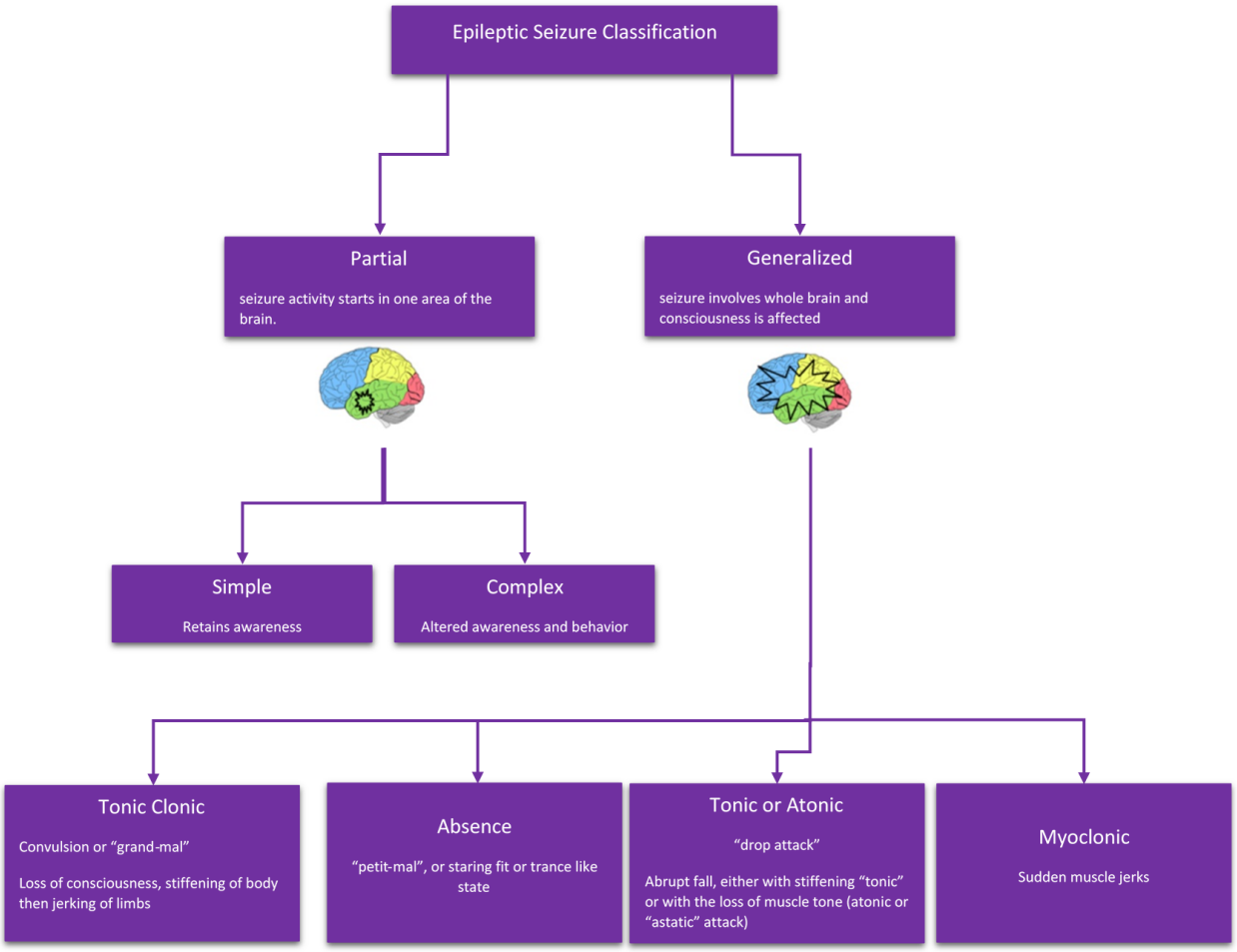

Figure 4: A block diagram of epileptic seizure classification, that consists the partial seizure which starts at a specific area in the brain, and the convulsive seizure that may involve the whole brain.

three stages. The first two stages are known as light sleep while the third stage is known as deep sleep, or Slow-Wave Sleep (SWS) [55]. Stage one of the NREM sleep lasts for approximately 10 minutes during which muscles are relaxed, whereas, in stage two, breathing and the heart rate are observed to slow

down. This stage lasts around 20 minutes and it has been observed that patients with epilepsy experience seizures during this sleep stage which is characterized by sudden and unusual movements of arms and legs, screams, and jerky movements. Such seizures may lead to injuries, including concussions, broken bones, or even Sudden Unexpected Death in Epilepsy (SUDEP) if the patients are not attended to in a timely manner [56], [53], [55]. It is therefore important to reliably detect the occurrence of seizures during sleep. This motivated our search for affordable, low-power, contact-free solutions to this problem. This led us to the investigation of pyroelectric IR sensors for epilepsy detection based on our prior knowledge of the effectiveness of pyroelectric IR sensors in motion detection applications. Detection of an epileptic seizure during sleep may be used to issue alerts to caregivers to provide timely help to the patients. The contact-free nature of the pyroelectric IR sensors and their ability to detect seizures even in the dark make them attractive for patient use. We note that while a sleep stage can trigger the epilepsy, which is noticeable in some epilepsy syndrome cases like Rolandic seizures, epilepsy may in turn disorganize and confuse sleep during epileptic seizures [57].

2.6 An overview of Respiratory Rate (RR) and Heart Rate (HR) measurements

Breathing and pulse rates are vital signs that are routinely measured by healthcare providers to assess a human body's basic functions and diagnose diseases. The Respiratory Rate (RR) and Heart Rate (HR), alongside with blood pressure and body temperature are the vital signs which are indicators of the human body's most basic functions [58]. The leading cause of death among males and females in United States is heart disease. According to the Centers for Disease Control and Prevention (CDC), about 6.5 million in the United States have a heart failure every year, and a heart failure was a contributing of one in 8 deaths in 2017 [59]. Continuous monitoring and accurate measurement of the HR and RR is

important in monitoring patients with Cardiovascular Diseases (CVDs). The HR is the number of times that the heart beats in one minute for a subject, and the heartbeat pulses can be sensed from any artery close to the skin. The respiration rate is the number of breaths per minute, and it can provide an early warning of disease or a health status deterioration [60]. The normal respiratory rate range for adults is between 12 to 20 breaths per minute [61]. The respiration process is related functionally with the brain, lungs, respiratory muscles, and blood vessels [62]. A large number of clinical situations can affect the respiration rate such as: heart failure, asthma, COPD, sleep apnea, diabetes, pain, and lately the acute respiration due to COVID- 19 disease [63], [64], [65]. Therefore, continuous monitoring of respiration rate is a useful and important tool to trigger an early warning of the patient's condition in hospitals and during in-home health care services [66–72]. The respiration rate can roughly be assessed by humans using visual and palpation methods but these are prone to errors. Many healthcare scenarios point to the need for a reliable automated system for continuous monitoring of respiration rate without requiring measurements by a human observer, usually a caregiver. For example, conditions like arrhythmia and mental stress alter the respiration rate significantly. These factors can also significantly affect the sleep quality of a subject. Obesity and aging have been observed to result in the sleep apnea syndrome (SAS). A cause of SAS is the deposition of fat in neck causing obstruction in air flow leading to reduced levels of alertness during daytime. Hence, a device for monitoring respiratory rate through the night would be valuable. Several systems have been proposed for monitoring the heart rate and respiratory rate. Based on how the heart rate and respiratory rate are measured, these systems are classified into contact-based systems and contact-free systems [69, 70, 73–75]. In contact-based systems the measurements devices used in monitoring the HR and RR are in direct contact with the subject's body, while in the

contact-free systems, the devices measure the HR and RR without touching the subject's body. One of the advantages of the contact-free systems over the contact-based systems is the comfort of the subjects during the monitoring, especially if the subjects need to be monitored for a long period of time such as during sleep. The traditional contact-based methods to measure the HR rely on different type of sensors and electronic devices such as oximeter sensor [76], [77], electrocardiogram (ECG) [78], smart watches, and wrist bands that need skin contact to measure the heart rate [79], [80]. These traditional methods can cause discomfort and inconvenience to the subjects. They may also cause damage to the skin, especially for the infants and the elderly whose skin is fragile. Interest is growing towards using contact-free methods to measure the HR. Many potential applications use commercial cameras to estimate the heart rate by capturing the skin color change due to the cardiac pulse [81], [82], [83]. Although contact-free methods are successful in estimating the heart rate from the captured video of the stationary subjects, the variation of the illumination factor can affect the performance and the outcomes of camera-based methods. This is because the strength of the cardiac pulse is small compared to the varying illumination factor [84]. Active sensing using Microwave beams is used in estimating the heart rate and measure the human subjects breathing [85]. In addition to that, the Fiber Optic Respiratory Plethysmograph (FORP) is used for respiratory monitoring [86]. Although these approaches can estimate the HR and RR, but they need specialized hardware and have other shortcomings including cost.

Another approach uses Radio Frequency (RF) wireless signal for emotion recognition by estimating the HR of the human subjects [87]. An infrared sensor is also used to estimate the heart rate and respiratory rate by monitoring the chest movements of the subjects [87]. One way to monitor the respiratory rate using contact-based devices is to measure the sound of respiration using a microphone that is

placed over the throat or mounted on the neck. In combination with microphone, a frequency analysis is applied to detect the variation of the sound. This method can be affected by speech or coughing of the subjects during the monitoring process [88]. Nasal pressure transducer sensor is another contact-based instrument to measure the respiratory rate. It detects the variation of the temperature between the inhaled and exhaled air. The detected variation is related to the respiratory rate. The airflow measurements can be done using this sensor via facemask or nasal cannula [89]. The limitation of this method is that the subjects may not feel comfortable with this type of sensor [90]. Impedance pneumography is another tool that is used to monitor the respiratory rate by measuring the change in thoracic impedance due to the abdominal chest wall movements during inhalation and exhalation. One of the limitations of this method is the patient's other movements that can cause inaccurate measurement of the respiratory rate. In addition, any obstruction of the air flow can cause inaccurate measurement because the chest wall will continue to move as a patient's tries to breathe [91]. The respiratory rate can be extracted from the Electrocardiogram (ECG) signal by measuring the fluctuation of the ECG signal. This technique is known as the ECG-Derived Respiration (EDR). Since the ECG electrodes has a direct contact with the subject's skin, the subjects may have some skin damages especially for long-term respiration monitoring [92]. Respiratory rate is measured using a pulseoximeter where a frequency spectral estimation method or a Continuous Wavelet Transform (CWT) is applied on the pulseoximeter waveform [93]. Plethysmogram is used to estimate the respiration by measuring the blood oxygen saturation (SpO2). Wavelet transform is used to process the plethysmogram signal to extract the respiratory rate [94], [95]. Radar-based monitoring, Fiber Grating (FG) vision sensor, video cameras, and passive infrared sensor are used as contact-free monitoring instruments to estimate the respiratory rate. Greneker [96] devel-

oped a Radar Vital Signs Monitoring (RVSM) method to estimate the respiratory rate by monitoring the chest movements using the Doppler phenomenon. This system is an early contact-free system to estimate the respiratory rate. Motion artifacts are considered as a limitation of this system because it can degrade the breathing signal. Aoki et al. [97] developed a respiratory rate monitoring system that uses a combination of viper grating projection with a Charge-Coupled Device (CCD) camera and an optical filter. The bright spots on the captured images were extracted and processed to estimate the respiratory rate. A webcam video camera is also used to estimate the respiratory rate by monitoring the chest and abdominal movements of children [98]. Regular and infrared camera-based monitoring systems violate the privacy of the subject and cannot be used at night during sleep. Infrared sensors have been proposed for HR estimation by us and other researchers [99], [100], [101]. A combination of Passive Infrared (PIR) sensor and a vibration sensor are used to estimate the respiratory rate from the chest wall movements of subjects during sleep. The empirical mode decomposition and a wavelet transform are used to extract the respiratory rate from the captured sensors signals [99]. Recently, a low-resolution thermopile array is used to monitor the flow of respiration for various observation settings from 20 cm [101].

CHAPTER 3

CONVULSIVE MOVEMENT DETECTION USING PASSIVE INFRARED PIR SENSOR

In this chapter we investigate the use of Passive InfraRed (PIR) sensor for convulsive movement detection based on our prior knowledge of the effectiveness of PIR sensors in motion detection applications. The PIR sensors can detect human body motion caused by epileptic seizures during sleep which makes the body shake and causes the PIR sensor to generate an oscillatory output signal. We distinguish this signal from that of ordinary motions during sleep by using analysis with different machine learning and deep learning algorithms. We classify the data set of the PIR sensor output into three classes: the occurrence of convulsive movements, ordinary motion, or absence of motion. We test the method on the PIR signals captured at 1 m from 33 healthy recruited subjects who, after watching seizure videos, either moved their body on a bed to simulate a seizure, ordinary motion, or lay still. Detection of an epileptic seizure during sleep may be used to issue alerts to caregivers to provide timely help to the patients. The contact-free nature of the PIR sensors and its ability to detect seizures even in the dark make them attractive for patient use.

3.1 Contribution

The contributions of this chapter can be summarized as follows:

1. We propose a novel approach to detect the convulsive seizures during sleep using low-cost, low-resolution, non-intrusive and contact-free PIR sensor.
2. For this study we received an Institutional Review Board (IRB) approval to examine the use of our sensing method on healthy recruited subjects for the purpose of carrying out a preliminary study using data from simulated motions of seizure.
3. Our approach is applied on 33 healthy recruited subjects (27 males and 6 female).
4. A supervised hidden Markov model algorithm (HMM) and a 1-D and 2-D convolutional neural network (ConvNet) are used to classify the data set of the PIR sensor output into the occurrence of epileptic seizures, ordinary motions, or absence of motion.
5. Our approach is reliable since all simulated seizures were successfully detected, with errors occurring only in distinguishing between ordinary motion and no motion.
6. Our approach is demonstrates the potential for using PIR sensors in the epileptic seizure detection.

The rest of this chapter is organized as follows. Section 3.2. presents the proposed method. Classification and feature extraction using deep learning networks are explained in Section 3.3. The performance metrics of the classification methods are described in Section 3.4. Finally, Section 3.5 discusses the performance results of the proposed method.

3.2 Proposed System Design

PIR sensors are low-cost devices which can be used in affordable detection systems. They consume very little power and they can be efficiently used to detect body motion based on the infrared energy emitted by the human body. Unlike camera-based detection systems, invasion of privacy is not a concern

with the use of PIR sensors. In contrast to visible-light devices, PIR sensors can also work in the dark [102], [103], [104], [105]. A pyro-electric infrared PIR sensor measures the change of infrared radiation (not the averaging of IR) emitted by moving objects within its range of view, and generate an electric potential corresponding to the rate of change of the detected infrared radiation. The electric potential generated by the PIR sensor is so small. Therefore, the PIR sensor cannot be used alone. To make the PIR sensor more powerful. We use a sensing unit (SU) instead of a standalone PIR sensor.

3.2.1 The Sensing Unit (SU)

The SU consists of an array of Fresnel lenses, an IR filter, and a PIR sensing element which consists of three pins (GND, V_{cc} and binary output), analog circuitry, and a microcontroller (Arduino Nano) as shown in (Figure 5).

3.2.2 Infrared (IR) Radiation

Infrared (IR) radiation is an electromagnetic radiation with a wavelength of 750nm to $100\mu m$. Its wavelength is longer than the visible light, therefore the human's eyes cannot detect the IR radiations but we can sense it as a heat. The IR can be classified into sub-bands based on its wavelength (see Figure 6). At normal body-temperature, the human radiates an IR roughly at a wavelength approximately equal to $10\mu m$.

3.2.3 Fresnel Lenses

Fresnel lenses are plano-convex lenses that permit the IR radiation to penetrate them. Basically, Fresnel lenses work as an antenna by increasing the range of captured IR and projecting it onto the sensing plates of the PIR sensor. Since the amplitude of the IR radiation decreases with distance, Fresnel lenses are also used to expand the range of the detecting distance for the PIR sensor.

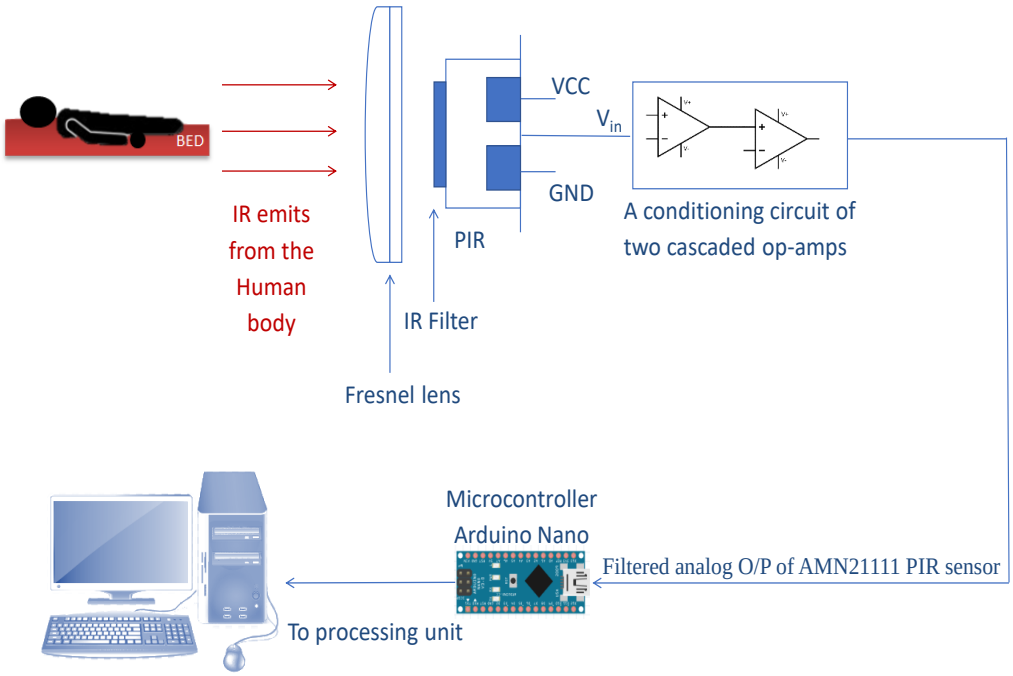

Figure 5: Sensing Unit (SU) in the proposed method that consists an array of Fresnel lenses, an IR filter, and PIR sensing elements.

3.2.4 PIR Sensor

A PIR sensor is made of two sensitive plates that can sense IR radiation, and the output of the sensor is proportional to the difference in the IR radiation impinging on the two plates. When there is no motion, a zero-output signal is generated because each plate detects the same amount of IR radiation. In contrast to that, a moving body causes a differential change in one plate when it moves in the sensing area. Most of the commercially available PIR sensors that are used for motion detection have a binary output [103], [105].

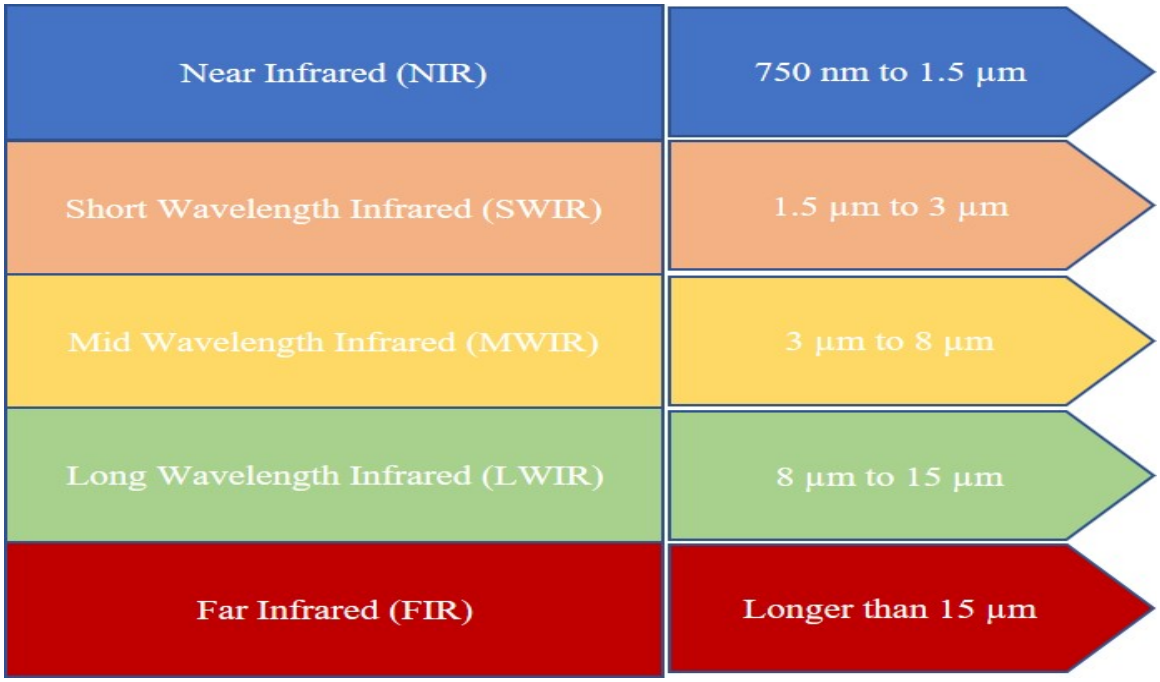

Figure 6: IR radiation sub-bands, the PIR detects the long wavelength infrared that is not visible to the humans eyes.

3.2.5 Analog Circuit

The analog circuit of the SU is used to generate an analog output of the PIR sensor instead of the digital output. The maximum amplitude voltage of the PIR sensor is 3.3v and, therefore, voltage divider resistors are used to prevent any clipping in the amplitude of the analog output signal. The PIR signal is a low-amplitude signal and its frequency is less than 5 Hz [102], [106]. Epileptic seizures are characterized by rhythmic jerks of the body, and the average jerking rate in a seizure is about 2 jerks/second, and this can be captured in the signal acquired with a PIR sensor. Two operational amplifiers (op-amps), OA1 and OA2 (see Figure 7) are used as a cascaded stage in order to increase the amplitude of the PIR

signal and bring it to a readable level. The two successive op-amps are also used to filter the signal from the unwanted noise. To filter noise from the signal, R_2, C_1 and R_5, C_4 at each stage act as a low pass filter with cut-off frequency equal to 1.6 Hz (see Equation 3.1 and 3.2). Because PIR sensors are intended to detect the human body motion with a frequency content less than 3 Hz, there is, therefore, no need to deal with high frequencies. R_4, C_3 and R_3, C_2 at each stage are used as a high pass filter to suppress the DC bias of the signal (see Equation 3.3 and 3.4).

$$f_{cutoff_1} = \frac{1}{2\pi R_2 C_1}, \tag{3.1}$$

$$f_{cutoff_2} = \frac{1}{2\pi R_5 C_4}, \tag{3.2}$$

$$f_{low_1} = \frac{1}{2\pi R_4 C_3}, \tag{3.3}$$

and

$$f_{low_2} = \frac{1}{2\pi R_3 C_2} \tag{3.4}$$

The gain for each stage is approximately equal to 100 (see Equation 3.5 and 3.6) which gives a total gain approximately equal to 10,000.

$$Gain_{OA1} = 1 + \frac{R_2}{R_4}, \tag{3.5}$$

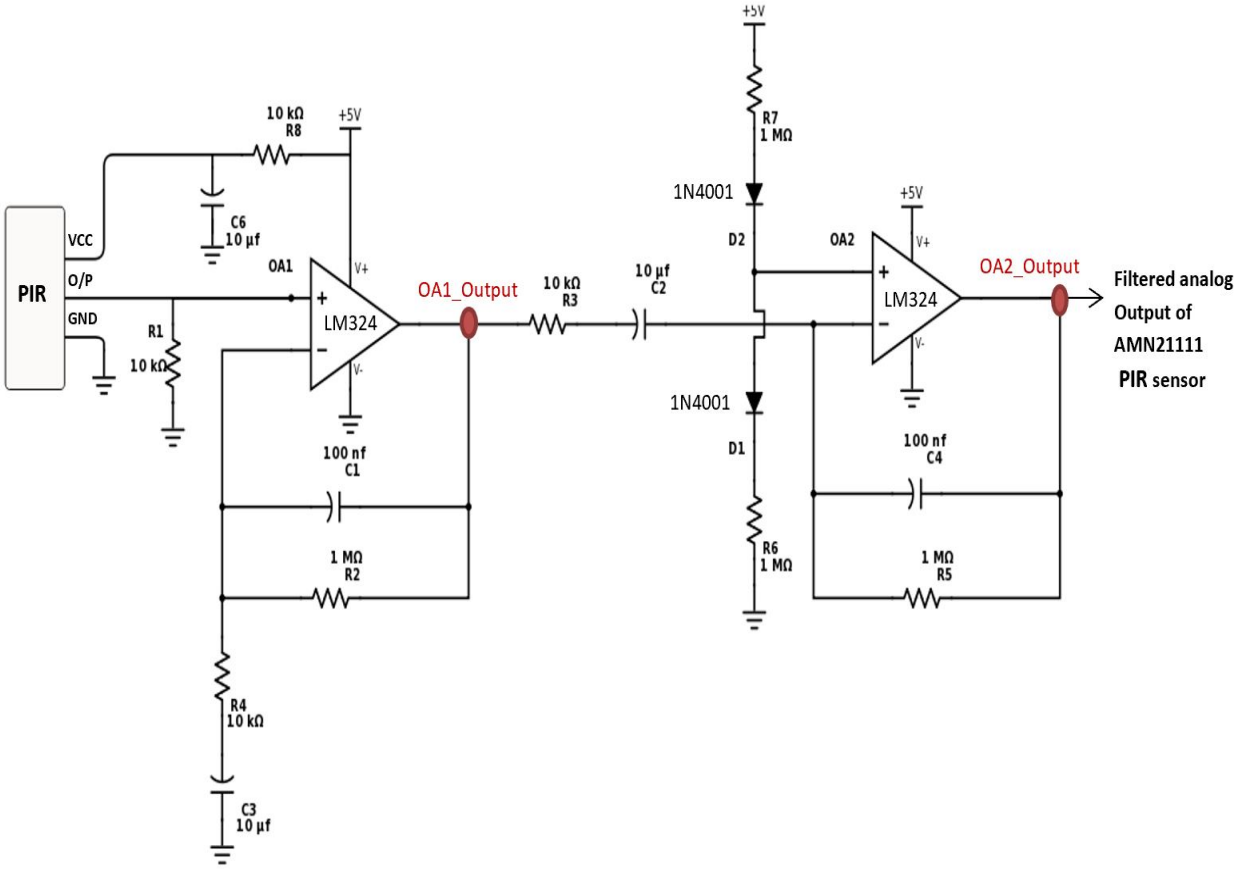

Figure 7: A conditioning circuit of two cascaded op-amps to filter the analog input of the PIR sensor. The output of the second amplifier OA2_Output is the filtered analog output of the Panasonic AMN21111 PIR sensor.

and

$$Gain_{OA2} = 1 + \frac{R_5}{R_3} \tag{3.6}$$

The output of OA2 is the filtered analog output signal of the PIR sensor. The filtered analog output is sampled and quantized with an Arduino nano microcontroller in order to be sent to the processing unit for classification. The sampling frequency used is 20 Hz with 10 bit quantization level.

The output signal of the PIR sensor contains a bias that can change with the room temperature. To remove this bias, the PIR sensor signal x[n] is convolved with a high-pass filter (HPF) with transfer function:

$$H(z) = h[0] + \sum_{n=1}^{10} h[n]\left(z^{-n} + z^{n}\right) \tag{3.7}$$

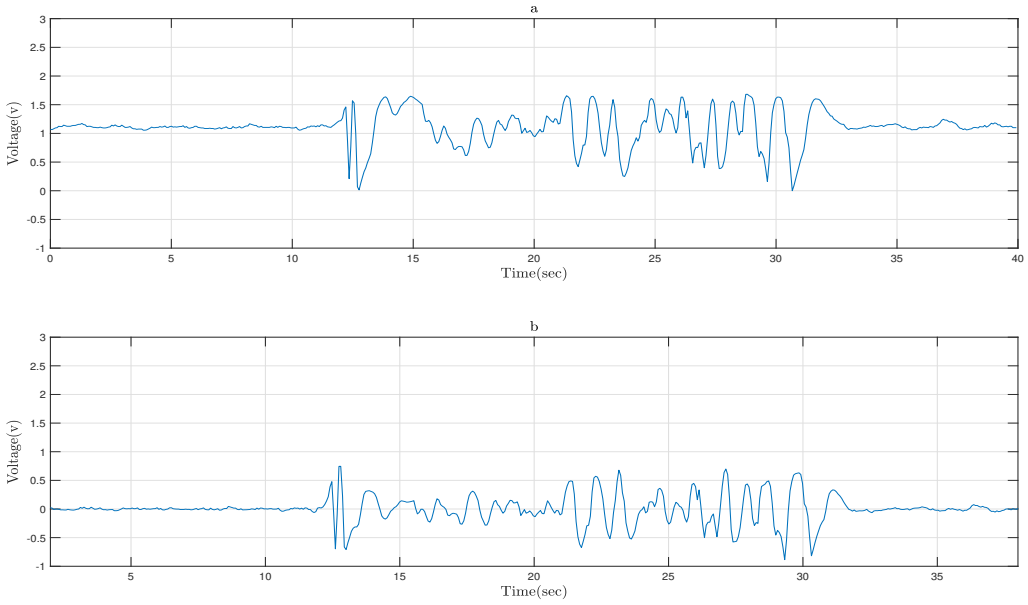

Figure 8: a) PIR sensor signal corresponding to an epileptic seizure case, and b) its high-pass filtered version.

The high-pass filter is designed using a minimax magnitude criterion, with a normalized angular passband edge frequency of 0.1π and stopband edge frequency of 0.05π. Figure 8 shows a filtered PIR signal. The output $y[n]$ is obtained using convolution, $y[n] = x[n] * h[n]$.

3.3 Feature Extraction and Classification

In order to design and build a precise model that can deal with a large amount of complex data and give accurate outcomes, many machine learning and deep learning algorithms are being used for the task of classification. In this study three different algorithms are used to extract features and classify the data captured from the PIR sensor, a) a Hidden Markov Model, b) a 1-D ConvNet, and c) a 2-D ConvNet and they are compared to each other.

3.3.1 Supervised Hidden Markov Model (HMM):

A supervised Hidden Markov Model is used to classify epileptic seizures and absence of epileptic seizures during a subject's sleep. In our study, we considered the normal movement during sleep and no movement during sleep as absence of epileptic seizure. Figure 9 shows three HMMs corresponding to three classes: Model E corresponds to the occurrence of epileptic seizures, model M corresponds to the normal movement of the subjects during sleep, and finally, model N corresponds to no-movement case during deep sleep.

We design three Markov models corresponding to epileptic seizures, normal movement during sleep, and no-movement during deep sleep from our training data [107]. The filtered PIR signal $y[n]$ is quantized into three levels using a threshold value of Th which is used to define the observation symbols, states and the corresponding transition probabilities for each model. An estimated threshold $Th = 0.05v$ is used in our method. We have three states S_0, S_1 and S_2 and three observation symbols O_0, O_1 and O_2 in the three Markov models. The output $y[n]$ of the high-pass is quantized into three levels. The symbol O_0 represents the data when $y[n]$ is within the interval $[-Th, Th]$. O_1 represents the data when $y[n]$ is

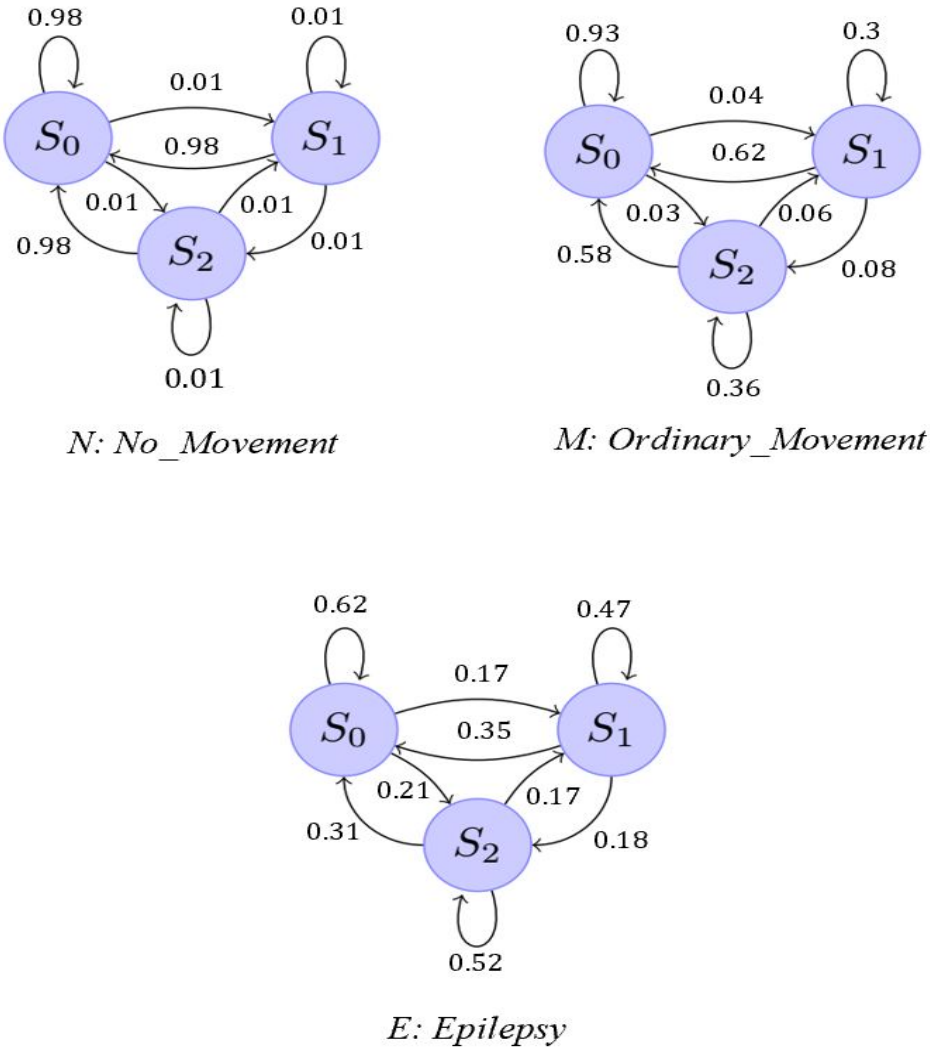

Figure 9: Three HMM chains with three classes, No-movement (N), Movement (M), and Epileptic seizures (E).

above the threshold Th, while O_2 represents the data when $y[n]$ is below $-Th$. In HMM framework, we cannot exactly know how the Baum-Welch training algorithm assigns the states [107]. Ideally, state S_0 may correspond to the case of $y[n]$ being in the interval $[-Th, Th]$. State S_1 may represent the data when $y[n]$ is above the threshold Th, while state S_2 may represent the data when $y[n]$ is below $-Th$. The states are hidden from us. Hence the designation Hidden Markov Model. We estimate the transition probabilities from our training data. Each model has different state transition probabilities estimated by the Baum-Welch training algorithm [107]. The probability of observing a sequence of symbols $O = \{o_1, \cdots, o_n\}$ given a state sequence $W = \{w_1, \cdots, w_n\}$ and the Markov model (No-Movement) is expressed as follows:

$$P(O \mid N) = \pi(w_1) P(O_1 \mid w_1) \prod_{t=2}^{n} P_r(t), \tag{3.8}$$

where

$$P_r(t) = A_{ij} B_{jk} = P(w_t \mid w_{t-1}) P(o_t \mid w_t), \tag{3.9}$$

where π is the initial probability of starting with state w_1, n is the number of states in S, o_t represents the observed symbol at time t, A_{ij} is the state transition probability, $A_{ij} = p(w_t = S_j \mid w_{t-1} = S_i)$ and B_{jk} is probability of observing the k^{th} symbol o_k at the state $w_t = S_j$, $B_{jk} = P(o_k \mid w_t = S_j)$.

Similarly, we calculate

$$P(O \mid M) = \pi(w_1)P(O_1 \mid w_1)\prod_{t=2}^{n} P_r(t), \tag{3.10}$$

and

$$P(O \mid E) = \pi(w_1)P(O_1 \mid w_1)\prod_{t=2}^{n} P_r(t), \tag{3.11}$$

which represent the probabilities of movement and epilepsy classes, respectively. Finally, the classification decision is made based on the most probable class. Fast algorithms for computing the probabilities in (3.8), (3.10), and (3.11) are described in [107].

Each Markov model has different transition probability values because when there is no seizure the signal stays mostly within the threshold interval $[-Th, Th]$. Therefore, the model N has very high probability $p(S_0 \mid S_0)$ compared to other models. When there is an epileptic seizure, the signal oscillates between states frequently due to rhythmic jerks. Therefore, the state transition probabilities $p(S_i \mid S_j)$ $(i \neq j)$ of the model E is higher than those of the other models. In the "Ordinary_Movement" Markov model, the state transition probabilities of moving back to the resting state (S_0), $p(S_0 \mid S_1)$ and $p(S_0 \mid S_2)$, are higher than other state transition probabilities, because the subject goes back to static state after body movements or a turning up to the left or to the right.

3.3.2 1-D ConvNet

Deep learning techniques are modeled to mimic the human brain ability to make an accurate decision for different complex problems [108]. A ConvNet is a discriminative deep learning model that is used to extract and classify features based on a combination of non-linear transformation operations and linear

filters [108], [109]. The main building blocks of the 1-D ConvNet are convolution, activation function, and pooling [110]. The input to the 1-D ConvNet is a set of 396 time series vectors of PIR data collected from 33 subjects, as described below. The size of each vector is ($1\times$ 764), where 764 represents the number of feature samples in each vector. The feature detector size is equal to ($64\times$ 1) with a depth of 32 filters. To add a non-linearity to the ConvNet, an activation function must be applied after the convolution.

In this system, a Rectified Linear Unit (RELU) function is applied to the convolution layer. A max pooling or down sampling filter of size ($1\times$ 701) (as shown in equation 12) is used to reduce the activation map dimensions, the network computations, and the number of parameters. The output of the max pooling layer, which represents the high-level extracted features of the input, is flattened and fed into a fully connected layer. A fully connected layer used in this system is a Neural Network (NN) of 300 hidden layers and three outputs. Finally, to prevent over-fitting, a dropout of 0.2 is applied to the output of the 1D-ConvNet. The softmax function is used to squash the output vector to ensure that the sum of the output probability is equal to one. Generally, the 1D-convolution and the max pooling layers are used to extract features from the input while the fully connected layer classifies the extracted features.

Figure 10 shows the 1D-ConvNet design that is used to classify the captured data signal via PIR. The size of activation map filter and the output of the max pooling layer depends on the size of the feature detector and the max pooling filter, the stride and the zero padding as shown in equation 3.12.

$$Filter\_Size = \left(\frac{W - F + 2P_d}{S_t}\right) + 1 \tag{3.12}$$

where W in this equation represents the height or width of the input image, F represents the size of the feature detector filter. P_d refers to the number of zeros padded and S_t is equal to the number of samples that the feature detector slides during the convolution operation.

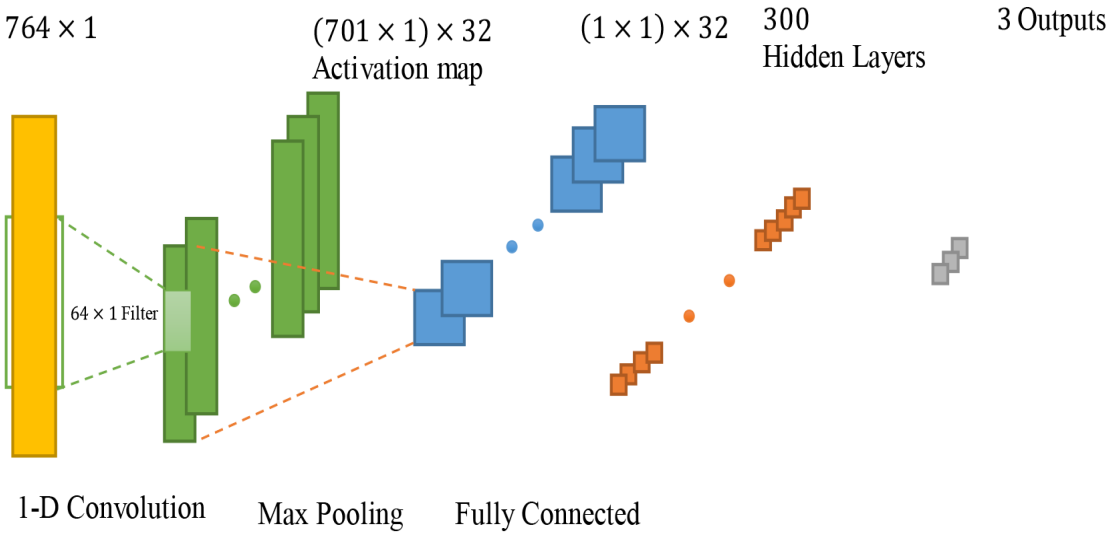

Figure 10: The structure of 1D-ConvNet with max pooling layers, fully connected layer, and three outputs is used to classify the captured real-time series data using PIR sensor.

3.3.3 2-D ConvNet

The 2-D ConvNet layer consists of two convolutional layers, two max pooling layers and a fully connected layer. The data captured by the SU system are converted into spectrogram images, prepro-cessed, reshaped into (64 × 64) arrays with three input channels (RGB) and fed to the ConvNet. The

input image matrices are convolved with a feature detector of size (3×3). An activation map of size ($62 \times 62 \times 32$) is produced. A down-sampling filter of size (2×2) is applied to reduce the size of the activation map.

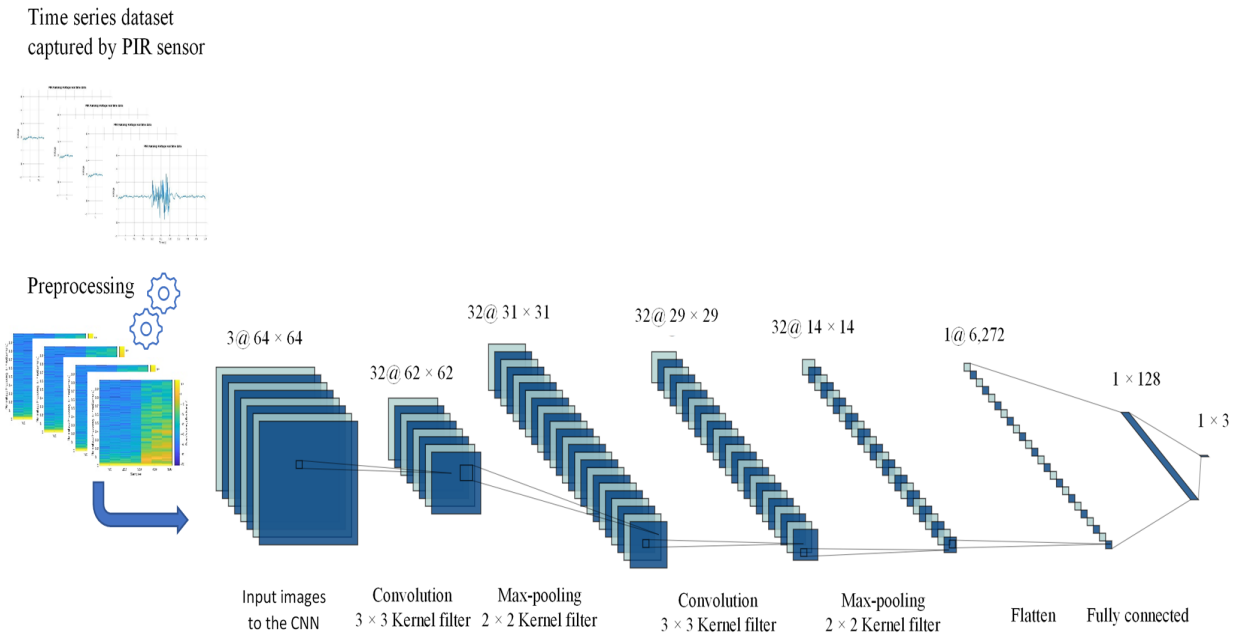

Figure 11: 2D-ConvNet deep learning structure with two convolution layers and two max pooling layers that used to classify the spectogram images of the collected data.

While there is loss of information due to down-sampling, the down-sampling or max pooling process reduces the number of calculations required for the next layers. The size of the filter after the first max pooling is ($31 \times 31 \times 32$) , this filter is convolved with a feature detector of size (3×3) and down-sampled with a (2×2) filter before it flattened and fully connected to 128 hidden layers. The output

of this network maps to to one of three different classes. Figure 11 shows the structural layers of the proposed 2d ConvNet.

3.3.4 Captured DataSet

The sensor signal of our proposed SU system are sampled at 20 Hz frequency with 10-bit quantization. A total of 396 records (132 record for each class) are fed to the 1-D ConvNet. In order to measure the accuracy of our system and compare it with the activation accuracy of 1-D ConvNet, the data are mapped into spectrogram images and fed into a 2-D ConvNet. Figure 12 shows the signal corresponding to normal movements of the SU system. Figure 13 shows the PIR signal during epileptic seizure. For HMM, the observation data sets are partitioned into an observation data set for each class. The data set per each class are trained individually. The max loglikelihood of each test set data per class is computed to classify each observed window. Figure 14 shows the spectrogram images for the cases of no motion, normal movement, and epileptic seizure.

3.4 Evaluation Metric of the SU System

In many classification problems, one of the most important steps to get an optimum classifier is the selection of metrics. Confusion matrix is a measurement metric, it is an array of size n$\times$n (true labels $\times$ predicted labels), where n is equal to the number of different classes [111], [112]. For a binary classifier (n=2), if the actual and predicted values are true, the class cell refers to true positive (TP). If both are false, then the class cell refers to true negative (TN). The confusion matrix gives a false positive (FP) when the actual value is false and predicted value is true. If the opposite happens, the class cell refers to false negative (FN). The related metric parameters can be represented mathematically as:

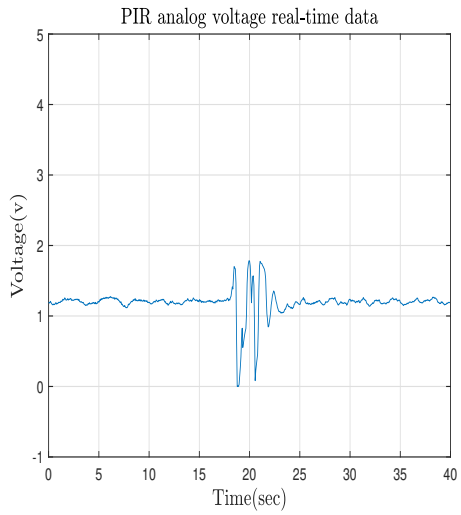

Figure 12: The PIR signal due to normal movements selected from one of the 33 subjects, the session period is 40 second.

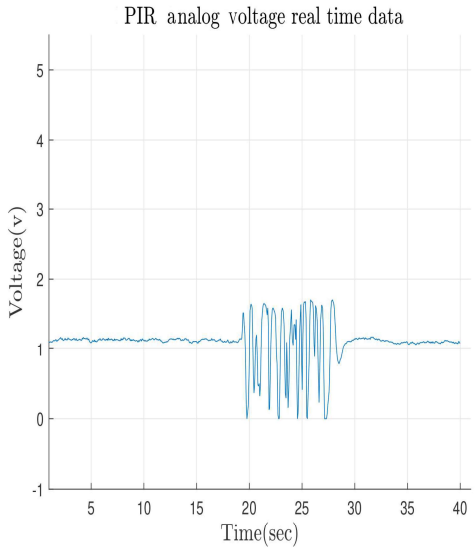

Figure 13: The PIR signal due to epileptic seizure selected from one of the 33 subjects, the session period is 40 second.

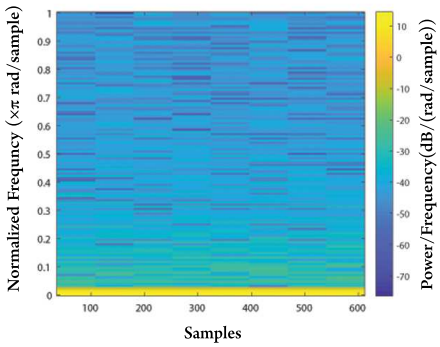

(a)

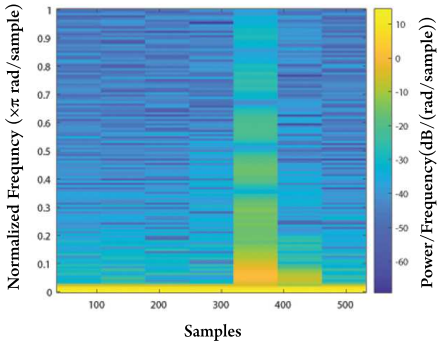

(b)

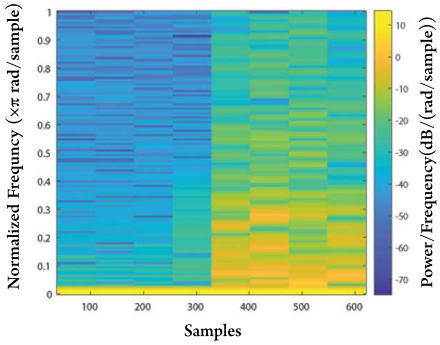

(c)

Figure 14: Spectogram image of captured PIR signal for a) no motion, b) a normal movement, C) an Epileptic seizure, all the three images which selected randomly are belong to one of 33 subjects.

$$P_R = \frac{TP}{TP+FP}, \tag{3.13}$$

$$R_C = \frac{TP}{TP+FN}, \tag{3.14}$$

$$F1\_Score = 2 \times \frac{P_R \times R_C}{P_R + R_C}, \tag{3.15}$$

$$A_{CC} = \frac{TP+TN}{TP+FP+TN+FN}, \tag{3.16}$$

where P_R (Precision) is the ratio of correctly detected epileptic seizures to the total detected seizures, R_c (Recall or sensitivity) is the ratio of correctly detected epileptic seizures to all the class observations, $F1\_Score$ is harmonic mean of precision and sensitivity, and A_{cc} (Accuracy) is the probability of the model's correct predictions [112]. Since we have three classes in our work (Epileptic seizures, Normal-movement and No-movement), a confusion matrix of size 3×3 was used as shown in Figure 15. The measurements of sensitivity and precision metrics for a certain class such as epileptic seizure class can be represented mathematically as follows:

$$Sensitivity_{Epilepsy} = \frac{C_{Epilepsy,Epilepsy}}{\sum_n T_{Epilepsy}}, \tag{3.17}$$

$$Precision_{Epilepsy} = \frac{C_{Epilepsy,Epilepsy}}{\sum_n P_{Epilepsy}}, \tag{3.18}$$

where $C_{Epilepsy,Epilepsy}$ is the confusion matrix element that represents the intersection of true label and predicted label of epileptic seizures class, $T_{Epilepsy}$ is the row elements of epileptic seizures class, $P_{Epilepsy}$ is the column elements of epileptic seizures class. The evaluation metrics for other classes are defined in a similar way [112].

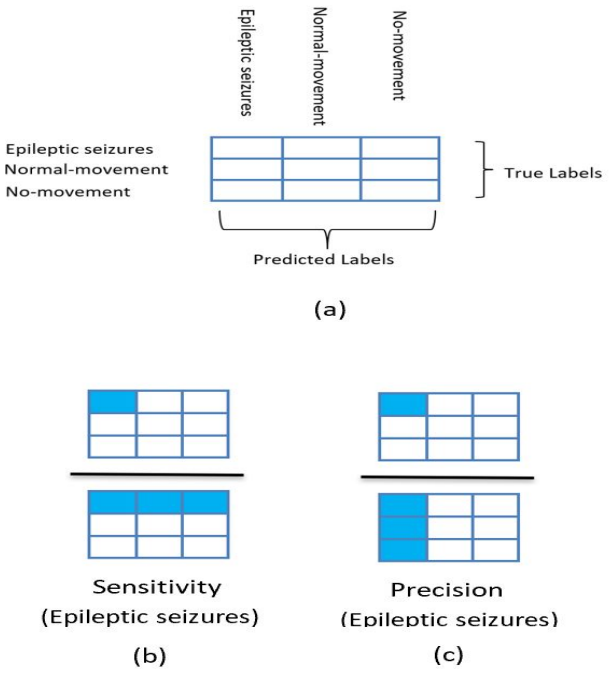

Figure 15: a) Confusion matrix, (b) sensitivity measurement of the epileptic seizures class, and (c) precision measurement of the epileptic seizures class.

3.5 Results and Discussion

For this study we received an Institutional Review Board (IRB) approval to examine the use of our sensing method on healthy recruited subjects for the purpose of carrying out a preliminary study using data from simulated motions of seizure. This will enable us to establish an early proof of concept for epileptic seizure detection using PIR sensors. For access to patients experiencing real seizures, we are waiting for IRB approval in collaboration with physicians studying epilepsy patients. We recruited 27 male and 6 female healthy subjects for this study.

The subjects were asked to perform a set of activities following procedure that consists of 12 sessions of activities where each session lasts 40 seconds. Half of the sessions (6) are done in a lit room while the other half are done in a dark room.

Before the start of the procedure, the subjects were asked to watch a YouTube video of a patient experiencing a compulsive epileptic seizure. In each session, each subject was asked to lie down on a couch and perform a set of activities consisting of 1) pretending to sleep without moving; 2) mimicking motions of an epileptic seizure while pretending to be a sleep; 3) moving the body to change position during sleep to mimic normal occasional body movement. The data are collected through the SU system that we designed and transmitted to a dedicated PC. The PIR sensor is the central unit of the SU system and it works based on the IR energy received from the subject. There was no contact between the sensor and the subjects through the entire procedure.

To process and classify the captured data set, we initially examined the use of the signal frequency content for classification. Since the epileptic seizure class has the highest frequency content among the three classes (epileptic seizure, movement, and no movement), we computed the Discrete Fourier

Transform (DFT) of the signal and defined features based on the fraction of the signal frequency content energy in suitably defined bands. We investigated features with different choices of frequency band boundaries and among these we chose the features that yielded the highest accuracy which was equal to 84.6%. The count of false positives was high, and we sought to improve the classification performance. Therefore, we examined the use of machine learning algorithms in order to enhance recognition accuracy.

A HMM algorithm was used to classify the collected data sets. As described before, three Markov models (epilepsy, ordinary movement and no-movement) were trained individually. The maximum log-likelihood of each test data set per class was measured to classify each suitable selected window of observation. The validation accuracy using HMM is 97.032%. In addition to that, two deep learning classification methods were used to classify the captured data. For the 1-D ConvNet, the data set are converted into 396 records. These records are split into 297 training records and 99 testing records (i.e. 75% training set and 25% test set). The data are fed into a multi-layer network that consists of a 1D Convolution layer, a flattening layer, and a fully connected layer (see Table I).

To prevent overfitting, a drop out of 0.2 and a softmax activation function are applied to the output [113]. All the epileptic seizure cases were correctly detected, and no false positive values appeared. On the other hand, 3 normal movement cases were misclassified as no-movement cases. Therefore, the validation accuracy of the system classification is equal to 96.97%, while the validation loss is equal to 0.06. Figure 16 shows the confusion matrix of the designed network. 1D-ConvNet successfully detected all the seizures. The precision, recall and $F1\_Score$ evaluation metrics are also calculated (see Table II).

TABLE I: THE STRUCTURAL LAYERS AND NUMBER OF PARAMETERS OF THE 1D CONVNET

Layer type	Output shape	parameters #
Conv 1d, 1 stride, 0 Padding	32 x 701 x 1	2080
RELU (Activation Function)	32 x 701 x 1	0
Max_poling, 1 stride, 0 Padding	32 x 1 x 1	0
Flatten_Hidden	32	0
Dense_Hidden	300	9900
Dropout (0.2)	300	0
Dense_Output	3	903
Softmax (Activation Function)	3	0

In the second method of data classification, the captured data was converted into spectrogram images. All the spectrogram images are reshaped into a (64×64) arrays and fed into a 2D ConvNet. The network designed consists of two convolutional layers with feature detector size (3×3) and depth 32 for each, two max pooling layers with down sampling filter of size 2×2 (2 stride and depth length 32) and a fully connected layer with 128 hidden layers and three outputs (see Table III).

Excessive training causes the classifier to memorize the input data. In order to avoid the poor performance of the classifier, a *K*-fold cross validation is applied on the input data images to estimate the generalized performance of the classifier [114]. The set of images were divided into 12-fold groups of equal size (33 records). The first fold is used as a test dataset while the remaining folds are used as

TABLE II: EVALUATION METRIC OF THE 1D CONVNET WHICH SHOWS THE VALUE OF PRECISION, AND RECALL, F1 SCORE FOR EACH OF THE THREE CLASSES: EPILEPTIC SEIZURE, NORMAL MOVEMENT, AND NO MOVEMENT

	Precision	Recall	F1-Score	Support
Class0(Epileptic Seizure)	1.00	1.00	1.00	33
Class1(Normal Movement)	1.00	0.91	0.95	33
Class2(No Movement)	0.92	1.00	0.96	33
Avg / total	0.97	0.97	0.97	99

a training dataset. The accuracy and the other performance metrics are then calculated. The procedure was repeated twelve times. The total accuracy, precision, recall and $F1\_Score$ of this network are equal to the average of the K-fold cross validation trials (see Table 3.4). The validation accuracy of the 2D-ConvNet designed is equal to 98.98%. Figure 17 shows the confusion matrix of 2D-ConvNet design. Because of the use of the K-fold, all the spectrogram input images were used as a training set and as a data set during classification.

It is observed in this study that the 2d_ConvNet gives better performance than the 1d_ConvNet, with higher accuracy and precision. However, in terms of speed HMM is the fastest machine learning algorithm (see Table VI, and Table V). The total number of parameters that are used in both networks depend on the size, the number of filters, the number of neurons that are used, and the way that they connect to the other neurons. This system is used to detect the generalized epileptic or generalized tonic-clonic seizure but not the partial seizure that happens in a certain part of the brain [115]. To use this

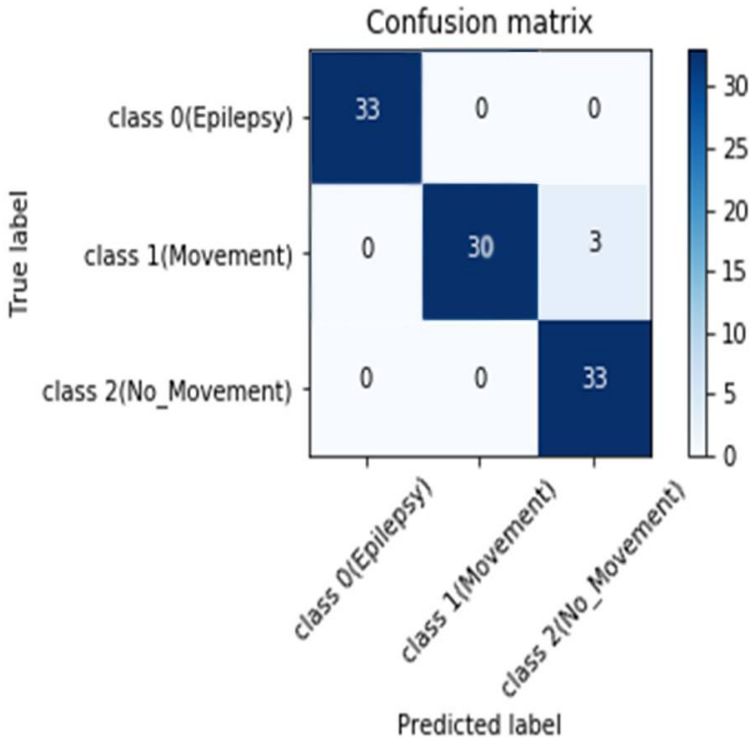

Figure 16: A 3 × 3 two-dimensional (true label vs predicted label) confusion matrix of 1D-ConvNet.

system in patient monitoring, the sensor can be connected to a wireless network to alert a first response or a caregiver.

A variety of high-level machine learning and deep learning techniques were used to classify the captured signals from the PIR sensor. All the programs were implemented using a CPU E5-1620 V3, 3.5 GHz with 8 cores, Memory size 32 GB, and an operating system Centos 6.9. A comparison between the applied algorithms was done based on the validation accuracy, implementation time (See Table V), evaluation metric, confusion matrix, and structural design. We observe that the accuracy in Table V

TABLE III: THE STRUCTURAL LAYERS AND NUMBER OF PARAMETERS OF THE 2D CONVNET THAT GIVES THE TYPE OF LAYERS USED, THE SIZE OF EACH LAYER, AND THE NUMBER OF PARAMETERS EXTRACTED FROM EACH LAYER

Layer type	Output shape	no. of parameters
Conv 2d, 1 stride, 0 Pad	32 x 62 x 62	896
RELU (Activation Function)	32 x 62 x 62	0
Max_Pooling 2d, 2 strides, 0 Pad	32 x 31 x 31	0
Conv 2d, 1 stride, 0 Padding	32 x 29 x 29	9248
RELU (Activation Function)	32 x 29 x 29	0
Max_poling 2d, 2 strides, 0 Pad	32 x 14 x 14	0
Flatten	6272	0
Dense_Hidden	128	802944
Dense_Output	3	387
Softmax (Activation Function)	3	0

is equal to 97.03% for HMM, 96.97% for 1D_ConvNet, and 98.98% for 2D_ConvNet. We compared our results with the accuracy of the other motion-based epileptic seizure detection systems (seeTable VI). We observe that our method shows significantly improved performance, while noting that it was achieved with data obtained from simulated epileptic seizures.

For real-time monitoring of a patient, the collected sensor data will be processed and classified using overlapping data segments. It is adequate to process and analyze the data segments at the rate of 15 to

TABLE IV: EVALUATION METRIC OF THE 2D CONVNET WHICH SHOWS THE VALUE OF PRECISION, AND RECALL, F1 SCORE FOR EACH OF THE THREE CLASSES: EPILEPTIC SEIZURE, NORMAL MOVEMENT, AND NO MOVEMENT

	Precision	Recall	F1-Score	Support
Class0(Epileptic Seizure)	1.00	1.00	1.00	33
Class1(Normal Movement)	1.00	0.97	0.98	33
Class2(No Movement)	0.97	1.00	0.98	33
Avg / total	0.99	0.99	0.99	99

TABLE V: VALIDATION ACCURACY AND IMPLEMENTATION TIME OF EACH CLASSIFIER, HMM, 1D, AND 2D CONVNET

Classifier	Validation accuracy	Implementation time (μsec)
HMM	97.03%	00.02
1D_ConvNet	96.97%	07.10
2D_ConvNet	98.98%	92.20

20 times per minute. This provide 3-4 seconds of data acquisition and processing time to analyze the data. Given the processing times shown in Table V, it is clear that we can accomplish the processing and analysis within 3 seconds to support real-time monitoring. To improve the performance of the system we plan to investigate the use of an array of sensors.

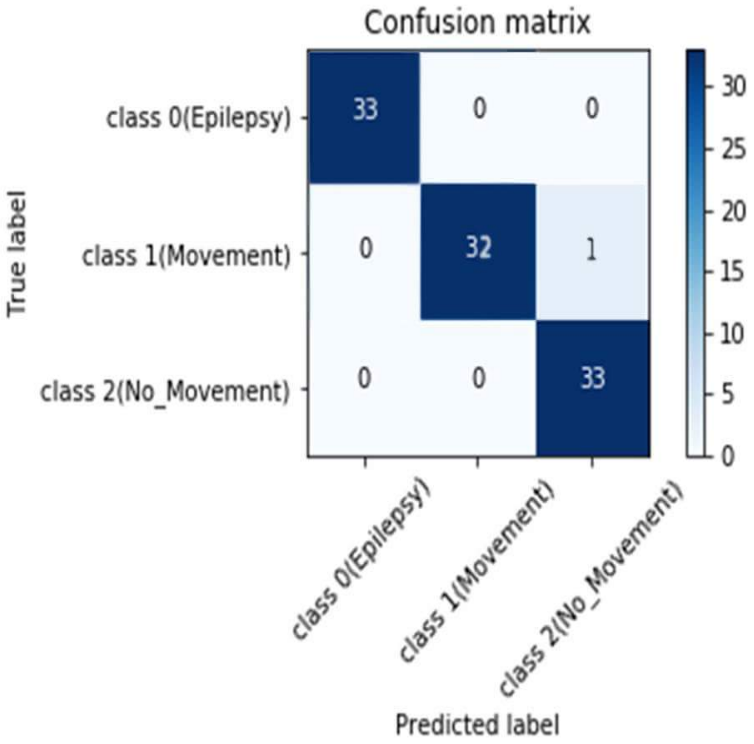

Figure 17: A 3 $\times$ 3 two-dimensional (true label vs predicted label) confusion matrix of 2D-ConvNet.

TABLE VI: VALIDATION ACCURACY COMPARISON WITH OTHER MOTION SENSORS TO DETECT EPILEPTIC SEIZURES

Method	Type of sensor	Accuracy
Proposed	**PIR**	**98.98%**
Beniczky [36]	Wireless wrist accelerometer	89.00%
Nijsen [37]	3D-accelerometer	55.56%
Narechania [41]	mattress sensor	80.00%

CHAPTER 4

CONVULSIVE MOVEMENT DETECTION USING LOW-RESOLUTION THERMOPILE SENSOR ARRAY

Sudden Unexplained Death in Epilepsy (SUDEP) is a fatal threat to patients who suffer from convulsive seizures. The causes of the SUDEP are still not well-understood, and the patients who suffer from epileptic seizures may face death during sleep, likely after an unwitnessed convulsive seizure. An important step towards SUDEP prevention is reliable seizure detection during sleep that is inexpensive and unobtrusive. In this Chapter, we investigate the use of a non-contact, non-intrusive, privacy-preserving system that can detect convulsive movements experienced by human subjects. Detection is accomplished by a combination of uncooled low-cost, low-power, low-resolution (8×8) IR sensor array, and a deep learning algorithm implemented with a Convolutional Neural Network (CNN). The thermopile sensor array is placed 1m from subjects who are reclining in bed. The CNN training set consists of thermal video streams from 40 healthy subjects mimicking convulsive movements or lying in bed without making convulsive movements.

4.1 Contribution

The contributions of this chapter can be summarized as follows:

1. We propose a novel approach to detect the convulsive movements during sleep using low-cost, low-resolution, non-intrusive and contact-free (8×8) thermopile IR sensor array.
2. For this study we received an Institutional Review Board (IRB) approval to examine the use of our sensing method on healthy recruited subjects for the purpose of carrying out a preliminary study using data from simulated Convulsive motions of seizure.
3. Our approach is applied on 40 healthy recruited subjects (28 males and 12 female).
4. A deep learning Convolutional Neural network (CNN) algorithm is used to classify convulsive movements and non-convulsive episodes.
5. Our approach is reliable since it produces no false negatives to distinguish between the occurrence and non-occurrence of convulsive movements.
6. The performance results show that the thermopile sensor array has the potential to detect convulsive seizures while maintaining patient privacy and not requiring direct patient contact.

The rest of this chapter is organized as follows: Our proposed system design is described in Sec. 4.2. The data acquisition using thermopile sensor array is shown Sec. 4.2.1. The input data processing is presented in Sec. 4.2.2. The feature extraction and classification are shown in Sec. 4.3. The supervised 2-D Convolutional Neural Network (CNN) description is explained in Sec. 4.3.1. The Evaluation metric of the proposed system design is shown in Sec. 4.4. The experimental results and discussion are provided in Sec. 4.5. Finally a comparison between the PIR sensor and the thermopile sensor array to detect the convulsive seizures is presented in sec. 4.6.

4.2 System Design

The seizure-detection system consists of a low-resolution (8×8) Grid-eye thermopile sensor to capture the thermal images due to body movements within its field of view, an Arduino uno microcontroller with 10 Hz sampling rate, 10-bit quantization level, and a processing unit for feature extraction and classification, as seen in Figure(18).

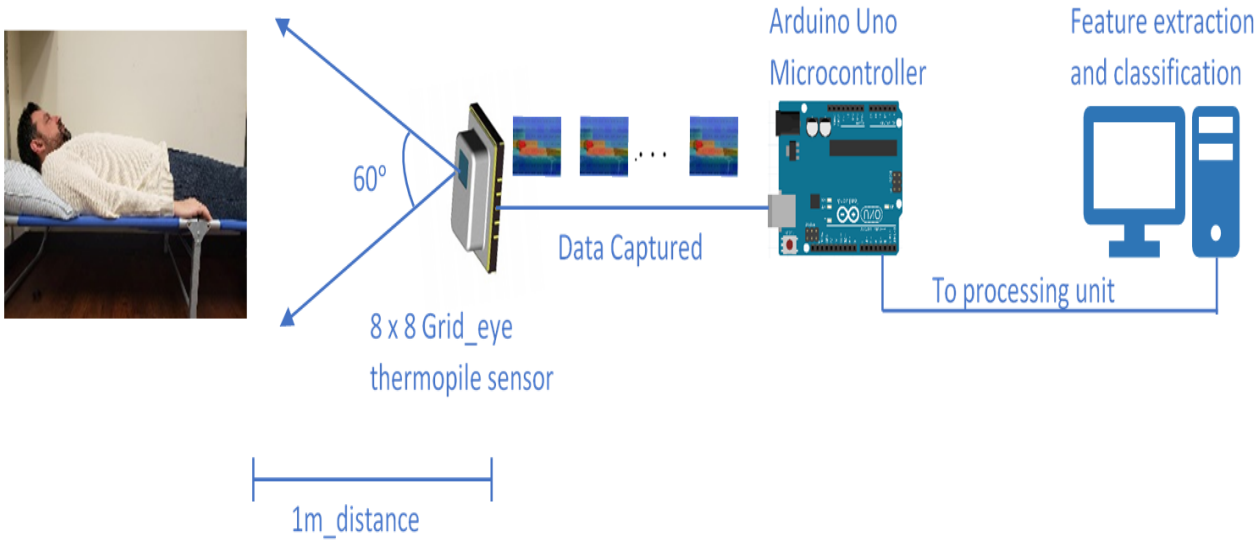

Figure 18: The proposed system consists of a thermopile sensor array, Arduino Uno micro controller, and a processing unit for extracting and classifying data.

4.2.1 Data Acquisition using the Thermopile Sensor Array

A thermopile sensor array consists of low-cost, highly sensitive, uncooled sensors that generate an electrical signal proportional to the detected infrared radiation when infrared radiation is incident on their active area. Individual thermoelements are made of two different thermal activity materials and can detect light with a wavelength between 8 and 13μm, which is not perceivable by the human eye. Their operation is based on the Seeback effect phenomena in which the heat difference between two different thermal activity materials generates an electrical signal between the two ends of the thermoelement [116]. The thermopile sensors generate a thermal image from the infrared radiation displayed as a matrix (Figure 19) [117]. We used an 8×8 Panasonic Grid-EYE sensor array that captures a thermal 64-pixel images every 100msec, with a power consumption of $\simeq$ 15 mW. The low resolution of the sensor array is advantageous in preserving the privacy of the observed subjects.

Data for this study were collected from normal recruited subjects under a protocol approved by an Institutional Review Board of the University of Illinois at Chicago. Before the start of the data acquisition, we presented to the subjects, two different YouTube videos of patients experiencing a convulsive epileptic seizure. In each session, each subject was asked to lie down on a couch, located one meter away from the thermopile sensor array, and perform a set of different activities consisting of 1) pretending to sleep without moving; 2) mimicking normal incidental body movements by changing the position during sleep; 3) mimicking the convulsive epileptic seizure movements while pretending to be asleep (Figure 20 and Figure 21).

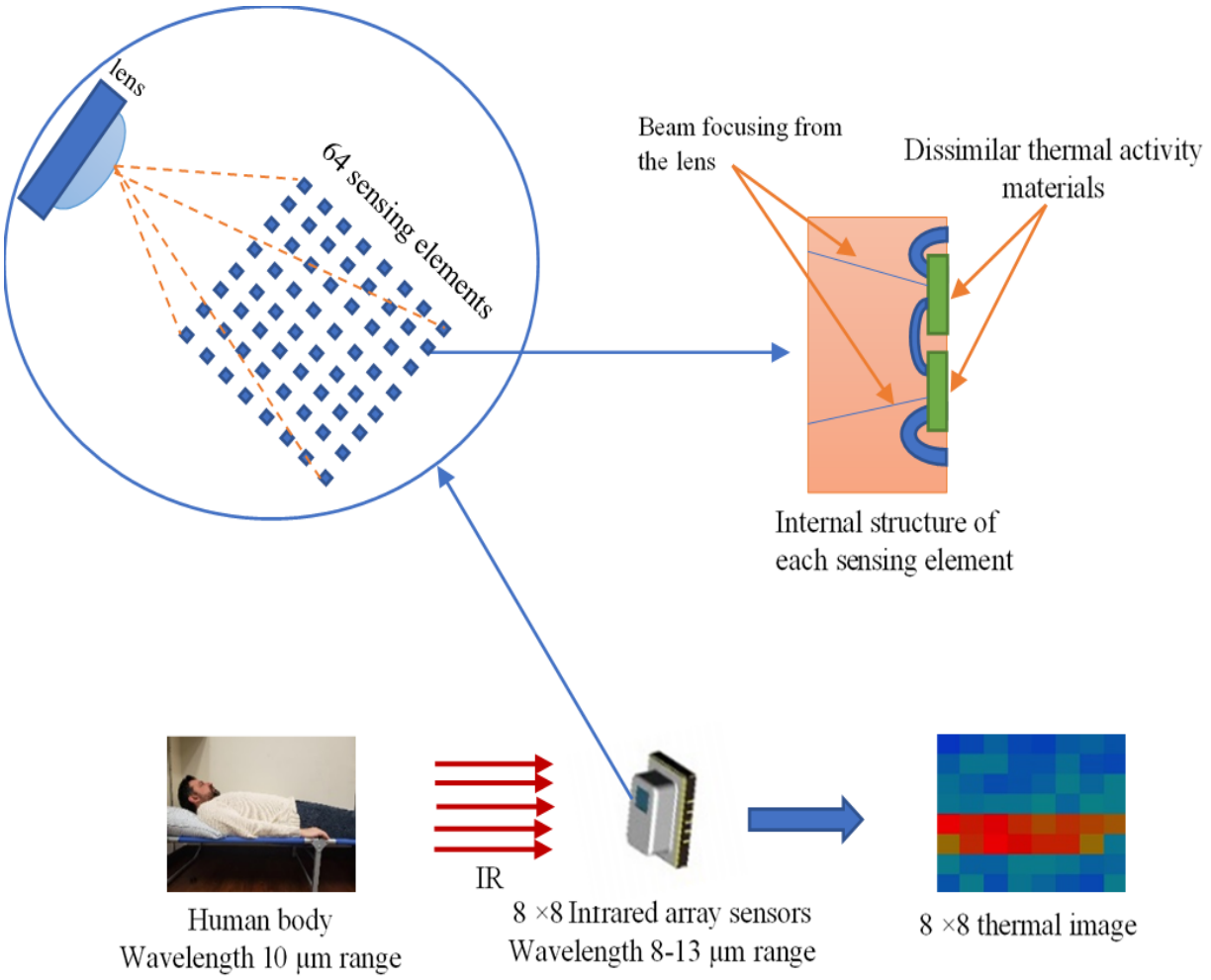

Figure 19: The thermopile sensors that generate a thermal image from the infrared radiation displayed as a matrix.

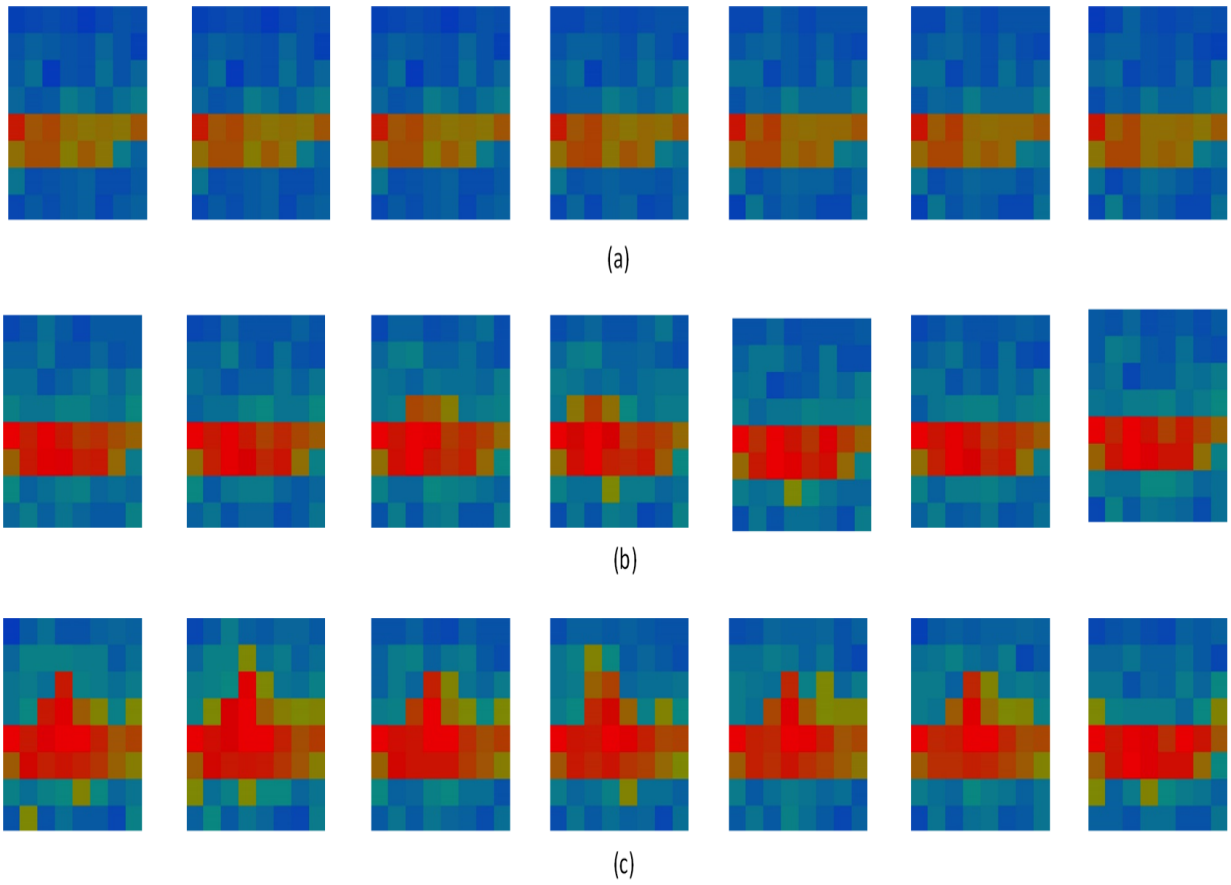

Figure 20: a) A sequence of frames captured by an (8×8) sensor array due to no movement (sleep mode). b) A sequence of frames captured by an (8×8) sensor array due to normal movements. c) A sequence of frames captured by an (8×8) sensor array due to convulsive movements.

4.2.2 Input Data Preprocessing

Image preprocessing consisted of calculating the absolute difference between two consecutive frames before feeding the information to the neural network as seen in equation (4.1).

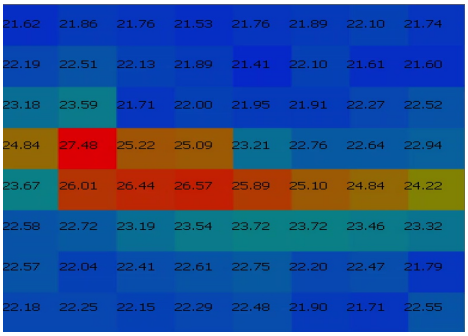

Figure 21: a) A thermal image with corresponding temperature values captured by an (8×8) sensor array due to no movement (sleep mode).b) A thermal image with corresponding temperature values captured by an (8×8) sensor array due to convulsive movement.

$$I_{diff}[n] = |I[n] - I[n-1]| \tag{4.1}$$

where $I[n]$ and $I[n-1]$ represent two consecutive frames captured at time n and $n-1$ respectively by thermopile sensor array and $I_{diff}[n]$ represents the input frame to the neural network. In the absence of motion, the difference is zero and a stationary subject is not detectable. Since we seek to detect the motion not the presence of the subject, the absence of the subject in a difference image used as neural network input is not a concern (Figure 22).

4.3 Feature Extraction and Classification

Deep learning algorithms are now commonly used to extract and classify features in complex data sets [118]. In this work we used a 2-D Convolutional Neural Network (CNN) as a binary classifier to detect the occurrence and non- occurrence of convulsive motion.

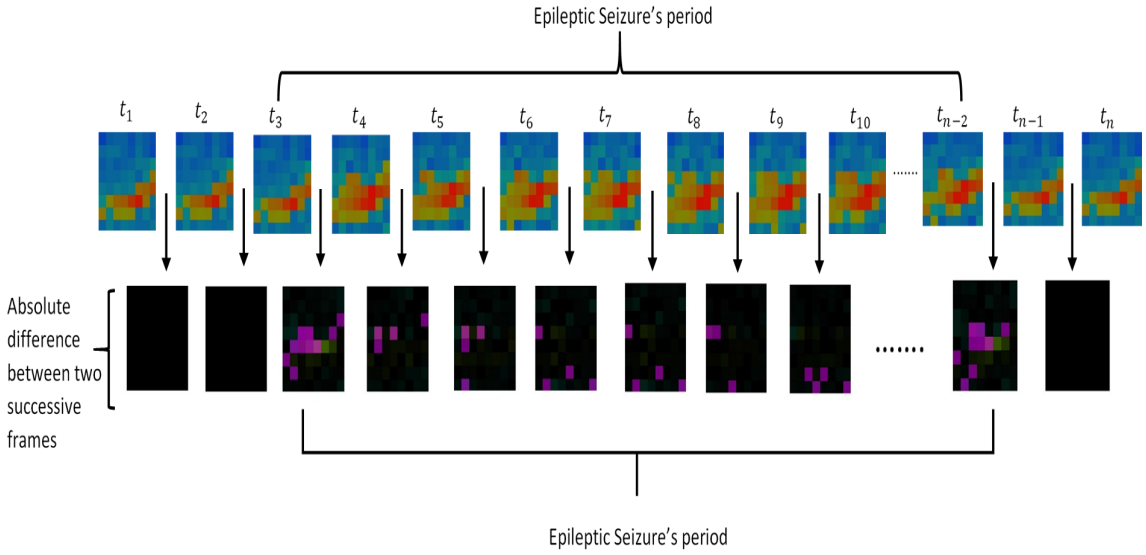

Figure 22: An absolute difference between two consecutive thermal images that captured using an (8×8) thermopile sensor array.

4.3.1 2-D CNN Description

The number of parameters that are used in the 2D-CNN depends on the size and depth of the filters, type of filters (kernel filter in our design), and the number of hidden layers and neurons that are used and the way that they connect to each other [119].

Our deep CNN design consists of two convolutional layers, a max pooling layer, and a fully connected layer. Generally, the convolution stage and max pooling stage are responsible of extracting the features from the input images, while the fully connected layer stage classifies the extracted features from the previous stages. The input to the CNN, which represents the set of an (8×8) thermal images, is convolved with 32 kernel filters of size (3×3). An activation map of size $(6 \times 6 \times 32)$ is produced. A batch normalization is used in order to make the learning process more stable, and to reduce the

number of epochs that are needed to train the deep network. A Rectified Linear Unit (RELU) activation function is applied to the convolved data to add a non-linearity. A down-sampling or max-pooling filter of size (2×2) is used to reduce the activation map dimensions. The output of the max pooling layer $(3 \times 3 \times 32)$ is convolved with another 16 kernel filters of size (3×3) and down-sampled with a filter of size (2×2). The output of the feature extraction layers $(2 \times 2 \times 16)$ is flattened and fully connected to two hidden layers of size 128 and 64 respectively (see Table VII and Figure 23).

The batch size of this network is 32 with 50 epochs. Excessive training can cause the classifier to memorize the input data. A dropout of 0.2 and a Ridge Regression L_2 regularization with regularization parameter value equal to 0.001 are used to prevent overfitting. In addition to that a K-fold cross validation is applied to the input data images to avoid the poor performance of the classifier [120].

In order to ensure that the sum of the output probabilities is equal to one, the SoftMax function is used to normalize the output vector. An Adam optimizer is used as stochastic gradient descent optimizer with cross-entropy loss to estimate the error of our model and to measure the performance of classification, for which the probability of its output lies between [0,1]. If the predicted probability diverges from the actual label, the loss function increases and vice versa. Equation (4.2) shows the cross-entropy loss J_{CH} function for multi classes.

$$J_{CH} = -\sum_{c=1}^{C} P_{o,c} \ln \tilde{P}_{o,c} \tag{4.2}$$

where C represents the number of classes, $P_{o,c}$ is the actual label of observation o, $\tilde{P}_{o,c}$ is the predicted probability of class c, and ln is the natural log. Since we are dealing with two classes, occurrence and

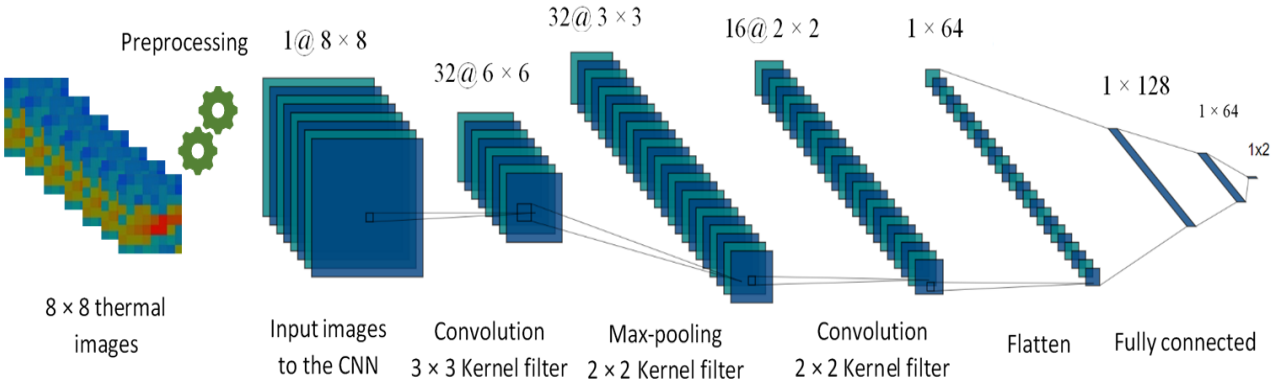

Figure 23: A structural diagram of the proposed 2-D CNN that used to classify captured thermal images into occurrence or non occurrence of convulsive movements.

non-occurrence of convulsive movements, the equation of cross entropy loss of our proposed network can be written as follows:

$$J_{CH} = -\left(P \ln\left(\tilde{P}\right) + (1-P)\ln\left(1-\tilde{P}\right)\right) \tag{4.3}$$

Figure 23 shows the 2-D CNN structural design that is used to classify the captured data of the thermal sensor array.

4.4 Evaluation Metric of System Design

The selection of the evaluation metric is a crucial step in many classification problems to get an optimum classifier, and to measure the quality of the machine learning or deep learning models. One

such metric is the confusion matrix, which is an array of size $(m \times m)$ (Predicted labels $\times$ Actual labels), where m represents the number of the classes of the classifier model [121]. Since we have two classes in our model, occurrence and non-occurrence of convulsive movements, m is 2, and the model is a binary classifier. If the predicted label and actual label of the confusion matrix are both false, the class cell of the confusion matrix indicates true positive (TN), while if both are true, then the class cell refers to true positive (TP). A false positive (FP) is generated when the predicted value is true, and the actual value is false. In our design the (FP) refers to a false alarm generated in response to a non-convulsive state. The converse situation (i.e. a convulsive movement is misclassified as a non-convulsive movement), is a false negative (FN). All the metric parameters can be represented mathematically as:

$$P_R = \frac{TP}{TP+FP}, \tag{4.4}$$

$$R_C = \frac{TP}{TP+FN}, \tag{4.5}$$

$$F1_{Score} = 2 \times \frac{P_R \times R_C}{P_R + R_C}, \tag{4.6}$$

$$A_{cc} = \frac{TP+TN}{TP+TN+FP+FN}, \tag{4.7}$$

in which Precision (P_R), or Positive Predicted Value, is the ratio of the number of cases with correctly detected convulsive movements to the total number of cases that the CNN classifies as having convulsive movements. Recall (R_C), or sensitivity, is the ratio of number of cases with convulsive movements that were detected correctly to the number of all cases with convulsive movements. $F1-Score$ is the

harmonic mean of the recall and precision. A_{cc} is the diagnostic accuracy, or the probability that the model's prediction is correct [121].

4.5 Results and Discussion

Twenty-eight male and 12 female healthy subjects were recruited to be monitored with the IR array while acting out either 12 seconds of convulsive movements or 12 seconds of simulated rest or normal movements.

Altogether 4800 frames were collected for each of the two class $\left(12seconds \times 10\frac{frames}{second} \times 40subjects\right)$. The total preprocessed images are fed into the CNN for training. In order to avoid the small data set issues, the data were augmented using an image data generator.

The image data set was split into 10 groups of equal size for each group. The first group was used as a test dataset while the remaining groups were used as training dataset. The performance metrics and the classification accuracy were then calculated. The procedure was repeated 10 times, each time trained with nine groups and tested with the remaining group. The test set contains 1600 images, and the classification accuracy of the network is 99.2% (Table VIII).

The 2D-CNN classifier had no false negatives. meaning that it identified all the cases with convulsive movements. Thirteen episodes of normal movement were misclassified as convulsive, giving a false positives rate of 1.6% (Figure 24). A comparison between the original captured thermal images data sets, and absolute difference images data sets $I_{input}[n]$ is shown in Table IX. Absolute difference image based classification is far superior to single image based classification. This is due to the fact that we classify movement information not the thermal images using the CNN.

TABLE VII: THE STRUCTURAL LAYERS AND NUMBER OF PARAMETERS OF THE 2D_CNN.

Layer type	O/P shape	no. of parameters
Conv 2d, 1 stride, 0 Pad	32 $\times 6 \times 6$	896
Batch-Normalization	32 $\times 6 \times 6$	128
RELU (Activation Function)	32 $\times 6 \times 6$	0
Max-Pooling 2d, 1 strides, 0 Pad	32 $\times 3 \times 3$	0
Conv 2d, 1 stride, 0 Padding	16 $\times 2 \times 2$	2064
Batch-Normalization	16 $\times 2 \times 2$	64
RELU (Activation Function)	16 $\times 2 \times 2$	0
Flatten	64	0
Dense_Hidden	128	8320
Activation	128	0
Dense_Hidden	64	8256
Activation	64	0
Dropout	64	0
Dense_Output	2	130
Soft-max (Activation Function)	2	0

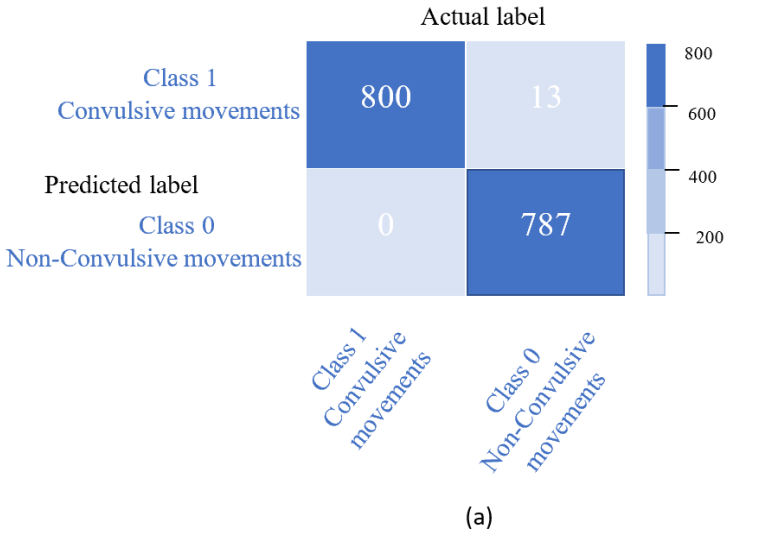

(a)

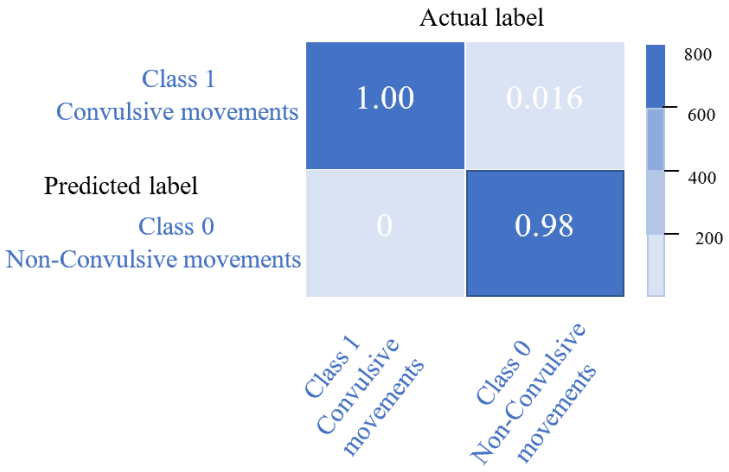

(b)

Figure 24: Evaluation metric of the 2D_CNN.

TABLE VIII: THE STRUCTURAL LAYERS AND NUMBER OF PARAMETERS OF THE 2D_CNN.

	Pre-cision	Re-call	F1-Score	Sup-port
Convulsive movements	1.00	0.98	0.99	800
Non-convulsive movements	0.98	1.00	0.99	800
Avg / total	0.99	0.99	0.99	1600

TABLE IX: A COMPARISON BETWEEN THE CAPTURED THERMAL IMAGES DATA SETS, BEFORE TAKING THE ABSOLUTE DIFFERENCE, AND AFTER TAKING THE ABSOLUTE DIFFERENCE.

I/P to CNN	TP	FP	TN	FN	Accuracy
$I_{diff}[n]$	800	13	787	0	99.2%
$I[n]$	669	131	672	128	83.3%

4.6 PIR sensor vs Thermopile Sensor Array

Both our novel approach studies were controlled studies due to the position of sensors, the distance of the sensor from the subjects, and the activities the recruited subjects were asked to do.

Although the PIR sensor and the thermopile sensor array have the ability to detect the convulsive movements, but each sensor can do it in different approaches. It should be noted that the number of subjects in the two studies is different which will affect a comparison of the two types of sensors. The PIR sensor uses the pyroelectric detectors to measure the changes in the infrared radiation received while

the thermopile sensor array uses the thermocouples to measure the temperature differences. Owing to this fact, both sensors are shown to be reliable to detect the epileptic seizures in a home environment. In clinical settings where the circumstances are different due to the fact that the patient's room may have more than one patient and the motion could be affected by other factors. The thermopile sensor array is advantageous over the PIR sensor because it can spatially distinguish multiple subjects in a scene. The PIR sensor may detect other movements due to other subjects in the room and may produce false alarms. In addition, the thermopile sensor array can detect the thermal energy of the static subject. One benefit of the PIR sensor over the thermopile sensor array, it has a wider bandwidth.

Both the low-resolution 8×8 thermopile sensor array; and the PIR sensor, can reliably detect simulated convulsive movements. Both systems are contact-free, noninvasive, and use passive sensors.

TABLE X: A COMPARISON BETWEEN A LOW-RESOLUTION 8×8 THERMOPILE SENSOR ARRAY AND PIR SENSOR.

	Thermopile sensor array	PIR sensor
Sampling rate	10 Hz	20 Hz
Detection distance	Up to 7m	Up to 5m
Type of data	Thermal images	Time series data
Accuracy	99.2%	98.98%

A comparison between the thermopile sensor array and the PIR sensor based on the detection distance, sampling frequency, activation accuracy to detect the convulsive seizure, and the type of collected data are shown in Table X.

CHAPTER 5

RESPIRATION RATE ESTIMATION USING A PASSIVE THERMOPILE INFRARED SENSOR ARRAY

The respiration rate alongside the heart rate, blood pressure and body temperature, is a vital sign for assessing the human's body functions. In this chapter, we investigate the use of a thermopile sensor array to estimate respiratory rate. We propose and experimentally validate a novel method that human respiration rate may be reliably estimated from respiratory-induced body movements captured using a low-cost, contact-free, passive thermopile sensor array. A thermopile sensor array detects the thermal infrared energy emanating from stationary human subjects within its area of detection. The sensed energy fluctuates with body movement. Low resolution 8×8-pixel thermal video clips were collected from 40 recruited subjects at rest positioned one meter away from the thermopile sensor array. Image frames are processed by Haar-like filters leading to the extraction of a one-dimensional feature signal from each video. A peak detection algorithm is used to identify each breath period. The proposed method is computationally efficient because it is based on multiplierless Haar-like feature extraction and peak detection.

5.1 Contribution

In this chapter we summarized our contributions as follows:

1. We propose and experimentally validate a novel approach to estimate the respiratory rate from respiratory-induced body movements.

2. We investigate the use of low-cost, low-resolution, and contact-free thermopile IR sensor array to estimate the respiratory rate. A thermopile sensor array detects the thermal infrared energy emanating from stationary human subjects within its area of detection. The sensed energy fluctuates with body movement.

3. For this study we received an Institutional Review Board (IRB) approval to examine the use of deidentified data that are collected from healthy recruited subjects during rest. Our approach is applied on 40 healthy recruited subjects (28 males and 12 female).

4. A Haar-like filters and peak detection algorithm are used to extract and estimate each breath period. Our proposed method is computationally efficient because it is based on multipliersless Haar-like feature extraction and peak detection algorithm.

5. We achieved a high positive correlation rate of 97.7% between the actual respiratory rate and the estimated rate in our dataset.

The rest of this chapter is organized as follows: The materials and methods of our proposed system are described in Sec. 5.2. The thermopile Infrared (IR) sensor array is presented in sec. 5.2.1. The thermopile data processing is shown Sec. 5.3. Finally, the experimental results and discussion are provided in Sec. 5.4.

5.2 Materials and Methods

In this work, we used the Panasonic Grid-Eye thermopile passive infrared sensor array to monitor subjects. The contact- free sensor array has a detection range of up to 7 meters. The sensor is placed 1m away from the subjects. It generates low- resolution 8×8 infrared images of subjects as shown in

Figure 26. In the following subsection we briefly review the basic features of the thermopile sensor array.

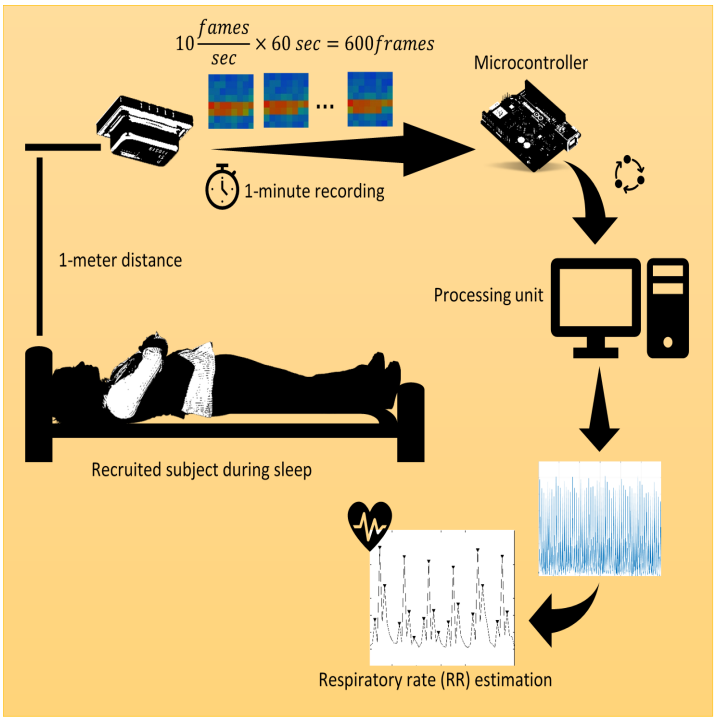

Figure 25: Proposed system design to monitor and estimate the respiration rate using a low resolution, contact-free thermopile sensor array.

In the following subsection we briefly review the basic features of the thermopile sensor array.

5.2.1 Thermopile InfraRed (IR) sensor array

The low-resolution thermopile IR sensor array is designed to measure the thermal energy by detecting the IR radiation from a subject within its area of detection. The subject need not be in motion to

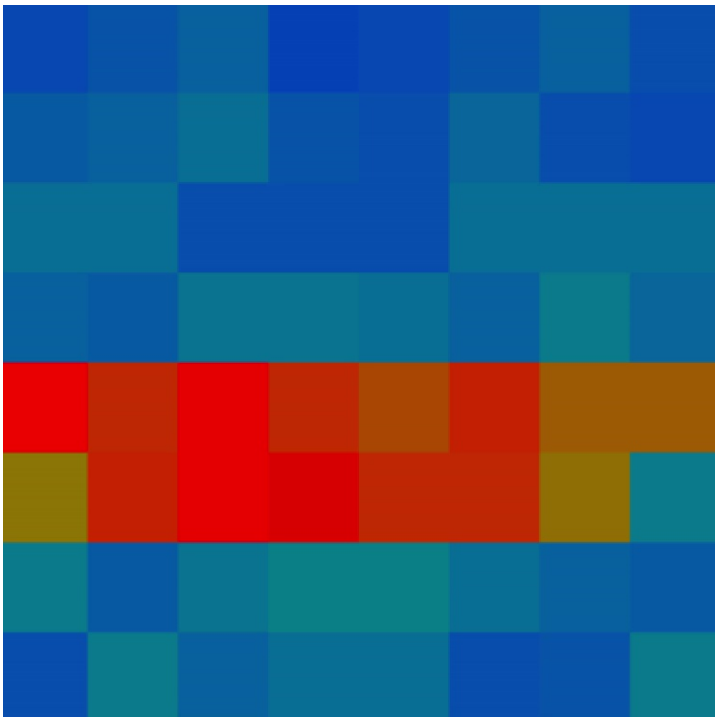

Figure 26: Thermopile InfraRed (IR) sensor array.

generate a non-zero sensor signal, as in the case of pyroelectric IR sensors. The thermopile IR sensor has several thermocouples connected in series. Each thermocouple has two junctions made of two dissimilar materials: the hot junction and the cold junction. The cold junction is isolated and, therefore, it does not absorb any IR radiation. On the other hand, the hot junction is sensitive to the IR radiation as shown in Figure 27. The thermopile sensor works based on the Seeback effect phenomena [122]. When the hot junction detects the IR radiation, a temperature difference between the two junctions is created and an electrical voltage V_{out} proportional to the difference between the hot junction temperature T_{hot} and the cold junction temperature T_{cold} is produced according to Equation (5.1):

$$V_{out} = N_{th} S_b \left(T_{hot} - T_{cold}\right) \tag{5.1}$$

where Nth is the number of thermocouples that are connected in series and Sb is the coefficient of the Seeback effect phenomena.

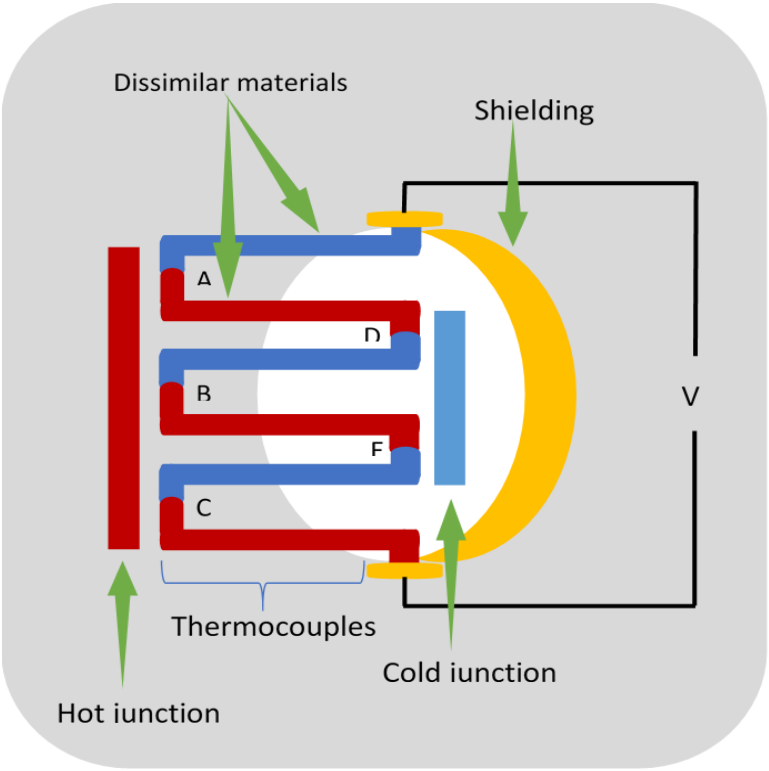

Figure 27: The internal structure of the thermopile sensor array that is made of several thermocouples connected in series.

Panasonic Grid-Eye passive IR thermal sensors array with a low power consumption of 15 mW is used in this work. The sensor can produce 10 images per second. The Panasonic Grid- Eye sensor can detect Long-Wave Infrared (LWIR) light in a wavelength range from 8 to 13μm. The sensor can therefore be used to monitor subjects during sleep at night as well. The low-resolution IR video streams

captured using the thermopile sensor array are sent to the processing unit via a microcontroller as shown in Figure 25.

5.3 Thermopile Data Processing

In order to extract the feature parameters from the captured low resolution 8×8 frames, we apply Haar-like filters [123] on each frame and obtain three different feature signals s_h, s_v and s_{vc} representing horizontal, vertical, and vertical central differences in the recorded low-resolution thermal video data, respectively. Figure 28 describes the feature extraction process from the thermopile sensor array data. The feature signal s_v is defined as follows:

$$s_v(k) = \left| \frac{\sum_{i=1}^{N} \sum_{j=1}^{N/2} I_k(i,j)}{N^2/2} - \frac{\sum_{i=1}^{N} \sum_{j=N/2+1}^{N} I_k(i,j)}{N^2/2} \right| \tag{5.2}$$

where $I_k(i,j)$ is the $(i,j)-$th pixel of the k-th frame of the infrared thermal data. Each recording is one-minute long with a frame rate of 10 frames/sec yielding 600 frames. Therefore $k \in \{1,2,...,600\}$.The image size is $N \times N$ and $N = 8$.

Similarly, s_h, and s_{vc} are defined as follows:

$$s_h(k) = \left| \frac{\sum_{j=1}^{N} \sum_{i=1}^{N/2} I_k(i,j)}{N^2/2} - \frac{\sum_{j=1}^{N} \sum_{i=N/2+1}^{N} I_k(i,j)}{N^2/2} \right| \tag{5.3}$$

and

$$s_{vc}(k) = \left| -\frac{\sum_{i=1}^{N} \sum_{j=1}^{N/4} I_k(i,j)}{N^2/4} + \frac{2\sum_{i=1}^{N} \sum_{j=N/4+1}^{3N/4} I_k(i,j)}{N^2/2} - \frac{\sum_{i=1}^{N} \sum_{i=3N/4+1}^{N} I_k(i,j)}{N^2/4} \right| \tag{5.4}$$

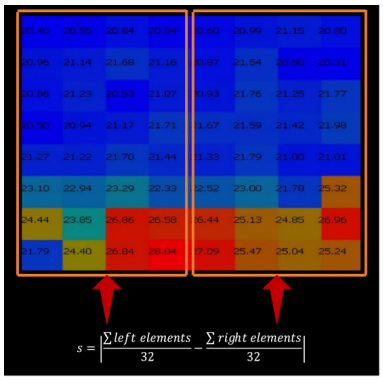

(a)

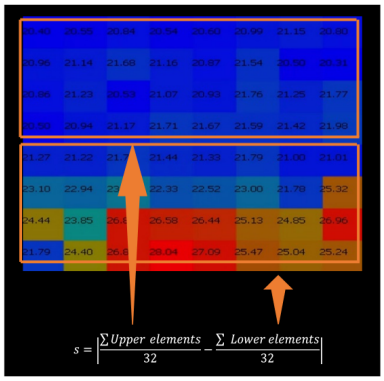

(b)

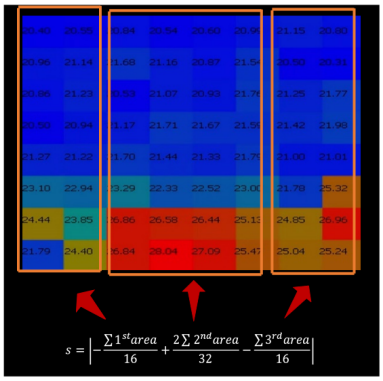

(c)

Figure 28: a) Haar-like filters are applied to capture the structural differences in each thermal image: (a) the first filter is applied on the left and right halves of each frame, b) the second Haar-like filter is applied on the upper and lower halves of each frame, and c) the third Haar-like filter is applied by dividing each frame into three zones as shown.

A typical one-minute-long feature signal s_v is shown in Figure 29. The other feature signals s_h and s_{vc} are similar to s_v. We observe an approximately periodic behavior due to respiration rate in these signals. The one-dimensional time-series feature signals $s_v(k)$, $s_h(k)$ and $s_{vc}(k)$ are decimated by a factor of 10 after applying a finite-duration impulse response (FIR) lowpass filter (LPF) of order 30 with normalized passband frequency= 0.03π, and the normalized stopband frequency = 0.1π. We decimate the feature signals because the frame rate of the sensor is 10 frame per second (fps) or 600 frames/minute and this rate is unnecessarily high for the respiration rate which has a range of 12 to 20 breaths per minute for adults. A down-sampled feature signal is shown in Figure 30. The down-sampling factor should set to a different value if our approach method is applied to measure the RR for children who have a RR range of 17 to 27 (bpm) [124]. Since all our datasets were recorded from adults subjects. Therefore, we did not change the set of down-sampling factor. We detect the peaks of the decimated feature signals to determine the respiration rate as shown in Figure 30. We modified the peak detection algorithm described in [125] to determine the peak locations. Since the peak is the data sample that is a local maximum, we calculated the local maximum value in a moving window of size $2w+1=7$. Our peak detection algorithm is described in Algorithm 1 and a typical detection result is shown in Figure 30. The peaks of the decimated feature signal are clearly identifiable, and the peak detection process is very accurate and efficient.

The total number of the maximum topological features of the decimated time series signal represents the number of respiration per minute (Figure 30).

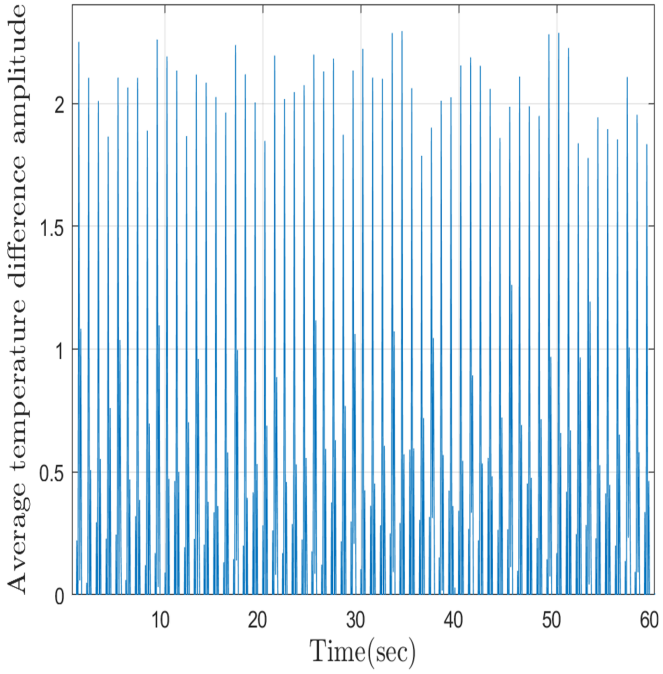

Figure 29: A feature signal after applying the vertical Haar-like filter on each captured IR frame.

5.4 Experimental Results

We collected IR data from forty healthy subjects (28 males, and 12 females). The subjects lay on a bed in a resting position as shown in Figure 25 and the distance between a subject and the sensor was about 1m. We recorded 60-second long 8×8 IR video clips with 10 fps frame rate using the thermopile sensor array.

Haar-like filters are applied to each frame of the data collected from the thermopile sensor array to measure the absolute average temporal difference values as shown in Figure 28. Each filter generates a single value for each frame. As a result, we obtain 3 time-varying feature signals s_h, s_v and s_{vc} for each video. Figure 29 shows the signal s_v after applying the vertical Haar-like filter on each captured

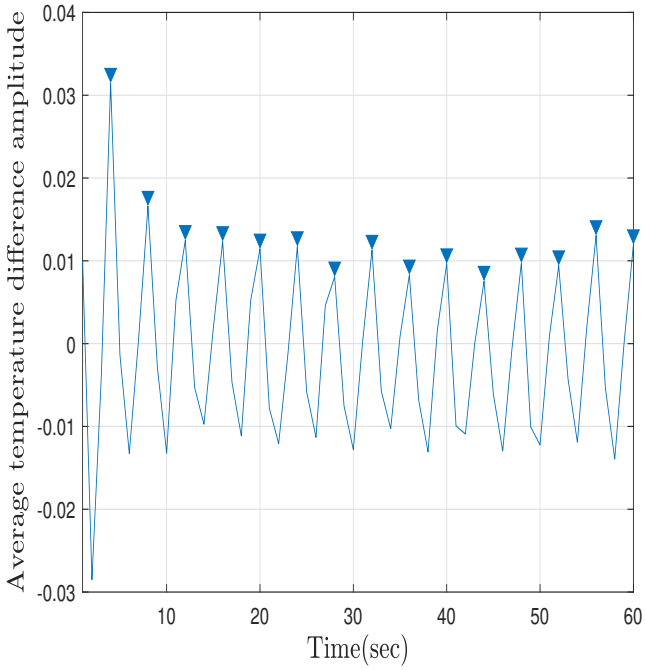

Figure 30: The downsampled feature signal and the detected peaks. The number of peaks per minute corresponds to the respiration rate (bpm=breath per minute).

IR frame. The frame rate of the sensor is 10 Hz which is well above the Nyquist rate for typical human respiration rate detection. We therefore decimate the data by a factor of 10 to reduce the sampling rate to 1Hz. We low-pass filter the feature signal signals s_h, s_v and s_{vc} using a Low-Pass Filter (LPF) with a cutoff frequency equal to 0.1 and down-sample the output by a factor of 10 and we obtain the signal shown in Figure 30. This signal is approximately periodic as it tracks the subject's respiration rate. We applied a modified version of a known peak detection algorithm to find the number of local maxima. The number of maxima per minute determines the respiration rate or the number of chest movements within one minute as shown in Figure 31.

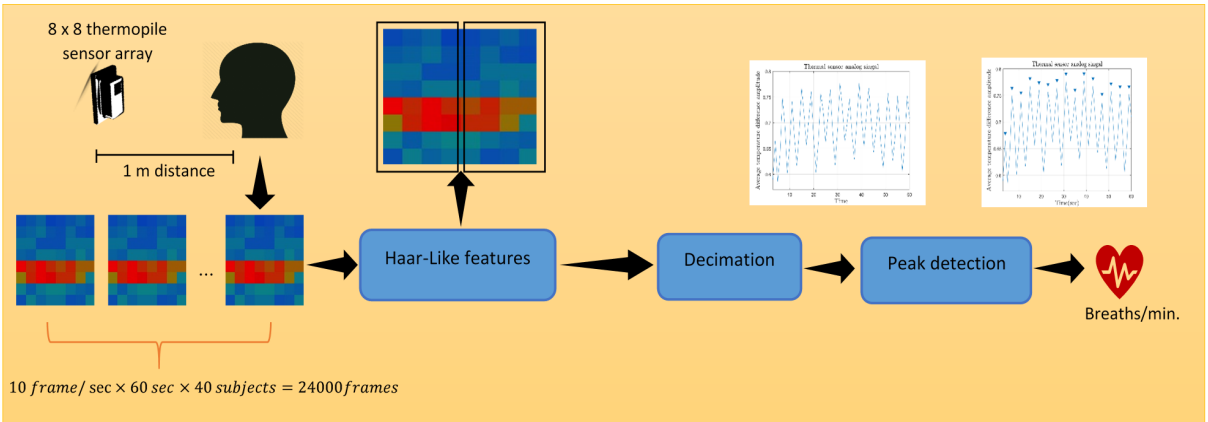

Figure 31: A block diagram of the proposed algorithm to extract the respiratory rate from the low-resolution thermal images by using Haar-Like filter and peak detection algorithm.

We measured the average Root Mean Squared Error (RMSE) for each Haar-like feature. We achieved an average RMSE equal to 0.387 breaths per minute when the Haar-Like filter is applied on three different regions of each frame, while an average RMSE equal to 0.274, and 0.591 are achieved when the Haar-Like filter is applied on the left and right side, and on the upper and lower side of each frame, respectively. The results are summarized in Table XI. We compared our system design with Lorato et al. [126] that used a thermopile sensor array from distance of less than one meter to monitor the respiration rate in Table XII. We measured the average Root Mean Squared Error (RMSE) for each Haar-like feature approach. We achieved an average RMSE equal to 0.387 breaths per minute when the Haar-Like filter is applied on three different regions of each frame, while an average RMSE equal to 0.274, and

0.591 are achieved when the Haar-Like filter is applied on the left and right side, and on the upper and lower side of each frame, respectively. The RMSE error is defined as follows,

$$Th_{RMSE} = \sqrt{\frac{\sum_{i=1}^{N} \left(Th_{RR}(i) - O_{RR}(i)\right)^2}{N}} \tag{5.5}$$

where Th_{RR} is the respiratory rate measurements extracted from the output signal of the thermopile sensor array, O_{RR} is the ground truth respiratory rate readings due to chest movements monitoring, and N is the total number of datasets recordings. Based on the observed results reported in Table XI, we chose the filter with the minimum average RMSE.

TABLE XI: AN AVERAGE RMSE OF THREE DIFFERENT HAAR-TYPE FILTERS THAT USED IN OUR WORK

Haar-like filters	s_v : Left and right rectangular	s_h Upper and lower rectangular	s_{vc} : Three regions rectangular
Average RMSE	**0.274**	0.591	0.387

In order to measure the reliability of this system, the chest movements of one subject out of the 40 subjects are visually recorded and used as a ground truth measurement [127]. A correlation coefficients is used to measure the relation between the actual and estimated respiratory rate value as follows

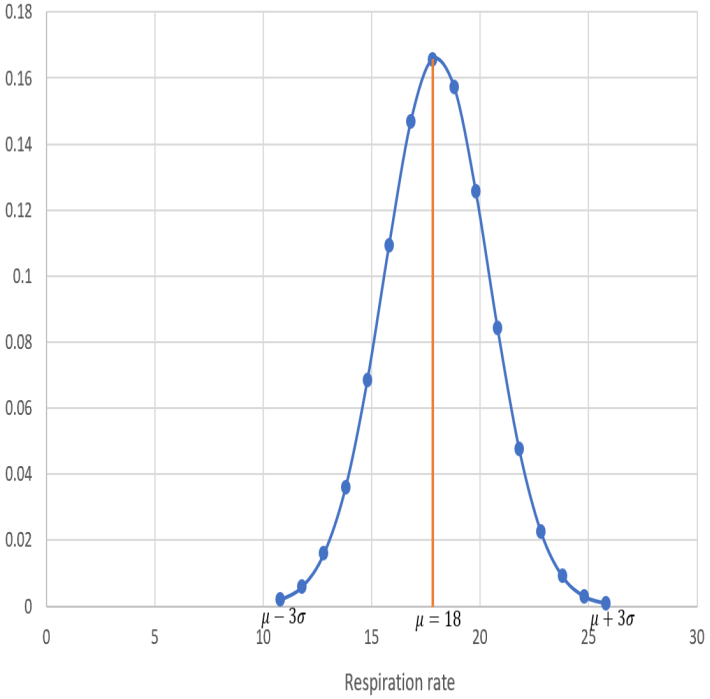

Figure 32: The distribution of the respiration rate values that are estimated from the recorded data.

$$r = \frac{\sum_{i=1}^{N}(Th_i - \bar{Th})(o_i - \bar{o})}{\sqrt{\sum_{i=1}^{N}(Th_i - \bar{Th})^2 \sum_{i=1}^{N}(o_i - \bar{o})^2}} \tag{5.6}$$

where Th is the estimated respiratory rate measured from the output streaming frames of an 8×8 thermopile sensor array,$\bar{Th}$ is the mean of the estimated respiratory rates from the thermopile sensor array signal, o is the ground truth respiratory rate measurements, $\bar{o}$ is the mean of the ground truth measurements, and N is the number of recordings. A high positive correlation coefficient equal to 97.77% is achieved between the monitored respiratory rate as a ground truth and the estimated respiratory rate

from the captured signal of the thermopile sensor array. The average respiratory rate is equal to 18 breaths per minute. Figure 32 shows the distribution of the estimated respiratory rate of the recorded data.

We compared our system design with Lorato et al. [126] that used a thermopile sensor array to monitor the respiration flow in Table XII. Lorato et al.'s method performs best when the distance between the sensor and the subject is about 0.2 meters, which is too close to the subject. On the other hand, our sensor can determine the respiration rate when the distance is about 1 meter, which is a much comfortable distance to monitor subjects. As a result, the sensor can be placed on an end table near the bed of the subject and it can be used to monitor subjects during the sleep. We have 40 healthy subjects in our study compared to 6 subjects in [126]. Although the datasets are different, we have slightly better accuracy compared to [126].

Our algorithm can also detect the respiration rate from the frontal head thermal infrared images. We did not have any frontal head recordings using the thermopile sensor array in our dataset. Unfortunately, we are currently unable to record new data due to restrictions of the COVID-19 pandemic. However, we found three thermal IR videos on YouTube and created low-resolution video-clips as shown in Figure 33. The human head makes slight movements whenever we take a breath [128]. The IR camera captures these subtle movements and the warm air coming out of nostrils and the mouth.

We extracted IR image sequences from the video clips and down-sampled them into the 8×8-pixel size, which is the image size of the thermopile sensor array that we use. We applied our algorithm on the low-resolution YouTube clips. The respiration rate estimation procedure is summarized in Figure 33. A 96.07% correlation rate are achieved between the actual respiratory rate and the estimated rate

TABLE XII: A COMPARISON BETWEEN OUR APPROACH THAT USED A THERMOPILE SENSOR ARRAY TO MEASURE THE RESPIRATORY RATE AND LORATO ET AL [126]

	Our proposed system	**Lorato et al. [126]**
Sensor type	8×8 thermopile sensor array	8×8 thermopile sensor array
Approach	Haar-like feature extraction and peak detection, count the number of peaks in the time domain	Hanning-windowed and 1DFFT, find the maximum peak in the frequency domain
Number of tested subjects	40 healthy subjects	6 healthy subjects
Sensor distance	1.0m	0.2m
Ground truth obtained	by counting the chest movements over a 60sec period	by impedance pneumography
Average RMSE	0.274 breaths per minute (bpm)	1.59 bpm
Correlation with the ground truth	97.77%	Was not specified

that detected from the thermal low-resolution images as shown in Figures 34 and 35. In these video clips subjects move their heads in the video clips. Despite head movements our algorithm was able to determine the correct respiration rate.

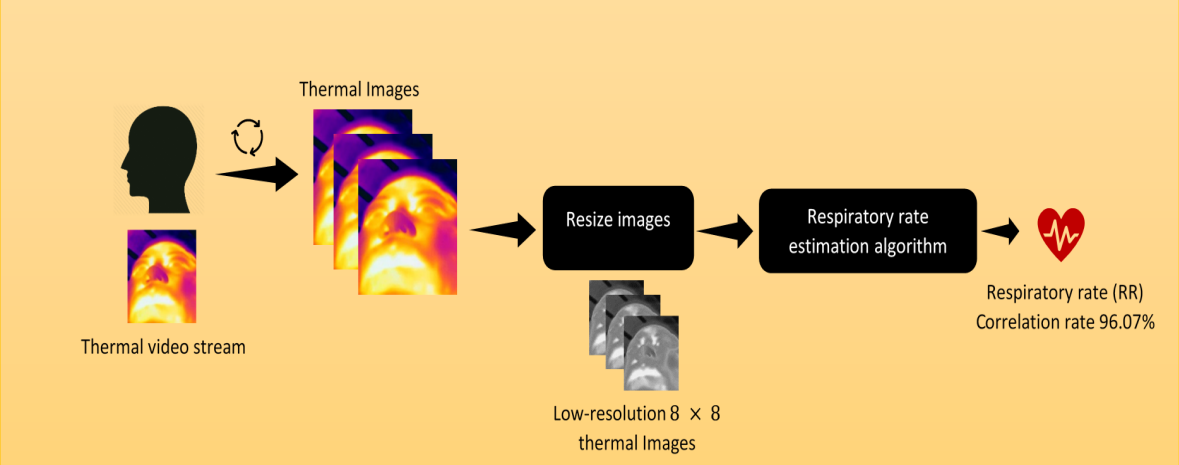

Figure 33: Steps of the proposed algorithm applied on three thermal YouTube videos.

We calculated the average RMSE values for each Haar-like filter as shown in Table III. The feature signal s_v obtained using the left-right Haar filter produces the best results in these three video clips. We can accurately detect the respiration rate as shown in Figure 35.

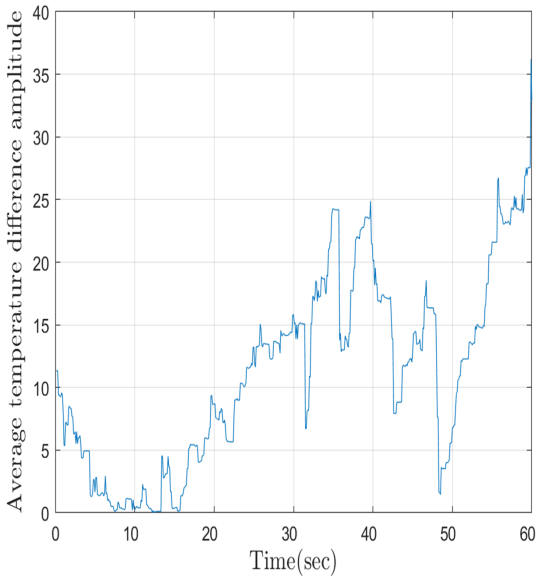

Figure 34: A horizontal feature signal after applying the Haar-like filter on each low-resolution 8x8 image extracted from thermal YouTube videos.

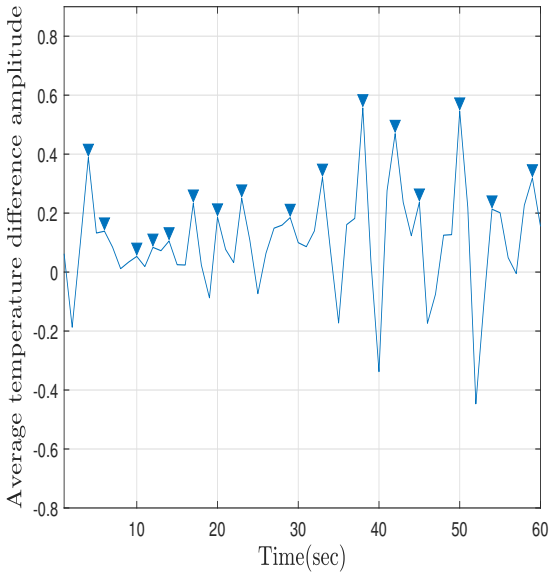

Figure 35: Low-pass filtered, down-sampled, and baseline removed feature signal corresponding to Fig.10. The number of local maxima corresponds to the respiration rate (16 bpm).

Algorithm 1 PEAK DETECTION ALGORITHM

S =s(1),s(2),...,s(k)

Respiratory ←Ø

Input k=60

Output Respiratory

j ← $j = 0$

for $i = 1,\ \ i{+}{+},\ \ i < k$ **do**

$j \leftarrow j + 1$

Peak[j]=P$_{local}$ (S, i, s_i, w)

end for

m=length(Peak)

for `j = 1, j++, while j < m` **do**

if Peak[j]> mean(Peak[j]) **then**

Respiratory ← Peak[j] $\bigcup$ Respiratory

end if

end for

for each adjacent pairs in Respiratory **do**

if $|l - k|$ <w) **then**

Remove the min(Respiratory[l],Respiratory[k]) from Respiratory

end if

end for

CHAPTER 6

RESPIRATION RATE AND HEART RATE DETECTION FROM SUBTLE HEAD MOTION USING THE PYROELECTRIC INFRARED (PIR) SENSOR

Breathing and pulse rates are vital signs that are routinely measured by healthcare providers to assess a human body's basic functions. In this chapter we investigate the use of a low-cost, contact-free, non-obtrusive, and non-invasive Pyroelectric Infrared sensor to estimate the Respiratory Rate (RR) and the Heart Rate (HR) from the subtle head movements. The RR and HR are inferred from the time-varying sensor signal due to the subtle movements of the head caused by the flow of air from the lungs and blood from the heart to the head via the carotid artery, respectively. The PIR sensor is placed behind the human's head without any contact to the human body and it can detect the motion from a distance of up to 50 centimeters. The sensor can be placed to the head rest of a chair or a bed and can continuously estimate both the RR and the HR at the same time.

6.1 Contribution

In this chapter we summarize our contributions as follows:

1. We propose a novel approach to estimate the respiratory rate and the heart rate from the subtle movements of the head caused by the flow of air from the lungs and blood from the heart to the head via the carotid artery, respectively.
2. We investigate the use of low-cost, contact-free, and passive Infrared sensor to estimate the respiratory rate and heart rate.

3. The pyroelectric IR sensor was found to detects the thermal infrared energy emanating from stationary human subjects within its area of detection. The analog output of the pyroelectric IR sensor is digitized and analyzed using appropriate signal processing algorithms. The pulse oximeter is used as a ground truth.

4. We achieved a high positive correlation of 96.4% between our estimates and the pulse oximeter measurements.

The rest of this chapter is organized as follows: The materials and methods of our novel system are described in Sec. 6.2. The concept of subtle head movements is shown in sec. 6.2.1. The pyro-electric IR sensor is presented in sec. 6.3. Heart rate and respiratory rate are described sec. 6.3.1. The heart rate estimation algorithm is described in sec. 6.3.2, while the respiratory rate estimation algorithm is presented in sec. 6.3.3. Finally, the experimental results and discussion are provided in Sec. 6.4.

6.2 Material and Methods

Our proposed system is based on a low-cost, contact-free, and non-intrusive PIR sensor that does not emit any type of radiation. A microcontroller is used to transfer the analog output of the PIR sensor to the processing unit which estimates the respiration and heart rates from the infrared sensor signal due to the subtle head motion of the subject (Figure 36).

6.2.1 Subtle head motion

During each cardiac cycle, the left ventricle contracts of the heart contracts and injects a blood to the aorta. Approximately 12 grams of the blood flow on either side of the head from the aorta via a carotid artery [129]. According to the Newton's third low, the blood's force on the head is equivalent to

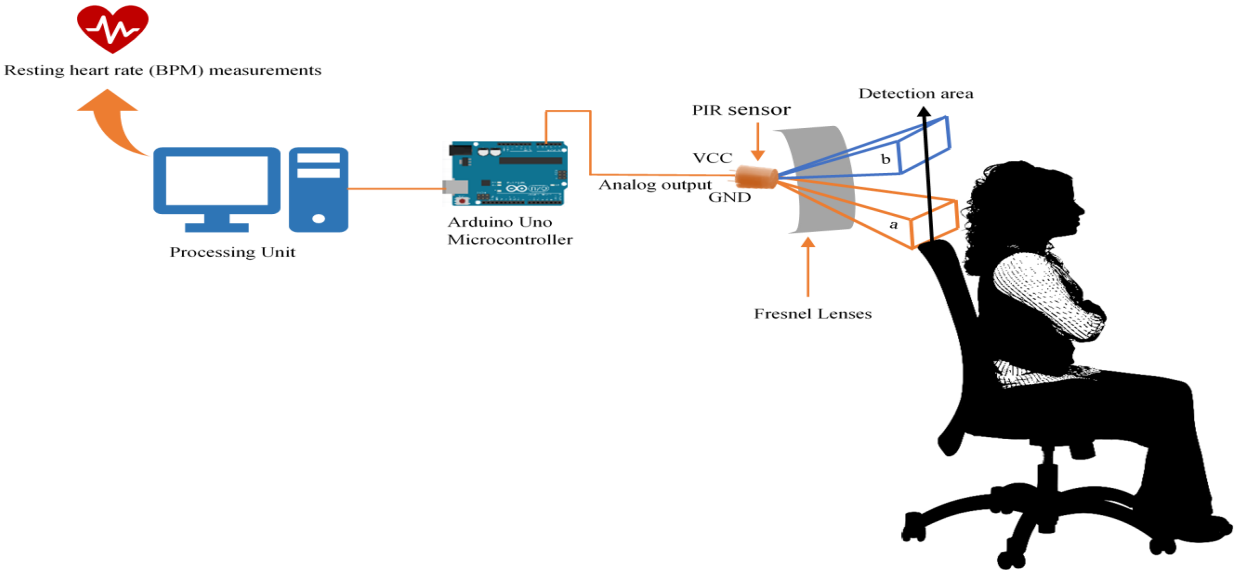

Figure 36: A proposed system that captured the subtle head motion of the subject using a low-cost, contact-free, non-intrusive pyroelectric IR sensor that placed behind the human subject.

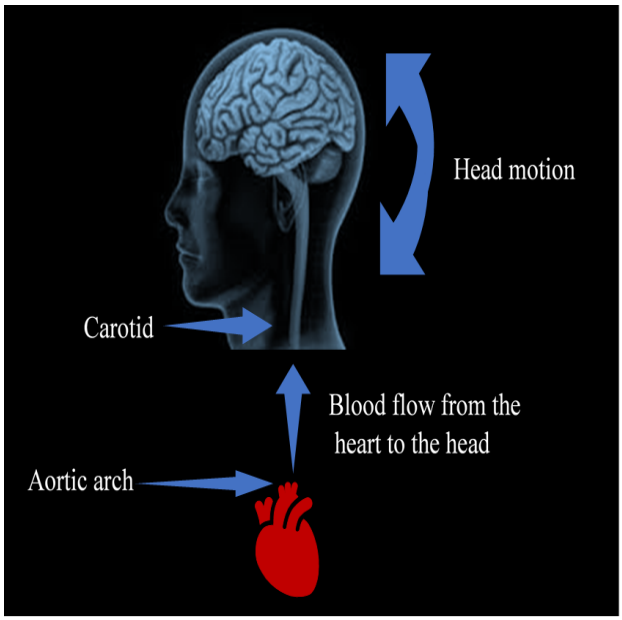

Figure 37: Subtle head motion during each cardiac cycle due to the flow of the blood from the aorta through the carotid artery into each side of the head.

the head's force that acting on the blood, and as a reaction it causes cyclic subtle head movements [130] (see Figure 37).

6.2.2 Pyroelectric IR sensor

Pyroelectric IR sensors are low-cost passive infrared sensors, that are well known as motion detection sensors. They are widely used in monitoring systems and energy savings systems [131]. Since the pyroelectric IR sensors are contact-free and non-intrusive sensors, in the recent years, they are involved in the healthcare applications such as detecting the epileptic seizures during sleep to avoid the Sudden Unexpected Death in Epilepsy (SUDEP) [1]. The pyroelectric IR sensors functionality is based on measuring the amount of the emitted infrared from the moving subjects. The output of the pyroelectric IR sensor can be affected by many factors including the distance of the moving subjects from the pyroelectric IR sensor, the speed of the moving subject, and the direction of the movement [131]. The pyroelectric IR sensor has two pyroelectric plates that are sensitive to the IR radiated from the moving objects and the two plates have the same amount of charge which is equal to the background ambient light. When there is no motion detected by the pyroelectric IR sensor, the IR difference between the two plates are equal to zero. If the moving subject enter the region of detection (RoD) of the pyroelectric IR sensor, the charge of the pyroelectric plate *a* will be higher than the charge on the plate *b* (see Figure 36). As a result, a positive differential charge will be generated. When the moving subjects leave the RoD, the amount of the IR charge on pyroelectric plate *b* will be higher than the IR charge on the other plate. Therefore, a negative differential charge will be generated. The pyroelectric IR sensor has Fresnel lenses that are used to increase the area of detection of the pyroelectric IR sensor. In addition to that, the Fresnel lenses use the same concept of a radar by focusing all the captured IR radiations that are emitted

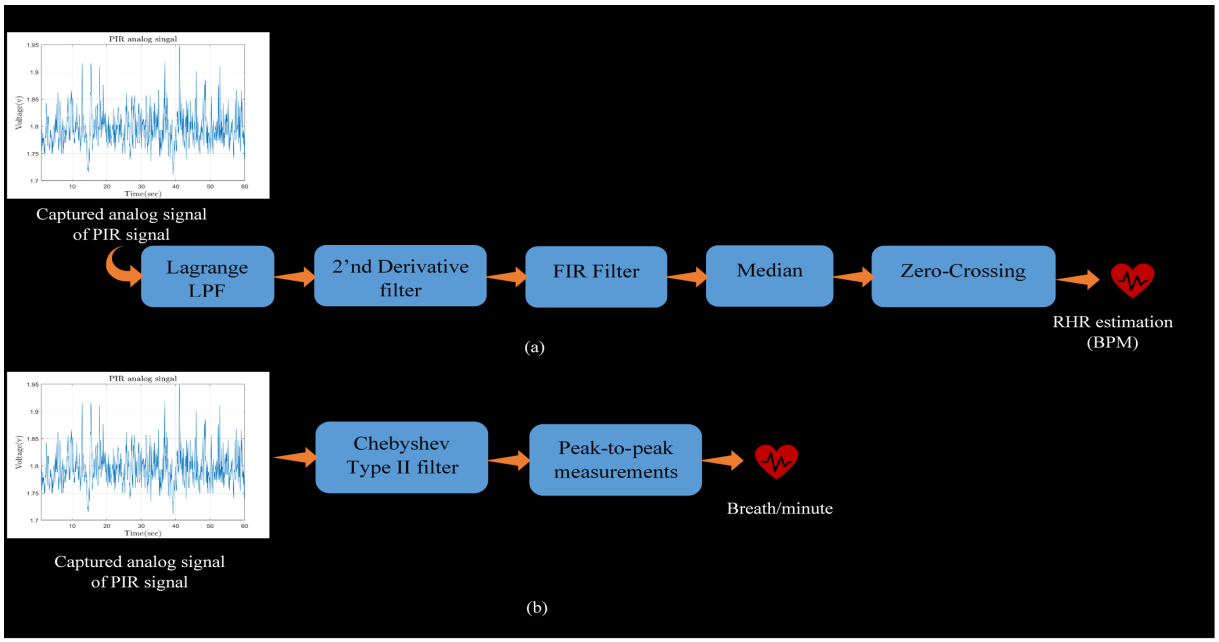

Figure 38: a) A block diagram of the algorithm that is applied on the captured PIR analog signal to estimate the RHR. b) A block diagram of the algorithm that is applied on the captured PIR analog signal to estimate the RR.

from the moving subject on the pyroelectric plates [132]. The pyroelectric IR sensor has no ability to detect more than one moving subject at a time [131].

6.3 Heart rate and respiratory rate extraction

The captured analog output of the pyroelectric IR sensor due to the subtle head motion is sent to the processing unit via a microcontroller with a 20 Hz sampling rate (Figure 1). We note that the magnitude of heart beat vibration is lower than the magnitude of respiration activity, and the heart beat acceleration is higher than the breathing acceleration [100]. The information of the HR and RR resides in different

frequency bands,therefore two different algorithms were applied on the captured PIR signal to extract the heart rate and respiratory rate.

6.3.1 Heart Rate Estimation algorithm

In order to attenuate the high frequency components that are generated due to the non-linearity of the Analog to Digital converter (A/D), the captured analog output of the PIR sensor is convolved with a Lagrange low-pass filter (LPF). Equation (1) shows the transfer function of the Lagrange Filter :

$$H(z) = -z^3 + 9z + 16 + 9z^{-1} - z^{-3} \tag{6.1}$$

The characteristic frequency of the filter should be half of the sampling frequency to avoid the aliasing that can affect the estimation of the heart rate of the subject. Therefore, the sampling rate of the signal is reduced by factor of 2 before applying the second derivative filter to the captured signal. Since the cardiac activity is much faster than the breathing, the second derivative filter is used to extract the heart rate by getting the acceleration of the subtle head movements [133]. The transfer function of the 1^{st}-derivative filter:

$$H_{1^{st}-deriv}(z) = 1 - z^{-1} \tag{6.2}$$

The first derivative filter is convolved with itself in the time domain to generate the 2^{nd}-derivative filter with transfer function:

$$H_{2^{nd}-deriv}(z) = z - 2 + z^{-1} \tag{6.3}$$

As a result, by convolving the 2^{nd}-derivative filter with Lagrange LPF we achieved the FIR filter that is used in this work to estimate the RHR as shown in Figure 3-a. The normalized FIR filter has the transfer function:

$$H_{FIR}(z) = -z^4 + 2 - z^3 + 8z^2 - 2z - 14 - 2z^{-1} + 8z^{-2} + 2z^{-3} - z^{-4} \tag{6.4}$$

$$H_{Normalized}(z) = \frac{1}{40}\left(h[0] + \sum_{n=1}^{4} h[n]\left(z^{-n} + z^{n}\right)\right) \tag{6.5}$$

To preserve the sharp edges of the signal and to remove the zero-mean additive noise before applying the zero-crossing algorithm to achieve the heart rate. A bandpass filter (BPF) of order 30, with normalized stopband frequencies 0.1π, and 0.6π $rad/samples$, and normalized passband frequencies 0.2π, and 0.4π $rad/samples$, and a median filter are applied on $H_{Normalized}(z)$.

Finally, the zero-crossing algorithm is applied on the filtered signal to measure the number of beats per minute (see Algorithm II).

6.3.2 Respiratory Rate estimation algorithm

The respiratory rate which is also known as the breathing rate is the number of breaths a human being takes per minute. The range of normal breathing rate for adults is between 12 to 20 breaths per minute. Below 12 or above 25 breaths per minute is considered as an abnormal respiratory rate which can be an indication to many unhealthy conditions that humans can suffer in their daily life, such as: anxiety, heart failure, asthma, and lung disease [134]. Lately the abnormal respiratory rate is linked with the symptoms of unprecedented COVID-19 disease [135].

Algorithm 2 HEART RATE ESTIMATION USING PIR SENSOR

System Initialization

$x[n] \leftarrow Captured - signal$

$h_1[n] \leftarrow -\delta[n+3] + 9\delta[n+1] + 16\delta[n] + 9\delta[n+1] - \delta[n+3]$

$h_2[n] \leftarrow \delta[n+1] - 2\delta + \delta[n+1]$ ▷ 2nd derivative filter

Processing the captured signal

$Y[n] \leftarrow x[n] \circledast h_1[n]$

$Y_{DS} \leftarrow Y[2n]$

$Y_{2nd-deriv} \leftarrow Y_{DS} \circledast h_2[n]$

$Y_{BPF} \leftarrow firpm[Y_{2nd-deriv}]$

$Y_{out} \leftarrow Median[Y_{BPF}]$

$L \leftarrow length[Y_{out}]$

while $\neq L$ **do**

    if $(Y_{out} < Th)$ & $(Y_{out} > -Th)$ **then**

        $Y_{out} \leftarrow 0$

    end if

end while

if $[Y_{out(present)} < 0$ & $Y_{out(next)} > 0]$ Or $[Y_{out(present)} > 0$ & $Y_{out(next)} < 0]$ **then**

    $beat \leftarrow beat + 1$

end if

To extract the respiratory rate from the captured signal we investigated the use of a filter that has the lowest phase distortion with a smooth amplitude response. A 30^{th} order Butterworth filter is applied to the analog output of the PIR sensor with normalized angular 0.35π, 0.65π, and stop band edge frequencies of 0.25π, 0.75π. A peak detection algorithm form [125] is used to detect the local maximums. The total number of the local maximums of the one minute duration of the filtered output signal represents the estimated respiratory rate. The local maximum counts of the filtered output signal represents the estimated RR as shown in Figure 3-b.

6.4 Results and discussion

A 100 recordings were collected with more than 9,000 heart beats. To measure the reliability of the infrared sensor, we used a pulse Oximeter sensor simultaneously with the PIR sensor to estimate the heart rate. In addition we consider the chest movements as the ground truth to estimate the respiratory rate. All the recordings are done using a low-cost, noninvasive, contact-free Panasonic AMN 21111 PIR sensor with 20 Hz sampling rate are placed 50 cm away from the back of the head of a stationary subject (see Figure 39).

The captured time series data are filtered using a Lagrange lowpass filter as shown in Figure 40. To extract the heart rate, the output of this filter is convolved with a 2^{nd} derivative filter as shown in Figure 41. Figure 42 shows the time series signal after removing the additive noise. Finally a zero-crossing algorithm is applied to estimate the heart rate.

Since the Butterworth filter has a flat response in the pass band and smooth amplitude response compared to other filters. Therefore, a Butterworth filter and a peak detection algorithm are applied to the captured PIR output to estimate the respiratory rate. The local maximum counts represent the

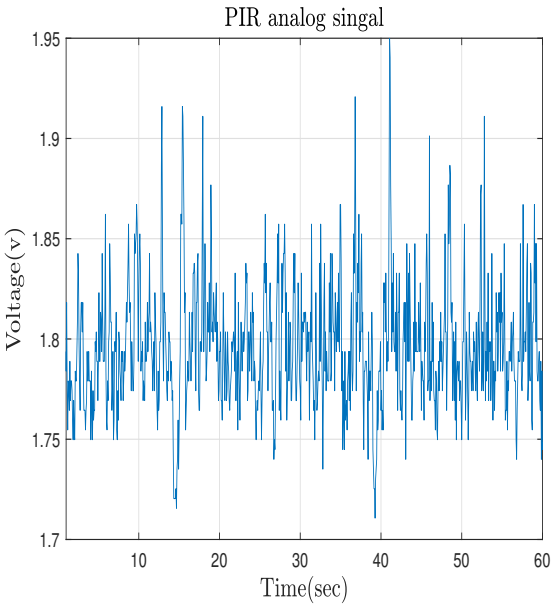

Figure 39: A captured time series signal from the subtle head motion using PIR sensor.

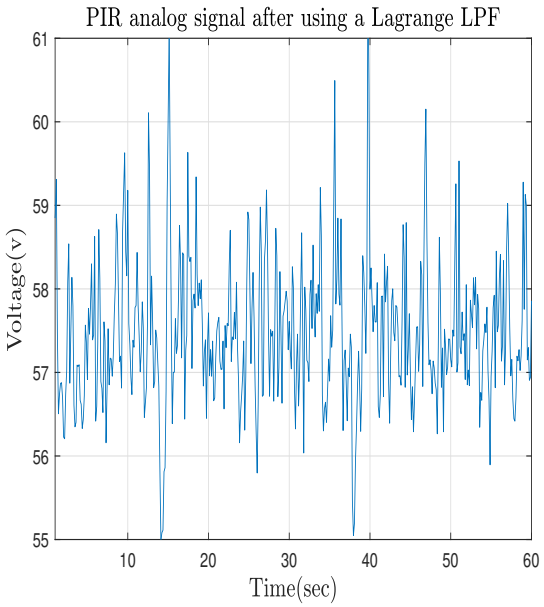

Figure 40: A Filtered time series signal using Lagrange LPF.

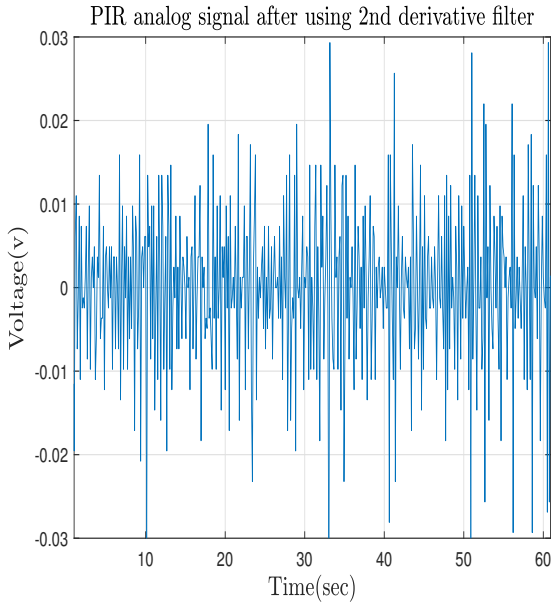

Figure 41: A time series signal after applying the 2^{nd} order derivative to estimate the RHR.

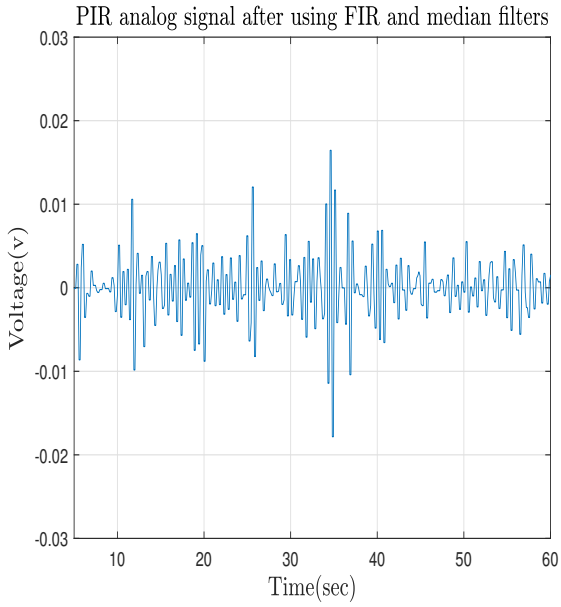

Figure 42: A time series signal after applying the BPF and median filters.

number of breathing per minute as shown in Figure 43. A high positive correlation coefficient equal to 95.37% is achieved between the estimated respiration from the captured signal of the PIR sensor and the actual reparations due to chest movements monitoring.

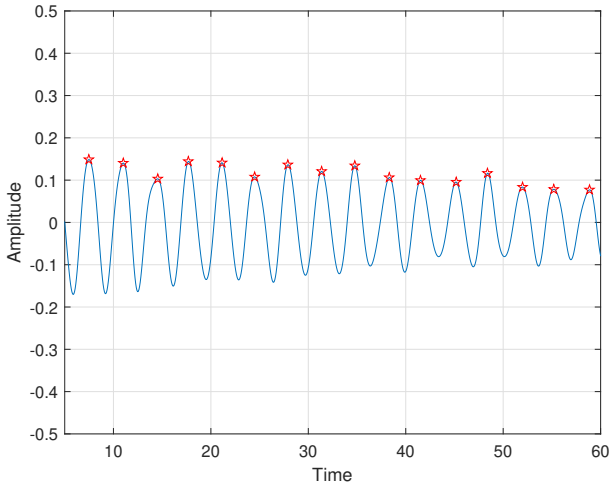

Figure 43: A PIR output signal after applying a Butterworth filter, the peak-to-peak values represent the number of breathing per minute.

To measure the reliability of our system, a commercial pulse Oximeter sensor is used simultaneously with the PIR sensor to measure the RHR. The correlation coefficients are used to measure the strength of relationship between the two sensors:

$$r_{po} = \frac{\sum_{i=1}^{N}(p_i - \bar{p})(o_i - \bar{o})}{\sqrt{\sum_{i=1}^{N}(p_i - \bar{p})^2 \sum_{i=1}^{N}(o_i - \bar{o})^2}} \tag{6.6}$$

where p is the PIR sensor recording, o is the pulse Oximeter sensor recording, $\bar{p}$ is the mean of the PIR recordings, $\bar{o}$ is the mean of the pulse Oximeter recordings, N is the number of recording and in our work N is equal to 100. We achieved a high positive correlation between the two sensors with a correlation coefficient equal to 96.4% as shown in Figure 44.

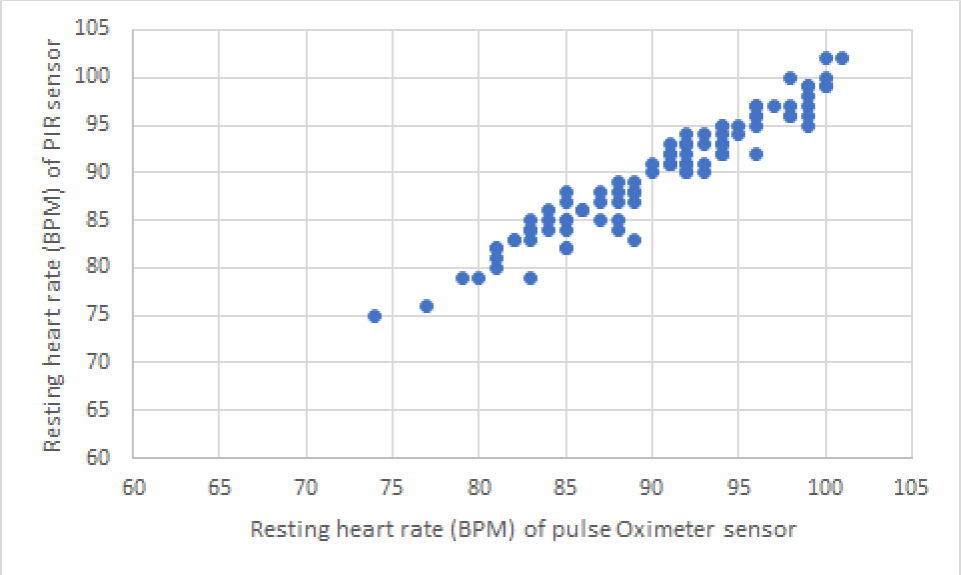

Figure 44: A correlation relation between the PIR sensor and the pulse Oximeter sensor.

We applied the chi-square test to measure the validity to estimate the heart rate from the subtle head movements using PIR sensor:

$$\chi^2 = \sum_{i=1}^{N} \frac{(p_i - o_i)^2}{o_i} \tag{6.7}$$

AS a result, the PIR sensor is significant at ($\alpha = 0.1$) compared to the commercial Oximeter sensor. Figure 45 shows the normal distribution of the estimated heart rate using the PIR sensor with a mean ($\mu = 89.92$) and standard deviation ($\sigma = 5.93$).

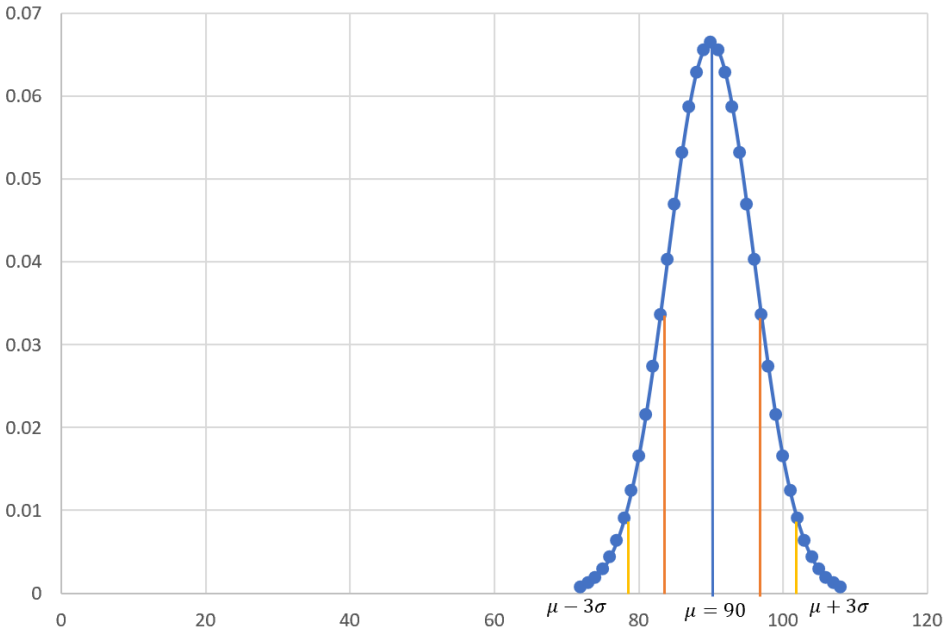

Figure 45: A normal distribution of the RHR that are estimated from the analog output of PIR sensor.

We compared our approach with the method in [130] that uses the Principal Component Analysis (PCA) to detect the pulse from head motion in videos (see Table XIII). In [130]. They used a video camera with 30 $frame/sec$ to record the head motion. The shortcomings of this approach is that the illumination and the skin color tone can affect their method unlike our approach that relies on detecting the IR radiation due to the subtle head movements of the subject. In addition, the video camera can not

TABLE XIII: A COMPARISON BETWEEN OUR APPROACH THAT USED A PIR SENSOR AND BALAKRISHNAN ET AL.

	Our proposed system	**Balakrishnan et al. [130]**
Sensor type	PIR sensor	Video camera
Way of connection	Contact-free	HContact-free
Sampling rate	20 Hz	30 frames / sec
Data type	Time series data	Image frames
Subject status	Stationary subject	Stationary subject

work in the dark, and it compromises the patient's privacy. On the other hand, in our method, we use a "one-pixel" passive sensor with a 20 Hz sampling frequency. In both methods, the data were collected from stationary subjects.

CHAPTER 7

CONCLUSION AND FUTURE WORK

In this thesis we proposed a novel approach that investigated the use of two passive sensors: the pyroelectic IR sensor and an 8×8 thermopile sensor array to detect the convulsive seizure during sleep. Chapter 3 presented a novel approach to detect the convulsive seizures using pyroelectic IR sensor. Our study shows that the system we devised has the potential to be applied to subjects with epileptic seizures. We note that the results have been obtained for simulated seizures. Since all the seizures were detected successfully, the low-cost, low-power pyroelectic IR sensor shows promise as a reliable device to detect epileptic seizures. Because of the contact-free nature of the pyroelectic IR sensor, it can avoid discomfort with the use of such sensors during sleep. Furthermore, this system can work in the dark as well as with illumination. Additionally, the ambient light does not affect the sensitivity of the system. Finally, the cost of this system is lower than the other available monitoring cameras and sensors.

A variety of high-level machine learning and deep learning techniques were used to classify the captured signals from the pyroelectic IR sensor. All the programs were implemented using a CPU E5-1620 V3, 3.5 GHz with 8 cores, Memory size 32 GB, and an operating system Centos 6.9. A comparison between the applied algorithms was done based on the validation accuracy, implementation time, evaluation metric, confusion matrix, and structural design. We achieved an accuracy equal to 97.03% for HMM, 96.97% for 1D_ConvNet, and 98.98% for 2D_ConvNet. We compared our results with the accuracy of the other motion-based epileptic seizure detection systems. We observe that our

method shows significantly improved performance, while noting that it was achieved with data obtained from simulated epileptic seizures.

Chapter 4 presented a novel approach to detect the convulsive seizures using an 8×8 thermopile sensor array. The pairing of a low-resolution IR sensor array with a CNN showed promise as a detecting convulsive movement. Since the thermal sensor array is contact-free and privacy preserving, it might eventually prove to be a practical tool for home monitoring of epileptic subjects at risk for SUDEP. While this study demonstrated the technical feasibility of a low-cost non-invasive system.

Chapter 5 presented a novel approach to estimating the respiratory rate using a low-cost, contact-free, privacy preserving, low-resolution 8×8 passive IR thermopile sensor array. We collected the data from healthy subjects resting on a bed. Our proposed system shows a promising result to estimate the respiratory rate which is one of the vital signs used in assessing a human's health status.

The respiration rate can also be determined using a pyroelectric IR sensor in a contact-free manner. However pyroelectric IR sensor observations are liable to interference from the movements of other people or pets within its viewing range and there is no way to separate the signal coming from the subject from other sources. Unlike the pyroelectric IR sensor, the thermopile sensor array generates a low-resolution image of the monitored area and we can identify the location of the person being monitored. The respiration rate monitoring system can focus on the person by resizing the windows of the Haar-like filters.

Chapter 6 presented a novel approach to estimate the respiratory rate and the resting heart rate from the subtle motion of the head using a low-cost, contact-free, and non-intrusive system. We used an algorithm based on 2^{nd} derivative filter, BPF, median filter and zero crossing to estimate the RHR from

the analog output of the yroelectric IR sensor. In measuring the RR, a Butterworth filter is applied to the output signal. To measure the reliability of the proposed system, we used an industrial pulse oximeter simultaneously with the pyroelectric IR sensor. Our system shows promising results for a reliably estimating two of the main vital signs that are indicators of the human body functions and can give an early indication for many of the diseases that are related to the respiratory system or the cardiac output.

In the future, there is a need to investigate the training and testing of both sensors on patients with epileptic seizures. Moreover, investigation is needed on the use of a combination of pyroelectric IR sensor and thermopile sensor array to design a real-time health monitoring and home assistive monitoring system that can monitor and estimate the heart rate and respiratory rate, and detect the epileptic seizure during sleep and send an alarm to the caregivers.

In addition, future works include investigation the use of multiple pyroelectric IR sensors to detect the epileptic seizure during sleep, and to estimate the heart rate and respiratory rate from the subtle head movements. This includes the study of the correlation between the multiple PIR sensors and measure the optimum location of the sensors.

APPENDIX

The IRB approved protocol 1026-2017 and the copyright permissions for all the manuscripts that are used in this dissertation is provided. Hanosh et al., 2019 [1] is published in IEEE Sensors Journal, 2019. and Hanosh et al., 2020 [2] is published in IEEE/CVF Conference on Computer Vision and Pattern Recognition (CVPR) Workshops, 2020.

APPENDIX (Continued)

Exemption granted

October 29, 2020

20201335-136172-2

20201335-136172-2

Rashid Ansari, Ph.D.
Electrical and Computer Engineering
Phone: (312) 996-5489 / Fax: (312) 996-6465

RE: Protocol # 2020-1335
"Respiratory estimation using passive infrared sensor array"

Sponsor: None

Dear Dr. Ansari:

Your application was reviewed on October 29, 2020 and it was determined that your research meets the criteria for exemption as defined in the U.S. Department of Health and Human Services Regulations for the Protection of Human Subjects [45 CFR 46.104(d)]. You may now begin your research.

UIC Exemption Granted Date: October 29, 2020
Sponsor: None

The specific exemption category under 45 CFR 46.104(d) is: 4

You are reminded that investigators whose research involving human subjects is determined to be exempt from the federal regulations for the protection of human subjects still have responsibilities for the ethical conduct of the research under state law and UIC policy.

Please remember to:

- → Use your research protocol number (2020-1335) on any documents or correspondence with the IRB concerning your research protocol.
- → Review and comply with the policies of the UIC Human Subjects Protection Program (HSPP) and the guidance *Investigator Responsibilities*.

We wish you the best as you conduct your research. If you have any questions or need further help, please contact me at (312) 355-2908 or the OPRS office at (312) 996-1711. Please send any correspondence about this protocol to OPRS via OPRS Live.

UNIVERSITY OF ILLINOIS AT CHICAGO
Office for the Protection of Research Subjects
201 AOB (MC 672)
1737 West Polk Street
Chicago, Illinois 60612
Phone (312) 996-1711

APPENDIX (Continued)

Approval Notice
Initial Review (Response To Modifications)

February 16, 2018

Rashid Ansari, Ph.D.
Electrical and Computer Engineering
1141 SEO 851 S Morgan Street
M/C 154
Chicago, IL 60612
Phone: (312) 996-5489 / Fax: (312) 996-6465

RE: Protocol # 2017-1026
"Real-Time Epileptic Seizure Detection during Sleep using Passive InfraRed (PIR) Sensors"

Dear Dr. Ansari:

Your Initial Review (Response To Modifications) was reviewed and approved by the Expedited review process on February 13, 2018. You may now begin your research

Please note the following information about your approved research protocol:

Protocol Approval Period: February 13, 2018 - February 13, 2019
Approved Subject Enrollment #: 100
Additional Determinations for Research Involving Minors: These determinations have not been made for this study since it has not been approved for enrollment of minors.
Performance Sites: UIC
Sponsor: None
Research Protocol:

a) Real Time Epileptic Seizure Detection during Sleep using Passive InfraRed (PIR) Sensors, Version 1.1, 01/11/2018

Recruitment Materials:

a) Eligible Checklist-V1.0, 02-04-2018
b) Flyer 2, Version 1.3, 02/04/2018
c) Flyer 1, Version 1.3, 02/04/2018

Informed Consents:

a) Consent Form-version 1.3-02/12/2018

Your research meets the criteria for expedited review as defined in 45 CFR 46.110(b)(1) under the following specific category:

(4) Collection of data through noninvasive procedures (not involving general anesthesia or sedation) routinely employed in clinical practice, excluding procedures involving X-rays or microwaves. Where medical devices are employed, they must be cleared/approved for marketing. (Studies intended to evaluate the safety and effectiveness of the medical device are not generally

APPENDIX (Continued)

APPENDIX (Continued)

Convulsive Movement Detection using Low-Resolution Thermopile Sensor Array

Conference Proceedings:
2020 IEEE/CVF Conference on Computer Vision and Pattern Recognition Workshops (CVPRW)

Author: Ouday Hanosh; Rashid Ansari; Naoum P. Issa; A. Enis Cetin

Publisher: IEEE

Date: 14-19 June 2020

Thesis / Dissertation Reuse

The IEEE does not require individuals working on a thesis to obtain a formal reuse license, however, you may print out this statement to be used as a permission grant:

Requirements to be followed when using any portion (e.g., figure, graph, table, or textual material) of an IEEE copyrighted paper in a thesis:

1) In the case of textual material (e.g., using short quotes or referring to the work within these papers) users must give full credit to the original source (author, paper, publication) followed by the IEEE copyright line © 2011 IEEE.
2) In the case of illustrations or tabular material, we require that the copyright line © [Year of original publication] IEEE appear prominently with each reprinted figure and/or table.
3) If a substantial portion of the original paper is to be used, and if you are not the senior author, also obtain the senior author's approval.

Requirements to be followed when using an entire IEEE copyrighted paper in a thesis:

1) The following IEEE copyright/ credit notice should be placed prominently in the references: © [year of original publication] IEEE. Reprinted, with permission, from [author names, paper title, IEEE publication title, and month/year of publication]
2) Only the accepted version of an IEEE copyrighted paper can be used when posting the paper or your thesis on-line.
3) In placing the thesis on the author's university website, please display the following message in a prominent place on the website: In reference to IEEE copyrighted material which is used with permission in this thesis, the IEEE does not endorse any of [university/educational entity's name goes here]'s products or services. Internal or personal use of this material is permitted. If interested in reprinting/republishing IEEE copyrighted material for advertising or promotional purposes or for creating new collective works for resale or redistribution, please go to http://www.ieee.org/publications_standards/publications/rights/rights_link.html to learn how to obtain a License from RightsLink.

If applicable, University Microfilms and/or ProQuest Library, or the Archives of Canada may supply single copies of the dissertation.

CITED LITERATURE

1. Hanosh, O., Ansari, R., Younis, K., and Cetin, A. E.: Real-time epileptic seizure detection during sleep using passive infrared sensors. IEEE Sensors Journal, 19(15):6467–6476, 2019.

2. Hanosh, O., Ansari, R., Issa, N. P., and Enis Cetin, A.: Convulsive movement detection using low-resolution thermopile sensor array. In Proceedings of the IEEE/CVF Conference on Computer Vision and Pattern Recognition Workshops, pages 300–301, 2020.

3. Yang, G.-Z. and Yang, G.: Body sensor networks, volume 1. Springer, 2006.

4. Aziz, O., Atallah, L., Lo, B., ElHelw, M., Wang, L., Yang, G.-Z., and Darzi, A.: A pervasive body sensor network for measuring postoperative recovery at home. Surgical innovation, 14(2):83–90, 2007.

5. Corbishley, P. and Rodriguez-Villegas, E.: Breathing detection: towards a miniaturized, wearable, battery-operated monitoring system. IEEE Transactions on Biomedical Engineering, 55(1):196–204, 2007.

6. Shneerson, J. M.: Sleep medicine: a guide to sleep and its disorders. John Wiley & Sons, 2009.

7. Erden, F., Velipasalar, S., Alkar, A. Z., and Cetin, A. E.: Sensors in assisted living: A survey of signal and image processing methods. IEEE Signal Processing Magazine, 33(2):36–44, 2016.

8. Chen, D., Malkin, R., and Yang, J.: Multimodal detection of human interaction events in a nursing home environment. In Proceedings of the 6th international conference on Multimodal interfaces, pages 82–89, 2004.

9. Pansiot, J., Stoyanov, D., Lo, C., and Yang, G.-Z.: Towards image-based modeling for ambient sensing. In International Workshop on Wearable and Implantable Body Sensor Networks (BSN'06), pages 4–pp. IEEE, 2006.

10. Lo, B. P., Wang, J. L., Yang, G.-Z., et al.: From imaging networks to behavior profiling: Ubiquitous sensing for managed homecare of the elderly. Citeseer, 2005.

11. Cardinaux, F., Bhowmik, D., Abhayaratne, C., and Hawley, M. S.: Video based technology for ambient assisted living: A review of the literature. Journal of Ambient Intelligence and Smart Environments, 3(3):253–269, 2011.

12. Chernbumroong, S., Cang, S., Atkins, A., and Yu, H.: Elderly activities recognition and classification for applications in assisted living. Expert Systems with Applications, 40(5):1662–1674, 2013.

13. Ganchev, I., Garcia, N. M., Dobre, C., Mavromoustakis, C. X., and Goleva, R.: Enhanced living environments: Algorithms, architectures, platforms, and systems, volume 11369. Springer, 2019.

14. Santo, H., Maekawa, T., and Matsushita, Y.: Device-free and privacy preserving indoor positioning using infrared retro-reflection imaging. In 2017 IEEE International Conference on Pervasive Computing and Communications (PerCom), pages 141–152. IEEE, 2017.

15. Witte, H., Iasemidis, L. D., and Litt, B.: Special issue on epileptic seizure prediction. IEEE transactions on biomedical engineering, 50(5):537–539, 2003.

16. Sveinsson, O., Andersson, T., Mattsson, P., Carlsson, S., and Tomson, T.: Clinical risk factors in sudep: A nationwide population-based case-control study. Neurology, 94(4):e419–e429, 2020.

17. Langan, Y., Nashef, L., and Sander, J.: Sudden unexpected death in epilepsy: a series of witnessed deaths. Journal of Neurology, Neurosurgery & Psychiatry, 68(2):211–213, 2000.

18. Rocamora, R., Sánchez-Álvarez, J. C., and Salas-Puig, J.: The relationship between sleep and epilepsy. The Neurologist, 14(6):S35–S43, 2008.

19. Benjamin, E. J., Muntner, P., Alonso, A., Bittencourt, M. S., Callaway, C. W., Carson, A. P., Chamberlain, A. M., Chang, A. R., Cheng, S., Das, S. R., et al.: Heart disease and stroke statistics-2019 update a report from the american heart association. Circulation, 2019.

20. Organization, W. H. et al.: Cardiovascular diseases (cvds) fact sheet. World Health Organization, 2017.

21. Trifan, A., Oliveira, M., and Oliveira, J. L.: Passive sensing of health outcomes through smartphones: systematic review of current solutions and possible limitations. JMIR mHealth and uHealth, 7(8):e12649, 2019.

22. Sendra Compte, S., Lloret, J., García Pineda, M., and Toledo Alarcón, J. F.: Power saving and energy optimization techniques for wireless sensor networks. Journal of communications, 6(6):439–459, 2011.

23. Tomas, J., Lloret, J., Bri, D., and Sendra, S.: Sensors and their application for disabled and elderly people. In Assistive Technologies: Concepts, Methodologies, Tools, and Applications, pages 357–376. IGI Global, 2014.

24. Kapre, S. S., Salunkhe, S. S., Thakkar, R. M., Pawar, A. P., and Malusare, O. A.: Advanced security guard with pir sensor for commercial and residential use. International Journal for Advance Research in Engineering and Technology, 2(XI), 2014.

25. Jeličić, V., Magno, M., Paci, G., Brunelli, D., and Benini, L.: Design, characterization and management of a wireless sensor network for smart gas monitoring. In 2011 4th IEEE International Workshop on Advances in Sensors and Interfaces (IWASI), pages 115–120. IEEE, 2011.

26. Othman, N. A. and Aydin, I.: A new iot combined body detection of people by using computer vision for security application. In 2017 9th International Conference on Computational Intelligence and Communication Networks (CICN), pages 108–112. IEEE, 2017.

27. Mainwaring, A., Culler, D., Polastre, J., Szewczyk, R., and Anderson, J.: Wireless sensor networks for habitat monitoring. In Proceedings of the 1st ACM international workshop on Wireless sensor networks and applications, pages 88–97, 2002.

28. Kuki, M., Nakajima, H., Tsuchiya, N., Kuramoto, K., Kobashi, S., and Hata, Y.: Mining multi human locations using thermopile array sensors. In 2013 IEEE 43rd International Symposium on Multiple-Valued Logic, pages 59–64. IEEE, 2013.

29. Gonzalez, L. I. L., Troost, M., and Amft, O.: Using a thermopile matrix sensor to recognize energy-related activities in offices. In ANT/SEIT, pages 678–685, 2013.

30. Witte, H., Iasemidis, L. D., and Litt, B.: Special issue on epileptic seizure prediction. IEEE transactions on biomedical engineering, 50(5):537–539, 2003.

31. Sveinsson, O., Andersson, T., Mattsson, P., Carlsson, S., and Tomson, T.: Clinical risk factors in sudep: A nationwide population-based case-control study. Neurology, 94(4):e419–e429, 2020.

32. Langan, Y., Nashef, L., and Sander, J.: Sudden unexpected death in epilepsy: a series of witnessed deaths. Journal of Neurology, Neurosurgery & Psychiatry, 68(2):211–213, 2000.

33. Jones, L. A. and Thomas, R. H.: Sudden death in epilepsy: Insights from the last 25 years. Seizure, 44:232–236, 2017.

34. M. Anil kumar, S. Kishore, N. K. K. C. s. and Shafi, S.: Realtime epileptic seizures detection and alert system using ni lab-view,. IEEE transactions on biomedical engineering, 5(5), 2014.

35. Christensen, J., Vestergaard, M., Pedersen, M. G., Pedersen, C. B., Olsen, J., and Sidenius, P.: Incidence and prevalence of epilepsy in denmark. Epilepsy research, 76(1):60–65, 2007.

36. Beniczky, S., Polster, T., Kjaer, T. W., and Hjalgrim, H.: Detection of generalized tonic–clonic seizures by a wireless wrist accelerometer: a prospective, multicenter study. Epilepsia, 54(4):e58–e61, 2013.

37. Nijsen, T. M., Arends, J. B., Griep, P. A., and Cluitmans, P. J.: The potential value of three-dimensional accelerometry for detection of motor seizures in severe epilepsy. Epilepsy & Behavior, 7(1):74–84, 2005.

38. Strong, V., Brown, S. W., and Walker, R.: Seizure-alert dogs—fact or fiction? Seizure, 8(1):62–65, 1999.

39. Strong, V., Brown, S., Huyton, M., and Coyle, H.: Effect of trained seizure alert dogs® on frequency of tonic–clonic seizures. Seizure, 11(6):402–405, 2002.

40. Li, Z., da Silva, A. M., and Cunha, J. P. S.: Movement quantification in epileptic seizures: a new approach to video-eeg analysis. IEEE Transactions on Biomedical Engineering, 49(6):565–573, 2002.

41. Narechania, A. P., Garić, I. I., Sen-Gupta, I., Macken, M. P., Gerard, E. E., and Schuele, S. U.: Assessment of a quasi-piezoelectric mattress monitor as a detection system for generalized convulsions. Epilepsy & Behavior, 28(2):172–176, 2013.

42. Pauri, F., Pierelli, F., Chatrian, G.-E., and Erdly, W. W.: Long-term eeg-video-audio monitoring: computer detection of focal eeg seizure patterns. Electroencephalography and clinical Neurophysiology, 82(1):1–9, 1992.

43. Rennie, J., Chorley, G., Boylan, G., Pressler, R., Nguyen, Y., and Hooper, R.: Non-expert use of the cerebral function monitor for neonatal seizure detection. Archives of Disease in Childhood-Fetal and Neonatal Edition, 89(1):F37–F40, 2004.

44. Waterhouse, E.: New horizons in ambulatory electroencephalography. IEEE Engineering in Medicine and Biology Magazine, 22(3):74–80, 2003.

45. Lockman, J., Fisher, R. S., and Olson, D. M.: Detection of seizure-like movements using a wrist accelerometer. Epilepsy & Behavior, 20(4):638–641, 2011.

46. Swami, P., Gandhi, T. K., Panigrahi, B. K., Bhatia, M., and Anand, S.: Detection of ictal patterns in electroencephalogram signals using 3d phase trajectories. In 2015 Annual IEEE India Conference (INDICON), pages 1–6. IEEE, 2015.

47. Tzallas, A. T., Tsipouras, M. G., and Fotiadis, D. I.: Epileptic seizure detection in eegs using time–frequency analysis. IEEE transactions on information technology in biomedicine, 13(5):703–710, 2009.

48. Gotman, J.: Automatic seizure detection: improvements and evaluation. Electroencephalography and clinical Neurophysiology, 76(4):317–324, 1990.

49. B. U. Toreyin, A. B. Soyer, I. O. and Cetin, E. A.: Falling person detection using multi-sensor signal processing,. EURASIP J. Adv. Signal Process., 2008(1), 2017.

50. Erden, F., Toreyin, B. U., Soyer, E. B., Inac, I., Gunay, O., Kose, K., and Cetin, A. E.: Wavelet based flickering flame detector using differential pir sensors. Fire Safety Journal, 53:13–18, 2012.

51. Engel, J.: A proposed diagnostic scheme for people with epileptic seizures and with epilepsy: report of the ilae task force on classification and terminology. Epilepsia, 42(6):796–803, 2001.

52. Töreyin, B. U., Soyer, E. B., Urfalıoglu, O., and Cetin, A. E.: Flame detection system based on wavelet analysis of pir sensor signals with an hmm decision mechanism. In 2008 16th European Signal Processing Conference, pages 1–5. IEEE, 2008.

53. Minecan, D., Natarajan, A., Marzec, M., and Malow, B.: Relationship of epileptic seizures to sleep stage and sleep depth. Sleep, 25(8):56–61, 2002.

54. Carskadon, M. A., Dement, W. C., et al.: Normal human sleep: an overview. Principles and practice of sleep medicine, 4:13–23, 2005.

55. Iber, C., Ancoli-Israel, S., Chesson, A. L., Quan, S. F., et al.: The AASM manual for the scoring of sleep and associated events: rules, terminology and technical specifications, volume 1. American academy of sleep medicine Westchester, IL, 2007.

56. Zainuddin, Z., Huong, L. K., and Pauline, O.: Reliable epileptic seizure detection using an improved wavelet neural network. The Australasian medical journal, 6(5):308, 2013.

57. Rocamora, R., Sánchez-Álvarez, J. C., and Salas-Puig, J.: The relationship between sleep and epilepsy. The Neurologist, 14(6):S35–S43, 2008.

58. Lockwood, C., Conroy-Hiller, T., and Page, T.: Vital signs. JBI reports, 2(6):207–230, 2004.

59. Benjamin, E. J., Blaha, M. J., Chiuve, S. E., Cushman, M., Das, S. R., Deo, R., De Ferranti, S. D., Floyd, J., Fornage, M., Gillespie, C., et al.: Heart disease and stroke statistics—2017 update. 2017.

60. Gandevia, S. C. and McKenzie, D. K.: Respiratory rate: the neglected vital sign. Medical Journal of Australia, 189(9):531–532, 2008.

61. Chourpiliadis, C. and Bhardwaj, A.: Physiology, respiratory rate. 2019.

62. McBride, J., Knight, D., Piper, J., and Smith, G. B.: Long-term effect of introducing an early warning score on respiratory rate charting on general wards. Resuscitation, 65(1):41–44, 2005.

63. Lima, C. M. A. d. O.: Information about the new coronavirus disease (covid-19). Radiologia Brasileira, 53(2):V–VI, 2020.

64. Parhizgar, F., Nugent, K., and Raj, R.: Obstructive sleep apnea and respiratory complications associated with vagus nerve stimulators. Journal of Clinical Sleep Medicine, 7(4):401–407, 2011.

65. Hanson, B., Child, N., Van Duijvenboden, S., Orini, M., Chen, Z., Coronel, R., Rinaldi, C. A., Gill, J. S., Gill, J. S., and Taggart, P.: Oscillatory behavior of ventricular action potential duration in heart failure patients at respiratory rate and low frequency. Frontiers in physiology, 5:414, 2014.

66. Droitcour, A. D., Seto, T. B., Park, B.-K., Yamada, S., Vergara, A., El Hourani, C., Shing, T., Yuen, A., Lubecke, V. M., and Boric-Lubecke, O.: Non-contact respiratory rate measurement validation for hospitalized patients. In 2009 Annual International Conference of the IEEE Engineering in Medicine and Biology Society, pages 4812–4815. IEEE, 2009.

67. Dellacà, R. L., Gobbi, A., Pastena, M., Pedotti, A., and Celli, B.: Home monitoring of within-breath respiratory mechanics by a simple and automatic forced oscillation technique device. Physiological measurement, 31(4):N11, 2010.

68. Seddon, P., Sobowiec-Kouman, S., and Wertheim, D.: Infant home respiratory monitoring using pulse oximetry. Archives of disease in childhood, 103(6):603–605, 2018.

69. Peng, Y.-T., Lin, C.-Y., Sun, M.-T., and Landis, C. A.: Multimodality sensor system for long-term sleep quality monitoring. IEEE Transactions on Biomedical Circuits and Systems, 1(3):217–227, 2007.

70. Folke, M., Cernerud, L., Ekström, M., and Hök, B.: Critical review of non-invasive respiratory monitoring in medical care. Medical and Biological Engineering and Computing, 41(4):377–383, 2003.

71. Erden, F., Velipasalar, S., Alkar, A. Z., and Cetin, A. E.: Sensors in assisted living: A survey of signal and image processing methods. IEEE Signal Processing Magazine, 33(2):36–44, 2016.

72. Erden, F. and Cetin, A. E.: Period estimation of an almost periodic signal using persistent homology with application to respiratory rate measurement. IEEE Signal Processing Letters, 24(7):958–962, 2017.

73. Pantelopoulos, A. and Bourbakis, N. G.: A survey on wearable sensor-based systems for health monitoring and prognosis. IEEE Transactions on Systems, Man, and Cybernetics, Part C (Applications and Reviews), 40(1):1–12, 2009.

74. Aarts, L. A., Jeanne, V., Cleary, J. P., Lieber, C., Nelson, J. S., Oetomo, S. B., and Verkruysse, W.: Non-contact heart rate monitoring utilizing camera photoplethysmography in the neonatal intensive care unit—a pilot study. Early human development, 89(12):943–948, 2013.

75. Gupta, O., McDuff, D., and Raskar, R.: Real-time physiological measurement and visualization using a synchronized multi-camera system. In Proceedings of the IEEE Conference on Computer Vision and Pattern Recognition Workshops, pages 46–53, 2016.

76. Tamura, T., Maeda, Y., Sekine, M., and Yoshida, M.: Wearable photoplethysmographic sensors—past and present. Electronics, 3(2):282–302, 2014.

77. Pietilä, J., Mehrang, S., Tolonen, J., Helander, E., Jimison, H., Pavel, M., and Korhonen, I.: Evaluation of the accuracy and reliability for photoplethysmography based heart rate and beat-to-beat detection during daily activities. In EMBEC & NBC 2017, pages 145–148. Springer, 2017.

78. Guo, H. W., Huang, Y. S., Chien, J. C., and Shieh, J. S.: Short-term analysis of heart rate variability for emotion recognition via a wearable ecg device. In 2015 International Conference on Intelligent Informatics and Biomedical Sciences (ICIIBMS), pages 262–265. IEEE, 2015.

79. Askarian, B., Jung, K., and Chong, J. W.: Monitoring of heart rate from photoplethysmographic signals using a samsung galaxy note8 in underwater environments. Sensors, 19(13):2846, 2019.

80. Nelson, B. W., Low, C. A., Jacobson, N., Areán, P., Torous, J., and Allen, N. B.: Guidelines for wrist-worn consumer wearable assessment of heart rate in biobehavioral research. NPJ Digital Medicine, 3(1):1–9, 2020.

81. Poh, M.-Z., McDuff, D. J., and Picard, R. W.: Non-contact, automated cardiac pulse measurements using video imaging and blind source separation. Optics express, 18(10):10762–10774, 2010.

82. Soleymani, M., Lichtenauer, J., Pun, T., and Pantic, M.: A multimodal database for affect recognition and implicit tagging. IEEE transactions on affective computing, 3(1):42–55, 2011.

83. Verkruysse, W., Svaasand, L. O., and Nelson, J. S.: Remote plethysmographic imaging using ambient light. Optics express, 16(26):21434–21445, 2008.

84. Li, X., Chen, J., Zhao, G., and Pietikainen, M.: Remote heart rate measurement from face videos under realistic situations. In Proceedings of the IEEE conference on computer vision and pattern recognition, pages 4264–4271, 2014.

85. Chen, K.-M., Huang, Y., Zhang, J., and Norman, A.: Microwave life-detection systems for searching human subjects under earthquake rubble or behind barrier. IEEE transactions on biomedical engineering, 47(1):105–114, 2000.

86. Augousti, A., Maletras, F., and Mason, J.: Improved fibre optic respiratory monitoring using a figure-of-eight coil. Physiological measurement, 26(5):585, 2005.

87. Zhao, M., Adib, F., and Katabi, D.: Emotion recognition using wireless signals. In Proceedings of the 22nd Annual International Conference on Mobile Computing and Networking, pages 95–108, 2016.

88. Shneerson, M.: Sleep medicine: a guide to sleep and its disorders, handbook, 2005.

89. Lee-Chiong, T. L.: Sleep: a comprehensive handbook. John Wiley & Sons, 2005.

90. Tobin, M. J.: Respiratory monitoring. Jama, 264(2):244–251, 1990.

91. Wilkinson, J. and Thanawala, V.: Thoracic impedance monitoring of respiratory rate during sedation–is it safe? Anaesthesia, 64(4):455–456, 2009.

92. Mazzanti, B., Lamberti, C., and De Bie, J.: Validation of an ecg-derived respiration monitoring method. In Computers in Cardiology, 2003, pages 613–616. IEEE, 2003.

93. Chon, K. H., Dash, S., and Ju, K.: Estimation of respiratory rate from photoplethysmogram data using time–frequency spectral estimation. IEEE Transactions on Biomedical Engineering, 56(8):2054–2063, 2009.

94. Minolta, K.: Basic understanding of the pulse oximeter. how to read spo2. Konica Minolta Sensing, Inc. Ramsey, 2006.

95. Wertheim, D., Olden, C., Savage, E., and Seddon, P.: Extracting respiratory data from pulse oximeter plethysmogram traces in newborn infants. Archives of Disease in Childhood-Fetal and Neonatal Edition, 94(4):F301–F303, 2009.

96. Greneker, E.: Radar sensing of heartbeat and respiration at a distance with applications of the technology. 1997.

97. Aoki, H., Takemura, Y., Mimura, K., and Nakajima, M.: Development of non-restrictive sensing system for sleeping person using fiber grating vision sensor. In MHS2001. Proceedings of 2001 International Symposium on Micromechatronics and Human Science (Cat. No. 01TH8583), pages 155–160. IEEE, 2001.

98. Tan, K. S., Saatchi, R., Elphick, H., and Burke, D.: Real-time vision based respiration monitoring system. In 2010 7th International Symposium on Communication Systems, Networks & Digital Signal Processing (CSNDSP 2010), pages 770–774. IEEE, 2010.

99. Erden, F., Alkar, A. Z., and Cetin, A. E.: Contact-free measurement of respiratory rate using infrared and vibration sensors. Infrared Physics & Technology, 73:88–94, 2015.

100. Kapu, H., Saraswat, K., Ozturk, Y., and Cetin, A. E.: Resting heart rate estimation using pir sensors. Infrared Physics & Technology, 85:56–61, 2017.

101. Lorato, I., Bakkes, T., Stuijk, S., Meftah, M., and De Haan, G.: Unobtrusive respiratory flow monitoring using a thermopile array: A feasibility study. Applied Sciences, 9(12):2449, 2019.

102. Erden, F., Toreyin, B. U., Soyer, E. B., Inac, I., Gunay, O., Kose, K., and Cetin, A. E.: Wavelet based flickering flame detector using differential pir sensors. Fire Safety Journal, 53:13–18, 2012.

103. Töreyin, B. U., Soyer, E. B., Urfalıoglu, O., and Cetin, A. E.: Flame detection system based on wavelet analysis of pir sensor signals with an hmm decision mechanism. In 2008 16th European Signal Processing Conference, pages 1–5. IEEE, 2008.

104. Erden, F. and Cetin, A. E.: Hand gesture based remote control system using infrared sensors and a camera. IEEE Transactions on Consumer Electronics, 60(4):675–680, 2014.

105. Erden, F., Velipasalar, S., Alkar, A. Z., and Cetin, A. E.: Sensors in assisted living: A survey of signal and image processing methods. IEEE Signal Processing Magazine, 33(2):36–44, 2016.

106. Erden, F., Soyer, E. B., Toreyin, B. U., and Cetin, A. E.: Voc gas leak detection using pyroelectric infrared sensors. In 2010 IEEE International Conference on Acoustics, Speech and Signal Processing, pages 1682–1685. IEEE, 2010.

107. Rabiner, L. R.: A tutorial on hidden markov models and selected applications in speech recognition. Proceedings of the IEEE, 77(2):257–286, 1989.

108. Deng, L. and Yu, D.: Deep learning: methods and applications. Foundations and trends in signal processing, 7(3–4):197–387, 2014.

109. Bengio, Y.: Learning deep architectures for AI. Now Publishers Inc, 2009.

110. LeCun, Y., Bottou, L., Bengio, Y., and Haffner, P.: Gradient-based learning applied to document recognition. Proceedings of the IEEE, 86(11):2278–2324, 1998.

111. Visa, S., Ramsay, B., Ralescu, A. L., and Van Der Knaap, E.: Confusion matrix-based feature selection. MAICS, 710:120–127, 2011.

112. Beleites, C., Salzer, R., and Sergo, V.: Validation of soft classification models using partial class memberships: An extended concept of sensitivity & co. applied to grading of astrocytoma tissues. Chemometrics and Intelligent Laboratory Systems, 122:12–22, 2013.

113. Srivastava, N., Hinton, G., Krizhevsky, A., Sutskever, I., and Salakhutdinov, R.: Dropout: a simple way to prevent neural networks from overfitting. The journal of machine learning research, 15(1):1929–1958, 2014.

114. Zainuddin, Z., Huong, L. K., and Pauline, O.: Reliable epileptic seizure detection using an improved wavelet neural network. The Australasian medical journal, 6(5):308, 2013.

115. Rocamora, R., Sánchez-Álvarez, J. C., and Salas-Puig, J.: The relationship between sleep and epilepsy. The Neurologist, 14(6):S35–S43, 2008.

116. Gonzalez, L. I. L., Troost, M., and Amft, O.: Using a thermopile matrix sensor to recognize energy-related activities in offices. In ANT/SEIT, pages 678–685, 2013.

117. Cerutti, G., Prasad, R., and Farella, E.: Convolutional neural network on embedded platform for people presence detection in low resolution thermal images. In ICASSP 2019-2019 IEEE International Conference on Acoustics, Speech and Signal Processing (ICASSP), pages 7610–7614. IEEE, 2019.

118. Deng, L. and Yu, D.: Deep learning for signal and information processing. Microsoft Research Monograph, 2013.

119. Bengio, Y. et al.: Learning deep architectures for ai. Foundations and trends® in Machine Learning, 2(1):1–127, 2009.

120. Zainuddin, Z., Huong, L. K., and Pauline, O.: Reliable epileptic seizure detection using an improved wavelet neural network. The Australasian medical journal, 6(5):308, 2013.

121. Beleites, C., Salzer, R., and Sergo, V.: Validation of soft classification models using partial class memberships: An extended concept of sensitivity & co. applied to grading of astrocytoma tissues. Chemometrics and Intelligent Laboratory Systems, 122:12–22, 2013.

122. Gonzalez, L. I. L., Troost, M., and Amft, O.: Using a thermopile matrix sensor to recognize energy-related activities in offices. In ANT/SEIT, pages 678–685, 2013.

123. Wang, Y.-Q.: An analysis of the viola-jones face detection algorithm. Image Processing On Line, 4:128–148, 2014.

124. Leonard, P. A., Clifton, D., Addison, P. S., Watson, J. N., and Beattie, T.: An automated algorithm for determining respiratory rate by photoplethysmogram in children. Acta paediatrica, 95(9):1124–1128, 2006.

125. Palshikar, G. et al.: Simple algorithms for peak detection in time-series. In Proc. 1st Int. Conf. Advanced Data Analysis, Business Analytics and Intelligence, volume 122, 2009.

126. Lorato, I., Bakkes, T., Stuijk, S., Meftah, M., and De Haan, G.: Unobtrusive respiratory flow monitoring using a thermopile array: A feasibility study. Applied Sciences, 9(12):2449, 2019.

127. Wang, Y.-Q.: An analysis of the viola-jones face detection algorithm. Image Processing On Line, 4:128–148, 2014.

128. Gupta, O., McDuff, D., and Raskar, R.: Real-time physiological measurement and visualization using a synchronized multi-camera system. In Proceedings of the IEEE Conference on Computer Vision and Pattern Recognition Workshops, pages 46–53, 2016.

129. Da He, D., Winokur, E. S., and Sodini, C. G.: A continuous, wearable, and wireless heart monitor using head ballistocardiogram (bcg) and head electrocardiogram (ecg). In 2011 Annual International Conference of the IEEE Engineering in Medicine and Biology Society, pages 4729–4732. IEEE, 2011.

130. Balakrishnan, G., Durand, F., and Guttag, J.: Detecting pulse from head motions in video. In Proceedings of the IEEE Conference on Computer Vision and Pattern Recognition, pages 3430–3437, 2013.

131. Yun, J. and Song, M.-H.: Detecting direction of movement using pyroelectric infrared sensors. IEEE Sensors Journal, 14(5):1482–1489, 2014.

132. Cirino, G. A., Barcellos, R., Morato, S. P., Bereczki, A., and Neto, L. G.: Design, fabrication, and characterization of fresnel lens array with spatial filtering for passive infrared motion sensors. In Photonics North 2006, volume 6343, page 634323. International Society for Optics and Photonics, 2006.

133. Zhao, M., Adib, F., and Katabi, D.: Emotion recognition using wireless signals. In Proceedings of the 22nd Annual International Conference on Mobile Computing and Networking, pages 95–108, 2016.

134. Lai, C.-C., Liu, Y. H., Wang, C.-Y., Wang, Y.-H., Hsueh, S.-C., Yen, M.-Y., Ko, W.-C., and Hsueh, P.-R.: Asymptomatic carrier state, acute respiratory disease, and pneumonia due to severe acute respiratory syndrome coronavirus 2 (sarscov-2): facts and myths. Journal of Microbiology, Immunology and Infection, 2020.

135. Gattinoni, L., Chiumello, D., Caironi, P., Busana, M., Romitti, F., Brazzi, L., and Camporota, L.: Covid-19 pneumonia: different respiratory treatments for different phenotypes?, 2020.

VITA

Name Ouday Hanosh

Key strengths

- Research and development
- Complex problem solver
- Signal processing
- Machine leaning Deep learning
- Biomedical signals
- Image and video processing Sensors
- Healthcare applications
- Technical documentation

Education

Ph.D., Electrical and Computer Engineering
University of Illinois at Chicago, Chicago, Illinois, United States, 2021

M.Sc., Electrical Engineering
University of Baghdad, College of Engineering, 2001
Thesis Title: Design and implementation of real time image processing using TMSC25

B.Sc., Electrical Engineering
University of Baghdad, College of Engineering, 1997

Publications

- **Hanosh, O.**, Ansari, R., Yusuf O. , and Cetin, A.E. "Respiratory rate estimation using a low-resolution infrared sensor array." Demos:Medical and Industrial Imaging, ICPR 2020.

- **Hanosh, O.**, Ansari, R., Issa, N. P. , and Cetin, A.E. "Convulsive Movement Detection Using Low-Resolution Thermopile Sensor Array." In Proceedings of the IEEE/CVF Conference on Computer Vision and Pattern Recognition Workshops, pp. 300-301. 2020.

- **Hanosh, O.**, Ansari, R., and Cetin, A.E. "Real-Time Epileptic Seizure Detection during Sleep using Passive Infrared (PIR) Sensors." Show and tell Demonstrations, ICASSP 2020.

- **Hanosh, Ouday**, Ansari, R., Younis, K., and Cetin, A.E. "Real-Time Epileptic Seizure Detection during Sleep using Passive Infrared (PIR) Sensors." IEEE Sensors Journal (2019).

- **Hanosh, O.**, and Salim, B.W. "11×11 Playfair Cipher based on a Cascade of LFSRs." Matrix 11 (2013): 11.

- **Hanosh, O.**,"Face Detection using Skin Color and Morphological Operation", pure and Engineering Sciences Journal, December 2009.

Academic Honors

- Recognized as the Mentor of the Fall 2017 Semester, University of Illinois at Chicago.
- Award for Graduate Research (Deiss-funded awards), Fall 2020 Semester, University of Illinois at Chicago.

Memberships

- IEEE Signal Processing Society member

Professional Activities

- **Reviewer**, Signal, Image and Video Processing (SIVP)
- **Reviewer**, Signal IEEE transactions on Neural Networks and Learning Systems

Teaching and Leadership Experience

- **University of Illinois at Chicago (2015-Present)**
- **Teaching Assistant** for the following courses: Introduction to Electrical and Computer Engineering, Circuit Analysis, Discrete and Continuous Signals and Systems, Digital Signal Processing I, Digital Signal Processing II, Pattern Recognition I.
- **Lead Instructor**, College of Engineering, Summer camp 2019.
- **Lead Instructor**, Women in Engineering Summer program; Summer 2017 and Summer 2019.

- **Teaching Assistant**, Science Technology Engineering Mathematics; Summer 2016.
- **Supervising** GPIP students.
- **Supervising** senior design students.
- **University of Nawroz (Duhok-Kurdistan region) (2007-2013)**
- **Lecturer**, taught Cryptography and Cipher Systems, Numerical Analysis.
- **University of Baghdad (Iraq) (2001-2006)**
- **Assistant Lecturer**, taught electrical engineering and computer science.